DISTRIBUTED STRUCTURAL ACTUATION AND CONTROL WITH ELECTROSTRICTORS

by
Michael Fripp

Submitted to the Department of Aeronautics
and Astronautics Engineering in Partial
Fulfillment of the Requirements for the
Degree of

MASTER OF SCIENCE
in Aeronautics and Astronautics
at the

Massachusetts Institute of Technology

January 1995

Signature of Author .....
Department of Aeronautics and Astronautics
January 13, 1995

Certified by .....
Professor Nesbitt W. Hagood
Thesis Supervisor

Accepted by .....
Professor Harold Y. Wachman
Chairman, Department Graduate Committee

ABSTRACT

DISTRIBUTED STRUCTURAL ACTUATION AND CONTROL WITH ELECTROSTRICTORS

Michael Fripp

This document develops a methodology for modeling the dynamic behavior of an electromechanical system with distributed electrostrictive coupling. A framework for the derivation of the governing equations is presented which is sufficiently general to model the dynamics of a broad range of nonlinear systems.

The modeling starts with a understanding of the constitutive relationships describing the electromechanical behavior of the electrostrictive relaxor ferroelectric, PMN-PT $0.9(Pb[Mg_{1/3}Nb_{2/3}]O_3\text{-}0.1(PbTiO_3))$. The practical limitations of the constitutive relationships are also presented. The relevant constitutive relationships for electrostrictors are introduced into a generalized form of Hamilton's principle. Approximate system equations are derived using the Rayleigh-Ritz assumed mode method.

The general equations which describe the dynamics of the electrostrictively coupled electromechanical system are experimentally validated by examining the static and dynamic response of a cantilevered beam actuated with an electrostrictive wafer. These equations are subsequently used in a control algorithm to regulate tip displacement of the cantilevered beam. A second-order controller with output linearization and temperature stabilitzation yielded a consistent 60% noise reduction across a wide range of temperatures and field levels. An adaptive control algorithm which gave 20% noise reduction was also implemented.

ACKNOWLEDGMENTS

I received a lot of help while performing this research. Gary Blackwood helped get me started by donating some of his extra electrostrictive wafers to me. Dave Warkentin, Kin Chan, John Rodgers, Aaron Bent, Lana Luoma, Kamyar Ghandi, Jaco DuPlessis, A.J. McFarland and Debby Redish helped keep me going. Dave helped with my Rayleigh-Ritz code. Kin provided the circuit which measured the charge on the electrostrictive wafer - sorry about destroying the circuit. John and Aaron provided some crucial experiment taking when time got tight. Lana's machining assistance saved me a lot of time. Kamyar's help in refocusing my efforts and in sanity preservation were greatly appreciated. Jaco, A.J., and Debby also provided some crucial sanity preservation during the writing and the catch-and-go revision process.

The assistance of my advisor, Nesbitt Hagood, proved crucial during my investigation. The monetary sponsorship of the National Defense Graduate Fellowship was greatly appreciated.

TABLE OF CONTENTS

LIST OF FIGURES

NOTATION

A	Helmholtz free energy: scalar or surface area: scalar
a	number of assumed structural displacement modes
b	number of assumed electrical modes (i.e. number of electrical surfaces)
$\mathbf{B}^f$	generalized coordinate conversion matrix for forces: [ax6] matrix
$\mathbf{B}^q$	generalized coordinate conversion matrix for charges: [bx3] matrix
C	stiffness matrix: [6x6] matrix
C^*	electric field varying stiffness: [6x6] matrix
$\mathbf{C}^d$	damping matrix: [6x6] matrix
d	piezoelectric coupling term: [3x6] matrix or amplified disturbance input to the piezoceramic: scalar
D	electrical displacement vector: [3x1] vector
E	electric field vector: [3x1] vector
e	control error: scalar
ε	dielectric of the electrostrictor: [3x3] matrix
F^*	hyperbolic field term: tensor
f	vector of applied forces: [6x1] vector
G	higher-order electrostrictive charge storage matrix: [bxb] matrix or Gibbs free energy function: scalar
g	linearization factor in the output linearization: tensor or magneto-mechanical coupling term: tensor
Γ	rate of adaptation: matrix
H	enthalpy of the system: scalar or transfer function: scalar
I	identity matrix: [axa] matrix
k	hyperbolic relaxation factor: scalar
K	stiffness matrix: [axa] matrix
$\tilde{\mathbf{K}}$	electric field correction to the stiffness term: tensor

$\mathbf{L}^u$ linear differential operator for elasticity: [6x6] matrix

$\mathbf{L}^v$ differential operator for electricity: [3x1] vector

$\mathbf{M}$ mass matrix: [axa] matrix

m electrostrictive constants relating electric field with strain: scalar

$\mathbf{m}^*$ electrostrictive coupling term. Includes a electric field term: [3x6] matrix

$\mathbf{N}^r$ modal vector of mechanical strains: [6xa] matrix

$\mathbf{N}^v$ modal vector of electric fields: [3xb] matrix

ν poisson's ratio

P electrical polarization: [3x1] vector

P^s spontaneous polarization: scalar

ψ^r modal vector of mechanical displacements: [6xa] matrix

ψ^v modal vector of voltages: [3xb] matrix

φ electrical potential: scalar

$\mathbf{q}$ applied electrode charges: [3x1] vector

q^m temperature factor relating m and temperature: scalar

q^k temperature factor relating k and temperature: scalar

$\mathbf{Q}$ electrostrictive capacitance matrix: [bxb] matrix

dQ infinitesimal quantity of heat: scalar

Θ electromechanical coupling matrix: [axb] matrix
or temperature: scalar

$\tilde{\Theta}$ electric field correction to the electromechanical coupling term: tensor

$\mathbf{R}$ elastostriction coupling term: tensor

$\mathbf{r}$ modal amplitudes of physical displacement: [ax1] vector
or elastostrictive coupling constants: tensor
or position

ρ density: scalar

$\mathbf{s}$ compliance matrix: [6x6] matrix
or system entropy: scalar
or Laplace transform variable: scalar
or velocity error: scalar

$\mathbf{S}$ strain vector: [6x1] vector

t time or ply thickness: scalar

$\mathbf{T}$ stress vector: [6x1] vector
or sampling interval: scalar

T^* complimentary kinetic energy: scalar

τ control output

$\mathbf{u}$ vector of mechanical displacements: [6x1] matrix
or amplified control input to the electrostrictor: scalar

U	potential energy: scalar
$\tilde{U}$	change in potential energy per unit volume at a particular state: scalar
$\mathbf{v}$	vector of generalized electric coordinates: [bx1] vector
V	volume: scalar
W_e^*	complimentary electrical energy: scalar
$\tilde{W}_e^*$	change in electric energy per unit volume at a particular state: scalar
W_m	magnetic energy: scalar
W	externally applied work: scalar
ω	natural frequency: scalar
x	control output: scalar
$\mathbf{Y}$	reference model: matrix
y	tip displacement: scalar
ζ	damping ratio: scalar
ξ	dummy variable indicating the state of the system: scalar
$\tilde{\xi}$	value of the dummy variable at the end of the path and reflecting the current state of the system: scalar
z	Z transform variable: scalar

Superscripts

a	pertains to the actuator or applied level after output linearization
c	pertains to the controller or commanded level before output linearization
d	desired value
o	bias point
r	reference value
s	pertains the structure
E	value measured at constant electric field
T	value measured at constant stress
t	transpose
-1	inverse
$()'$	derivative with respect to ξ
$(\dot{})$	derivative with respect to time
$(\hat{})$	estimated value
*	includes an electric field term

Subscripts

i, j, k, l, m, n, o, p, q, r, s, t, u, v, w, x, y	indices

Chapter 1

INTRODUCTION

Electrostrictors all are ceramic;
with voltage aid, tiny or gigantic.
Despite high voltage and incredible strain
during large deflections, they feel no pain.
Yet when temperature is thus applied,
sensitive electrostrictors subside.
Cold electrostrictors need not alarm-
they're only shivering to keep warm.
-M. Valere Masingill

1.1 Motivation

The performance required of future precision structures has motivated a new approach to structural design, where feedback control principles and advanced sensors and actuators are applied to the design of high performance structural systems. The optimization through modeling of these controlled structures will allow higher precision, lighter weight, and more robust structures.

Inherent to the design of controlled structures is the implementation of adaptive and sensory materials. These materials are referred to as active materials. New controlled structures demand increased levels of actuation and sensing capabilities from materials that have not changed significantly since the 1970s. As a result, improved performance is provided through a

better understanding of the material behavior and a more efficient use of the materials in the applications.

The basis of efficient material utilization lies in the advent of better modeling of the controlled structure. Such a model would need to include the coupled dynamics of the electrical and mechanical interactions of the system. Before an accurate electromechanical model can be created, however, a thorough understanding of the electrical and mechanical behavior of the materials is required. The material behavior is most often characterized in terms of constitutive relationships that detail the coupled interaction of the electrical and mechanical parts of the material. The limitations of the constitutive relationships needs to be understood as well as the dependence of the constitutive parameters on their operating environment, such as temperature and stress.

An increasing number of the applications involving active materials use the materials to actuate, control, and sense flexible structures. The large power density of the solid-state actuators makes them well suited to becoming an integral component of an adaptive structure. As a result, the interaction between the structure and the actuator or sensor becomes increasingly important. The constitutive relationships of the active materials are coupled with the mechanical behavior of the host structure and the electrical behavior of the electronics. The actuators and sensors can be configured as point sources or they can be distributed over the structure. Again, the need for accurate modeling is paramount.

By the nature of the material, the study of active materials is an interdisciplinary study. The dynamics of the material are governed by materials science. The dynamics of the active structure are described through structural dynamics. The dynamics of the controlled system are found with control theory. This thesis attempts to incorporate each of these disparate descriptions of electrostrictors with the goal being the unified understanding of actuation with electrostrictors.

1.2 Material Overview

There are many active materials that are currently commercially available for actuation and sensing: electrostrictors, piezoelectrics, magnetostrictors, shape memory alloys, shape memory ceramics, and polymer hydrogels. This study focuses upon electrostrictive ceramics, but the general models will be sufficiently general so that they can be applied to a broad class of the nonlinear active materials.

The objective of this study is to actuate a structure; hence, the most important property of the active material is that it must be able to input a large force over a wide range of frequencies. The available force for actuation is a product of the material stiffness and maximum strain. This product is known as the actuation potential since it is a rough measure of the amount of energy that can be imparted into a structure. Another feature of strong importance is the materials' bandwidth. The operating frequency of the material must be larger than the structural modes otherwise only limited actuation is feasible.

Of lesser importance is the amount of hysteresis and the brittleness of the material. The hysteresis in a cycle is a measure of the amount of energy lost and serves as an upper bound on the material efficiency. Excessive hysteresis leads to significant heating during high frequency excitation. Additionally, the hysteresis is a phase lag which can be problematic during control implementation. The brittleness given by a K_{Ic} value is a rough indication of the brittleness of the material. A small K_{Ic} is indicative of a brittle material.

There are several types of active materials which posses a large actuation potential and a high bandwidth. As indicated in figure 1.1, piezoceramics, magnetostrictors, and electrostrictors can deliver large forces at high frequencies. The other commercially available active materials are lacking one or the other of the two actuation parameters. Piezopolymers and polymer hydrogels lack the sufficient stiffness needed to actuate a structure. By their very nature of being shape memory, shape memory alloys and

ceramics can only successfully operate at low frequencies. The switching mechanism and tremendous hysteresis prohibits their cycling faster than a few hertz.

During the remainder of this subsection, a brief description of each material is presented. Figure 1.1 gives a quick reference for the material behavior, but each of the materials has more subtle advantages and disadvantages. Special focus is given to the material's actuation ability and to their electromechanical behavior.

Piezoceramics are the most widely used active materials for actuation. They have a high bandwidth and a large actuation potential. Piezoceramics have high temperature stability and a good linearity at low electric field levels (Cady, 1984) (Jaffe, Cook, and Jaffe, 1971). Although these materials are linear at low fields, the nonlinearity at moderate to high electric field levels is difficult to express in the form of a constitutive relationship (Chan and Hagood, 1994).

Magnetostrictive materials are nonlinear materials which are driven by magnetic field. Magnetostrictors are good materials for actuation because they posses a high frequency response, a large actuation potential, low hysteresis, and strong temperature stability (Butler, 1988). Although nonlinear, the constitutive relationships for magnetostrictive behavior can be simplified to a set of nonlinear algebraic equations (Carman, 1994) (Kannan and Dasgupta, 1994). This "friendly" nonlinearity can be easily expressed in the models developed in chapter 5. As a result, the general equations of motion for a distributed magnetostrictive system also will be developed. Actuation by magnetic field is a double edged sword. Significant extra hardware is required in order to produce a magnetic field, but the field geometry allows for large displacement rods of magnetostrictor. Thus, although providing 0.2% strain, magnetostrictive rods can give several hundred microns of displacement (Anjanappa and Bi, 1994).

Electrostrictors are nonlinear electroceramic materials which are typically composed of PMN ($Pb[Mg_{1/3}Nb_{2/3}]O_3$). These materials feature a large

actuation potential, high frequency response, and a negligible hysteresis (Uchino, 1986). Electrostrictors have a significant variation of the electromechanical coupling with respect to temperature (Blackwood and Ealey, 1993). Due to the material nonlinearity and the temperature sensitivity, electrostrictors have principally been used in specialty quasi-static applications. Models that describe the dynamic or distributed implementation of electrostrictors are just being developed (Fripp and Hagood, 1994). As a result, this thesis focuses upon electrostrictive materials. The properties of electrostrictors are discussed in more detail in chapters 2 and 3.

Shape memory materials come in two forms: alloys composed of nickel-based Nitinol and ceramics composed of lead-based PLZST. Both the shape memory alloys and the shape memory ceramics deliver large deflections and posses high material stiffness (Schetky, 1979) (Rogers, Liang, and Barker, 1989). However, by the nature of being shape memory materials, these materials perform at limited frequencies and require dissipative rate laws for their material description. The phase change in the alloys are triggered by temperature changes while the phase change in the ceramics can

	PZT-5H	Terfenol	PMN	PVDF	PAN	Nitinol	PLZST
Actuation Mechanism	piezo-ceramic	magneto-strictor	electro-strictor	piezo-polymer	Polymer Hydrogel	shape memory alloy	shape memory ceramic
Max Strain	0.13%	0.2%	0.1%	0.07%	50%	8%	0.9%
Stiffness	10 Msi	7 Msi	17 Msi	0.3 Msi	0.2 Msi	4-13 Msi	12 Msi
Density kg/m^3	7500	9250	7800	1780		7100	7500
Hysteresis	0%	2%	<1%	>10%	High	High	High
Bandwidth	100 kHz	10 kHz	100 kHz	100 kHz	<1 Hz	<5 Hz	<100 Hz
Brittleness, K_{1c}, MPa$\sqrt{m}$	1.4		0.9	polymer	polymer	metal	$\approx$ 1.5

Figure 1.1: Comparison of the commercially available active materials. For actuation the most important figures are the product of strain and stiffness and the bandwidth of the actuation.

be triggered by either a temperature change or an imposed electric field (Ghandi and Hagood, 1994).

Polymer hydrogels are a new actuator and are driven by pH variations. This actuator delivers large strains but is very slow and cannot deliver significant forces due to the material's low stiffness (Brock et al, 1994). Similarly, piezopolymers can deliver significant strains over a wide range of frequencies but lack sufficient stiffness to effectively actuate a structure. In fact, the low stiffness of piezopolymers lead to their principle application as a solid-state sensor (Broadhurst, Micheron, and Wada, 1981) (Kynar, 1987).

1.3 Previous Actuation Models

The previous models for structural actuation with adaptive materials are limited. An overwhelming majority of the models have focused upon the linear implementation of piezoceramic actuators. Few have looked at electrostrictive elements and no one else has considered electrostrictors distributed in a structure.

Piezoceramics have dominated structural actuation because they are easy to model at low actuation levels and because they have been commercially available for decades. At low electric field levels, piezoceramics are essentially linear elements; the mechanical displacement is proportional to the electrical displacement and vice versa. Thus, piezoceramics, like other adaptive materials, can be used as sensors or as actuators. For actuation, piezoceramics have been used in beams (Bailey and Hubbard, 1985) (Lee and Moon, 1989) (Hagood et al, 1990), plates (Crawley and Lazarus, 1989) (Lee, 1990) (Yu, 1993), trusses (Hagood and Crawley, 1988) (Geng and Haynes, 1992), shells (Tzou and Howard, 1992), box beams (Smith and Chopra, 1990) (Chandra and Chopra, 1991) and motors (Hagood and McFarland, 1994) (Zhang and Zhu, 1994)

The coupled structural and electrical interaction of "linear" piezoceramic elements has been investigated. The implementation of distributed linear electroceramic elements in a coupled electromechanical

system has been successfully modeled (Hagood et al, 1990). In this model, the linear constitutive properties of piezoceramics were introduced into Hamilton's principle. The resulting governing equations for the electroelastic system were approximated with a Rayleigh-Ritz assumed modes technique. The model was validated through experiments with piezoceramics on a cantilevered beam.

However, Hagood et al. did not include any of the nonlinear properties of piezoceramics. Later efforts in modeling actuation with piezoceramics also neglected the material nonlinearities (Tzou and Howard, 1992). Piezoceramics strains become nonlinear and strongly hysteretic at large electric fields. Additionally, the nonlinearity of piezoceramics is a strain based nonlinearity instead of an electric field based nonlinearity (Anderson, 1989). The nonlinear behavior of piezoelectrics have been extensively studied (Chan and Hagood, 1994). However, the resulting models are often sufficiently cumbersome so that engineering implementation is difficult. Attempts to model the nonlinear behavior of piezoelectric actuation invariably neglect the fundamental nonlinearities (Yu, 1993).

Electrostrictive actuators consisting of relaxor ferroelectric materials have also existed for decades. The modeling effort with electrostrictors has focused upon the material's constitutive relationships. Numerous authors have produced constitutive relationships in which the electromechanical relationships and the temperature dependence have been investigated. Polynomial parameterization in terms of electric field is most common (Blackwood and Ealey, 1993) but a few authors have utilized a transcendental function of the electrical polarization (Namboodri, 1992) (Hom and Shankar, 1994).

Although many of the material properties have been characterized, little attention has been paid to the coupled structural interaction. Experiments have been conducting utilizing electrostrictors, but the modeling effort is skimpy. Most often, the electrostrictor is given a large enough electric bias that the nonlinear behavior is effectively linearized (Regelbrugge et al,

1994). Although such approaches tend to work, they are inherently brutish and inefficient.

In summary, those implementing electrostrictors are working by intuition and by trial and error, essentially operating blindly. The constitutive parameters are documented but the models on utilization are nonexistent. The knowledge that has accrued on the linear modeling of piezoceramics in flexible structures has yet to be applied to the problems of modeling electrostrictors.

1.4 Objective

Applications involving electrostrictors primarily use the material in stacks and rely upon the longitudinal properties of the material as opposed to the smaller transverse properties. A large actuation potential, high set-point accuracy, and low hysteresis make electrostrictors a choice material for quasi-static micro-positioning devices. Despite these advantages, few applications have implemented electrostrictors as structural actuators due to the nonlinearity and temperature sensitivity of electrostrictors. Piezoceramics continue to dominate structural control applications.

This document attempts to create an analysis framework through which approximate governing equations of a nonlinear electroceramic system with distributed electrostrictive coupling can be expressed and thereby lower the barriers to application of this material. This general analysis is specifically applied to distributed electrostrictors in structural actuation. First, variational principles are reviewed. Then the variational concepts are used to derive the nonlinear governing equations for electrostrictors. These equations not only model the mechanical interaction between the electrostrictor and the structure but also model their electrical behavior. Using assumed elastic modes and electric field shapes allows the derivation of general equations of motion for an arbitrary structural system with distributed electrostrictive inclusions. Dynamic and static experiments upon a cantilevered beam corroborate the model. Finally, the governing equations are utilized in a

second-order controller with output linearization and adaptive control algorithm for vibration control.

1.5 Overview

This document seeks to provide a comprehensive treatise on the utilization of electrostrictive elements. The previous works on relaxor ferroelectrics are reviewed and then extended into the realm of application through a general model of an electrostrictively coupled electromechanical system. The methodology used to model the dynamics of electrostrictive materials is sufficiently broad so that it can be applied to any system which is composed of elements which can be described by a set of nonlinear algebraic constitutive relationships.

In chapter 2 the micromechanical world of electrostrictors is broached. The crystalline properties and configuration of the relaxor ferroelectric are reviewed. Some of the present and future applications of electrostrictors are given.

In chapter 3 the constitutive relationships for electrostrictors are derived in terms of electric field and of electrical polarization. The electromechanical coupling is modeled as hyperbolic tangent squared and as a quadratic relationship. The limitations of the different formulations are given. Methods to model the temperature behavior are also presented.

In chapter 4 the constitutive properties of electrostrictors are investigated experimentally. The material behavior is compared with the material models that were developed in chapter 3. The electrostriction, elastostriction and temperature dependence is presented. During this section, data on one-dimensional constrained actuation is also presented. The electric field correction to the material stiffness is presented as well as evidence that the nonlinearity of electrostrictors is fundamentally a electric field-based nonlinearity.

In chapter 5 models of an electrostrictively coupled electromechanical system are derived. Hamilton's principle is applied to a nonlinear electromechanically coupled system. The general form of Hamilton's principle is simplified for the case when a thermodynamic formalism was used to describe the constitutive relationships. The most general form of Hamilton's principle is used to derive the governing equations for the electromechanical system. The governing equations are applicable for finite elements analysis or an assumed modes method. Simplifications of the governing equations are presented for the case when there is only one actuator on the structure.

In chapter 6 experimental verification of the governing equations derived in chapter 5 is presented. Results from the model and the experiment are compared in the case of quasi-static actuation, dynamic charge control, and over a wide range of actuation frequencies. The effect of the material's quadratic nonlinearity is also presented.

In chapter 7 the results of using the electrostrictive actuator for vibration control are presented. A second-order control loop and an adaptive control algorithm are utilized. These closed loop tests are performed at different temperatures in an effort to explore the effect of temperature on the control algorithm.

In chapter 8 the effectiveness of the modeling effort is summarized as well as providing a synopsis of the experimental and control effort in this study. The contributions provided by this thesis are also listed. For the casual reader, the author suggests that section 8.2 be perused first. This should allow the readers to focus their time most efficiently.

Chapter 2

MATERIAL OVERVIEW

Electrostrictors, electrostrictors
straining with high energy.
Electrostrictors - in a few short years
what will you mean to me?

Activated at Curie temperature:
do you enjoy electrical abuse?
Bonded to larger structures,
just what will be your use?
-Greg Will

Modern electrostrictors provide strains as large as 0.1%, poses high mechanical stiffness, exhibit little hysteresis, are isotropic at zero electric field, and do not require poling. This chapter seeks to explain the micromechanical properties that lead to these material behaviors. The description starts with the crystalline properties of the material. The micro-mechanical properties are then described in context with existing applications of electrostrictive materials.

2.1 Crystalline Description

The piezoelectric effect was discovered in 1880 when Pierre and Jacques Curie discovered that crystals develop electrical polarization under the influence of an external mechanical force (P.G. DeGennes, 1982.). However, it

took until the 1950s before electrostrictors were popularized by G.A. Smolenskii (G.A. Smolenskii, et. al, 1961.). Modern electrostrictors were discovered during the development of integrated electronics in the 1950s and the push for higher dielectric materials. As the dielectric permittivity of the materials increased, it was recognized that the ferroelectric properties also increased. The rise of PMN ($Pb[Mg_{1/3}Nb_{2/3}]O_3$) as the electrostrictor of choice occurred during the late 1970s and 1980s.

All crystals, whether piezoelectric or not, exhibit an electrostrictive effect and produce strains proportional to the square of the electrical polarization. Electrostrictors which are used for actuation have a perovskite crystal structure and are ferroelectric in nature. These electrostrictors can be placed into a subgroup of ferroelectrics known as relaxor ferroelectrics (A.F. Devonshire, 1954). The placement of relaxor ferroelectrics in terms of the material symmetries can be seen in figure 2.1. Most of the noncentrosymmetric cystral structures are piezoelectric in nature. However, not all of the asymmetric piezoelectric crystal structures result in strain when

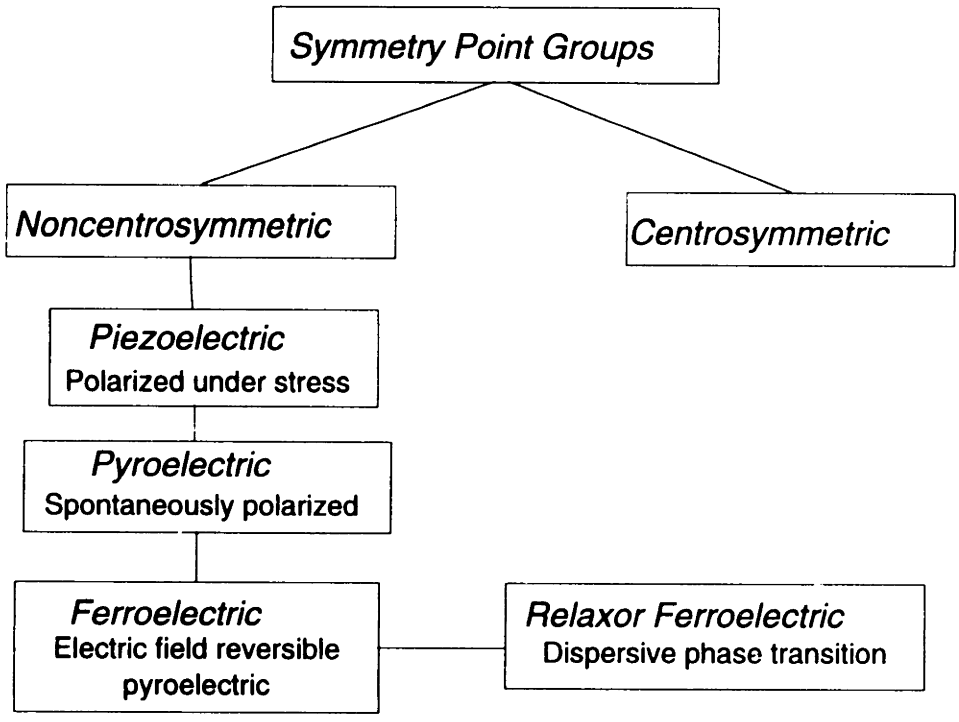

Figure 2.1: Classes of crystalline material. This thesis focuses upon the relaxor ferroelectric.

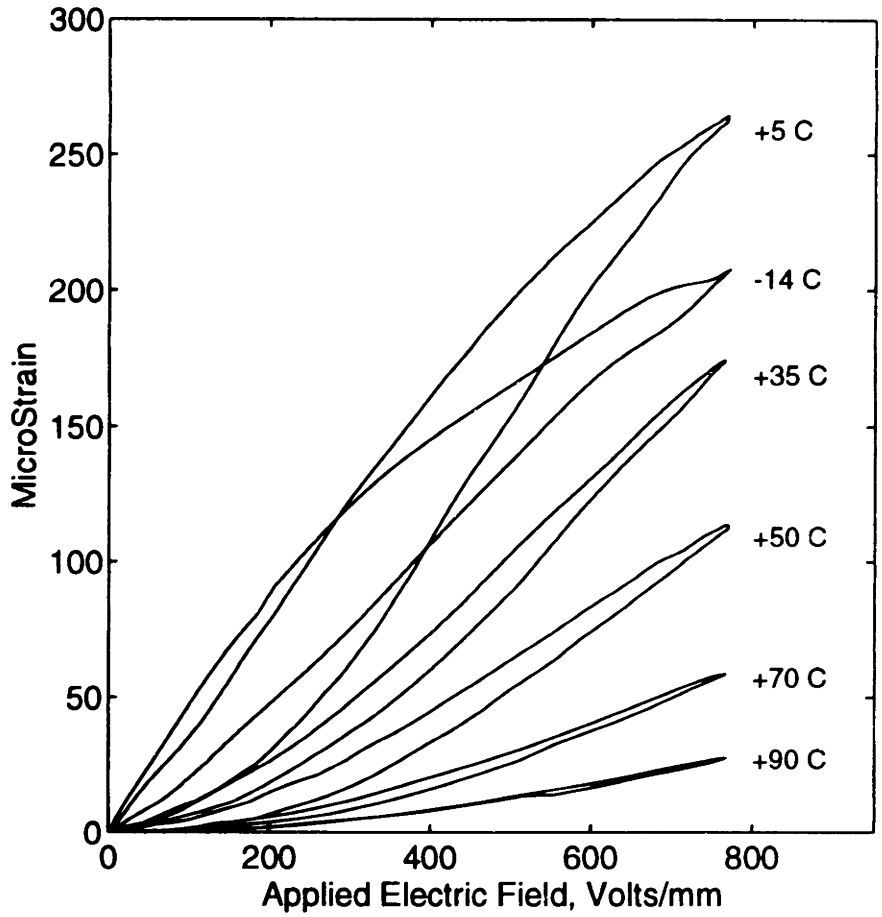

Figure 2.2: As temperature increases, the hysteresetic ferroelectric behavior degenerates into an algebraic nonlinearity. The transverse expansion of 0.9PMN-0.1PT is shown here.

polarized. A subgroup of piezoelectrics known as ferroelectric have the necessary structure that allow for useful strain when polarized. The piezoceramics used in engineering applications belong to the subgroup known as ferroelectrics (Haertling, 1986).

Relaxor ferroelectrics are a subgroup of ferroelectrics. In fact, relaxor ferroelectrics are ferroelectric at low temperature. The spontaneous polarization of relaxor ferroelectrics slowly diminishes over a range of temperatures during the phase transition known as the Curie range. The effect of this transition is that the hysteretic response slowly degenerates into an algebraic nonlinearity, as shown in figure 2.2. This diffuse phase

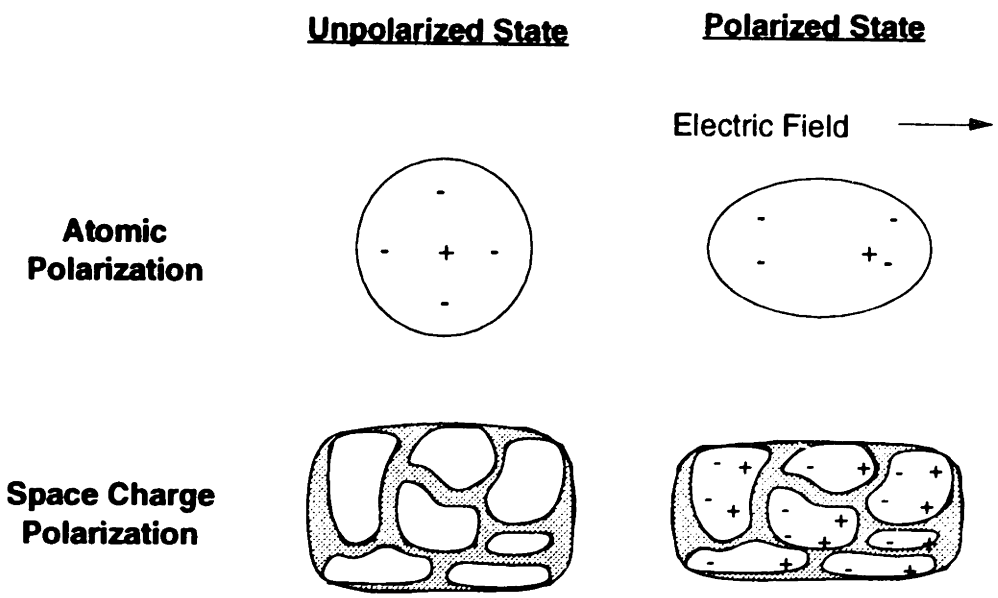

Figure 2.3: Different styles of polarization. Every material exhibits atomic polarization but relaxor ferroelectrics also exhibit space charge polarization. It is the space charge polarization that leads to the large strains in relaxor ferroelectric electrostrictors.

transition differentiates relaxor ferroelectrics from standard ferroelectrics (Cross, 1987).

It is often misconstrued that relaxor ferroelectrics are differentiated from standard ferroelectrics by their large dielectric permittivity. The peak relative dielectric permittivity of the typical relaxor ferroelectric is around 20,000, which is very large. However, most ferroelectric materials have a relative dielectric permittivity around 20,000 when heated to their Curie temperature. The true difference between the materials is that relaxor ferroelectrics do not experience a sharp phase change at the Curie point like typical ferroelectrics. Instead, relaxor ferroelectrics have a diffuse phase transition.

Although other materials also have large dielectrics, the electrostrictive effect is intimately associated with the relaxor ferroelectric's large dielectric permittivity. The electrostrictive effect that is present in all materials arises from a stretching of the atomic structure or an atomic polarization, as shown

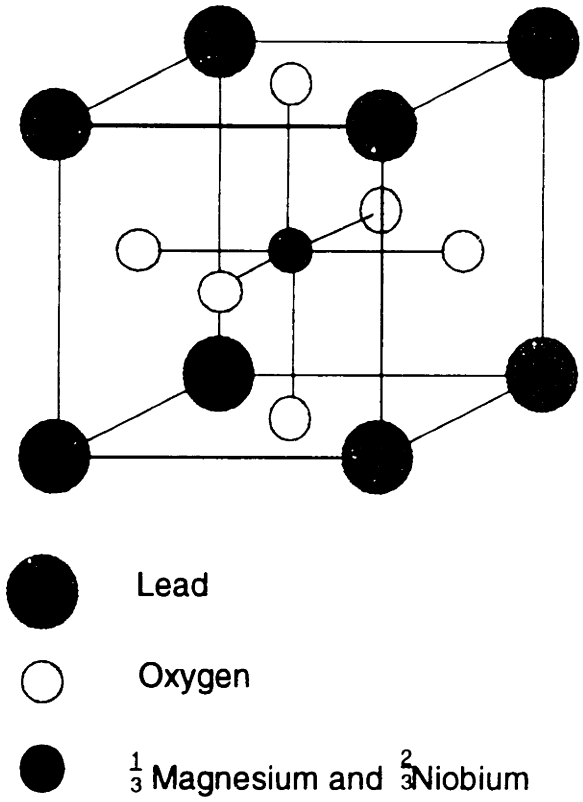

Figure 2.4: Unit cell of the perovskite crystal structure of PMN, $Pb[Mg_{1/3}Nb_{2/3}]O_3$. The actual crystal structure will be complicated by the addition of other dopants, such as $PbTiO_3$.

in figure 2.3 (Solymar and Walsh, 1988). Atomic polarization is based upon the deformation of the electron cloud by the applied electric field. As a result, this polarization can respond at high frequencies but delivers negligible strains. Relaxor ferroelectrics also exhibit a space charge polarization. This type of polarization features a limited transport of the ions. The magnitude of the deformation is related to the dielectric permittivity of the material (Moulson and Herbert, 1990).

Each of the preceeding "mesoscopic" behaviors is intimately related to the crystalline structure of relaxor ferroelectrics. In the unstressed state within the Curie temperature range, relaxor ferroelectrics exhibit a cubic perovskite crystal structure. Perovskites have the general formula of ABO_3

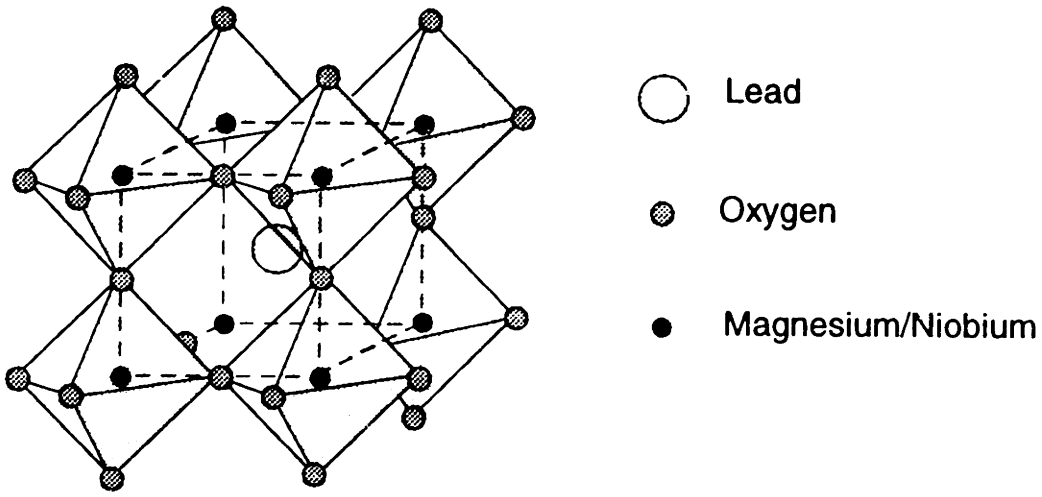

Figure 2.5: The perovskite structure is built of corner-shared octahedral cages.

where A and B are metals, the positive ions should have a *total* charge of +6; A and B must be of different sizes; and the smaller, higher charged ion must be a transition metal (Braithwaite and Weaver, 1990). In the case of PMN, the large lead ions (ionic radius of 0.132 nm, charge +2) fill the A position and are balanced with the small magnesium and niobium ions (radius of 0.078 nm, charge +2 and 0.070 nm, charge +5, respectively) which fill the B position in the Perovskite ABO_3 formulation. The total charge of the lead, magnesium, and niobium atoms balances the charges from the oxygen.

The simple perovskite structure of PMN is illustrated in figure 2.4. In this crystalline structure, the corners of the cubic structure are lead atoms, the face center positions are filled with oxygen and the body center is occupied by either a magnesium or a niobium atom. The ratio of lattice sites filled by magnesium or niobium is dictated by the stoichimetric ratio. The addition of lead titinate, $PbTiO_3$, replaces the magnesium and niobium ions with small titanium ions (ionic radius of 0.068 nm).

The magnesium, niobium, and titanium atoms are randomly distributed throughout the Perovskite crystal structure. This random distribution leads to two of the observered mesoscopic behaviors: the existance of a Curie *range* and the large strains. The Curie range arises

because the random distribution of magnesium, niobium, and titanium leads to random distributions of cation-ordered microvolumes throughout the crystal. These microvolumes exhibit widely different Curie temperatures. As a result, the Curie transition is smeared across a Curie range. The size of the microvolumes changes the behavior of the material. Thus, for example, changing the sintering temperature from 1100°C to 1200°C alters the size of the microvolumes and lowers the dielectric permittivity by 50% at the center of the Curie range (Nomura and Uchino, 1982).

The random distribution of cations also leads to a larger electrostrictive coupling. The disordered arrangement of cations gives a larger "rattling" space than an ordered arrangement. The larger magnesiusm atoms prop open the lattic framework and allow the smaller niobium and titanium atoms to rattle around. When an electric field is applied to a disordered perovskite, the niobium can shift easily within the rattling space. As a result, larger polarizations are expected. As a result, relaxor ferroelectrics with a disordered structure outperform normal perovskites (Nomura and Uchino, 1982). The octahedral cages which allow the ordered rattling are formed by shifting the unit cell in figure 2.4 by a half width. The resulting structure is shown in figure 2.5. Figure 2.5 does not show, however, the random distribution of magnesium, niobium, and titanium which amplifies the rattling and the resulting strains.

Above the Curie range, the bonds lengthen and the oxygen cages form a sloppy fit around the magnesium, niobium, and titanium atoms. Since there are no internal perturbations, the structure is symmetrical and cubic. As the material is cooled, the bonds shrink. In the Curie range, the fit within the lead cage is nearly bistable. This leads to the very large dielectric and large strains of the material in the Curie range. Below the Curie range, the bonds shrink further and the material is forced to assume a net polarization and behave as a ferroelectric material (Braithwaite and Weaver, 1990). As a result, electrostrictors are typically used near their Curie range. At these temperatures the material exhibits maximum strain. The result of operating near the Curie temperature is that the electromechanical coupling and the hysteresis are strongly temperature dependent.

There are several material behaviors resulting from perovskites being a symmetric cubic structure around the Curie range. Due to the internal symmetry, there is no macroscopic polarization of a relaxor ferroelectric when there is no applied electric field. The absence of spontaneous polarization at the crystalline scale translates on the macroscopic scale to very little hysteresis and an excellent zero electric field set point strain response for temperatures above or near the Curie range.

2.2 Applications

This section details many of the applications of electrostrictive materials. Relaxor ferroelectrics are most often utilized as quasi-static micro-positioning devices although there are some applications involving dynamic uses of electrostrictors.

The optical community was one of the first disciplines to embrace electrostrictors. The small hysteresis, long term stability, and high actuation potential allowed the development of solid-state adaptive optics (Uchino et al, 1981). Ground-based adaptive optics seek to utilize the electrostrictor's quick response to deform a mirror to cancel the refractive turbulence of the atmosphere. Space-based adaptive optics seek adaptive material which would be used to achieve a desired mirror contour and correct for gravity-induced curvature. Also precision alignment is an important space-based requirement. Electrostrictors are attractive for use in space due to the small power requirements inherent to a material with negligible hysteresis and for their good set point history when there is no power. Most of the adaptive optics configurations have utilized the material in stacks. The stacks deform the mirror by pushing against a rigid mount (Ealey and Davis, 1990). In a simple quasi-static scenario, the transverse properties of the electrostrictor have also been used to alter the shape of a mirror (Nomura and Uchino, 1983).

The optics community, as well as others, have used electrostrictive stacks as micropositioning devices. In the optics realm, electrostrictors have

been used to adjust the placement of mirrors in a bistable optical device in order to stabilize the intensity of a laser (Gomi et al, 1982). In the recent repair of the Hubble Space Telescope, electrostrictive stacks were used to adjust the placement of the replaced articulating fold mirror. Electrostrictive stacks have also been used in semiconductor mask alignment for VLSI and in X-ray lithography position control (Levinson, 1988).

The quick response of electrostrictors allows their utilization as on/off servo controllers. Some of the impact dot matrix printers have an electrostrictive stack to impact the printer ribbon. Another prototype printer has an electrostrictive bimorph to impact the printer ribbon (Uchino, 1986). In either configuration, mechanical magnification is required. The smart material printers are reported to offer faster performance with lower energy consumption and reduced noise than the standard mechanical design .

Dynamic utilization of electrostrictors as actuators has been limited. Martin Marietta is currently developing a line of active vibration isolators that utilize stacks of electrostrictors to provide high frequency and small displacement control. The electrostrictive stacks are used in conjunction with a shape memory alloy bimorph. The shape memory component provides low frequency, gross position control while the electrostrictor provides high frequency fine tuning (Hom and Shankar, 1994b).

Electrostrictors have also been utilized as sensors. A medical ultrasonic probe has been built with electrostrictors used as sensors. The development of advanced acoustic imaging systems has led to the necessity of different electromechanical gains at different positions within the probe. The new ultrasonic probe provides variable gains by capitalizing on the nonlinear electromechanical coupling offered by electrostrictors. The linear and phased array acoustic imaging system was constructed with PMN-PT in a 1-3 composite with polyurethane. The gain of the sensor was adjusted by altering the electric field bias across the electrostrictive elements (Takeuchi et al, 1989).

The transverse sensing properties of electrostrictors have also been utilized (Namboodri and Rogers, 1992). In this case, an electrostrictive wafer

was surface bonded to a cantilevered beam. The charge on the wafer was measured. By adjusting the DC electric field, different strain sensitivities were obtained. The ultimate goal of this style of variable gain sensor would be to produce a modal sensor.

In summary, the state of the art for electrostrictors consists primarily of electrostrictors in stacked configuration being used as micropositioning devices. In addition to further developments of the applications already mentioned, electrostrictors will also be utilized in solid state motors and in micromachining tool control. Future implementation of electrostrictors is hampered by two factors: the temperature dependence of the electromechanical coupling and a lack of modeling methodologies for distributed actuation and sensing configurations.

Chapter 3

CONSTITUTIVE EQUATIONS

I am an actuator. I am a sensor.
I live for voltages applied on my ends.
With the help of electricity,
I can change shape and even bend.
But temperature is my Achilles Heel,
The problem is the variation.
For in the fall I may work right,
Yet in the summer I take a vacation
-Mandy Malone

This chapter derives the form of the coupled equations describing the behavior of electrostrictive relaxor ferroelectrics. These constitutive relationships are simplified by noting material symmetry and employing experimental observations.

The electrostriction effect is defined as being the second-order relationship between strain and electrical polarization (Devonshire, 1954). Formulation of the constitutive relationships in terms of polarization is popular within the materials science community. Applications oriented engineers tend to prefer constitutive relationships in terms of electric field since the electric field tends to be prescribed instead of the polarization. The constitutive relationship may include hyperbolic tangents or algebraic powers of the fields. Each of these forms are merely variations of the thermodynamic potential.

This chapter starts by investigating the thermodynamic formalism. This formalism is applied to the symmetries inherent to electrostrictors. The constitutive relationships are parameterized in terms of electric field and in terms of electric polarization. The higher-order algebraic terms are simplified to quadratic functions and to hyperbolic tangent functions.

3.1 Thermodynamics

It is possible to describe an electro-mechanical system by three independent variables chosen from the pairs (stress, T, and strain, S), (electric field, E, and displacement, D), and (temperature, Θ, and entropy, s). The other three variables become the dependent variables of the system. The thermodynamics of the system give the relationship between the variables. In other words, the first and second laws of thermodynamics maintain the symmetry between each of the coupled equations. This section closely follows the corresponding section in Lines and Glass (Lines and Glass, 1977).

The first law of thermodynamics describes the conservation of energy in a unit volume. The change in internal energy, dU, is given by

$$dU = dQ + dW \tag{3.1}$$

where dQ is an infinitesimal quantity of heat and dW is the total work done on the unit volume. Assuming reversibility, the second law of thermodynamics relates the increment of heat to the absolute temperature, Θ, and the system's entropy, s, by

$$dQ = \Theta ds. \tag{3.2}$$

The work done on the system is the sum of the mechanical and electrical contributions

$$dW = \int_V \left(T_{ij} dS_{ij} + E_m dD_m \right) dV. \tag{3.3}$$

Substituting equations (3.2) and (3.3) into equation (3.1) the first law becomes†

$$dU = T_{ij}dS_{ij} + E_m dD_m + \Theta ds. \tag{3.4}$$

Clearly, if S, D, and s are chosen as the independent variables, then the dependent variables are

$$T_{ij} = \left(\frac{\partial U}{\partial S_{ij}}\right)^{D,s}, \quad E_m = \left(\frac{\partial U}{\partial D_i}\right)^{S,s}, \quad \text{and} \quad \Theta = \left(\frac{\partial U}{\partial s}\right)^{S,D} \tag{3.5}$$

where the superscripts indicates that the designated variables are held constant. Each of these equations are constitutive relationships for the system.

Often the form given in the previous equations does not lend itself to a particular application. In such cases additional thermodynamic potentials can be added without changing the inherent thermodynamics of the system. Since the three independent variables can be chosen in eight different ways, there are eight possible thermodynamic potentials. They are, in addition to U,

Helmholtz free energy	$A = U - \Theta s$
enthalpy	$H = U - T_{ij}S_{ij} - E_m D_m$
elastic enthalpy	$H_1 = U - T_{ij}S_{ij}$
electric enthalpy	$H_2 = U - E_m D_m$
Gibbs free energy	$G = U - T_{ij}S_{ij} - E_m D_m - \Theta s$
elastic Gibbs energy	$G_1 = U - T_{ij}S_{ij} - \Theta s$
electric Gibbs energy	$G_2 = U - E_m D_m - \Theta s$ (3.6)

† There is a discrepancy between the definition of internal energy between the form given in Devonshire (Devonshire, 1954) and the form given by Lines and Glass (Lines and Glass, 1977). Devonshire defines the differential of the internal energy as

$$dU = -T_{ij}dS_{ij} + E_m dP_m + \Theta ds.$$

which is clearly different from the form given by Lines and Glass in equation (3.4). The change in the sign leads to fundamental changes in the formulation of the thermodynamic relationships. I do not understand how Devonshire can say that work supplied by a force over a distance, TdS, *decreases* the energy in the system. Although I am loath to say this, it appears that Devonshire is wrong.

Each of the thermodynamic forms in equation (3.6) are equally valid forms from which to generate the material constitutive relationships. The differential forms describing infinitesimal changes in these thermodynamic potentials are, using equation (3.4),

Helmholtz free energy	$dA = -sd\Theta + T_{ij}dS_{ij} + E_m dD_m$
enthalpy	$dH = \Theta ds - S_{ij}dT_{ij} - D_m dE_m$
elastic enthalpy	$dH_1 = \Theta ds - S_{ij}dT_{ij} + E_m dD_m$
electric enthalpy	$dH_2 = \Theta ds + T_{ij}dS_{ij} - D_m dE_m$
Gibbs free energy	$dG = -sd\Theta - S_{ij}dT_{ij} - D_m dE_m$
elastic Gibbs energy	$dG_1 = -sd\Theta - S_{ij}dT_{ij} + E_m dD_m$
electric Gibbs energy	$dG_2 = -sd\Theta + T_{ij}dS_{ij} - D_m dE_m$ (3.7)

The astute reader might have noticed the preference for electrical displacement instead of the electrical polarization. Much of the ferroelectric and relaxor ferroelectric literature uses the polarization, P, explicitly rather than the electric displacement. Since $D=\varepsilon_o E+P$, the thermodynamic formalism can be easily applied to the conjugate pair (P, E) rather than (D, E) (Devonshire, 1954). This is not done here for engineering reasons. Firstly, imposing the experimental constraint of constant polarization is exceedingly difficult. Thus, defining material constants in terms of constant polarization makes little sense. Secondly, although a set of thermodynamic relationships analogous to equations (3.6) exists in terms of P and E, they do not possess the external properties normally associated with free energies in connection with questions of stability although the contrary is often assumed. The reason is that the variable D enters the work function and, as a result, enters the laws of thermodynamics in a simpler and more natural manner than P (Lines and Glass, 1977). Nevertheless, for high dielectric materials such as electrostrictors, the difference between electrical displacement and electrical polarization is largely academic.

3.2 Electric Field Expansion

3.2.1 Tensor algebraic form

The first question that must be addressed when forming the constitutive equations is what are the preferred independent variables. As indicated by the eight thermodynamic potentials shown in the previous subsection, there are numerous choices. For material characterization, it is easiest if the independent parameters are temperature, strain, and electrical displacement. Strain is more easiiy measured than stress and electric field is more easily specified than electrical displacement. From the thermodynamic expressions given in equation (3.7), it is clear that either the enthalpy function or the Gibbs free energy function should be used. This section will use Gibbs free energy where

$$dG = -sd\Theta - S_{ij}dT_{ij} - D_m dE_m \tag{3.8}$$

The direct electrical and mechanical effects are clearly expressed in equation (3.8) but the form of the electromechanical coupling is yet unknown. The electrostrictive term for the direct electrostriction effects is defined by (Blackwood and Ealey, 1993)

$$m_{ijmn} = \frac{1}{2}\frac{\partial^2 S_{ij}}{\partial E_m \partial E_n} \tag{3.9}$$

and converse electrostriction effects is given by

$$m_{mnij} = \frac{1}{2}\frac{\partial^2 D_m}{\partial T_{ij} \partial E_n}. \tag{3.10}$$

The other electromechanical coupling terms are defined by analogy.

At this point in the derivation, expansions are given for each of the terms in the Gibbs energy formulation. Assume a polynomial expansion for all of the internal energies. Neglecting temperature effects, the full Gibbs free energy function becomes

$$
\begin{aligned}
dG = &-\tfrac{1}{2}\varepsilon_{mn}E_mE_n - \tfrac{1}{3}\varepsilon_{mno}E_mE_nE_o - \tfrac{1}{4}\varepsilon_{mnop}E_mE_nE_oE_p - \cdots \text{h.o.t.} \\
&- \tfrac{1}{2}s_{ijkl}T_{ij}T_{kl} - \tfrac{1}{3}s_{ijklmn}T_{ij}T_{kl}T_{mn} - \cdots \text{h.o.t.} \\
&- u_{mijkl}E_mT_{ij}T_{kl} - r_{mnijkl}E_mE_nT_{ij}T_{kl} - n_{mnoijkl}E_mE_nE_oT_{ij}T_{kl} - \cdots \text{h.o.t.} \\
&- d_{mij}E_mT_{ij} - m_{mnij}E_mE_nT_{ij} - g_{mnoij}E_mE_nE_oT_{ij} - h_{mnopij}E_mE_nE_oE_pT_{ij} - \cdots \text{h.o.t.}
\end{aligned}
\tag{3.11}
$$

where constants have been added to the first two lines for later simplicity. The first line of the Gibbs energy expansion represents the electrical energy terms and the mechanical energy is represented in the second line. The last two lines of equation (3.11) couple the mechanical and electric energies.

Temperature has been removed from an explicitly representation in the thermodynamic formalism. The thermal variation will be included later in this chapter as a variation in the material constants. Either method of including the thermal effect will provide good experimental correlation. However, including the thermal effect as a variation on the material parameters is easier to measure.

Expressions for the electrical displacement and mechanical strain are obtained from the partial derivatives of equation (3.7);

$$
\left(\frac{\partial G}{\partial E_m}\right)^T = -D_m \qquad \text{and} \qquad \left(\frac{\partial G}{\partial T_{ij}}\right)^E = -S_{ij}. \tag{3.12}
$$

Evaluating the variation gives the constitutive relationships:

$$
\begin{aligned}
D_m = &\ \varepsilon_{mn}E_n + \varepsilon_{mno}E_nE_o + \varepsilon_{mnop}E_nE_oE_p + \cdots \text{h.o.t.} \\
&+ u_{mijkl}T_{ij}T_{kl} + 2r_{mnijkl}E_nT_{ij}T_{kl} + 3n_{mnoijkl}E_nE_oT_{ij}T_{kl} + \cdots \text{h.o.t.} \\
&+ d_{mij}T_{ij} + 2m_{mnij}E_nT_{ij} + 3g_{mnoij}E_nE_oT_{ij} + 4h_{mnopij}E_nE_oE_pT_{ij} + \cdots \text{h.o.t.} \\
S_{ij} = &\ s_{ijkl}T_{kl} + s_{ijklmn}T_{kl}T_{mn} + \cdots \text{h.o.t.} \\
&+ 2u_{mijkl}E_mT_{kl} + 2r_{mnijkl}E_mE_nT_{kl} + 2n_{mnoijkl}E_mE_nE_oT_{kl} + \cdots \text{h.o.t.} \\
&+ d_{mij}E_m + m_{mnij}E_mE_n + g_{mnoij}E_mE_nE_o + h_{mnopij}E_mE_nE_oE_p + \cdots \text{h.o.t.}
\end{aligned}
\tag{3.13}
$$

The form of the constitutive relationships in equation (3.13) are very general and, consequently, are not very useful for electrostrictive actuation. Knowledge of the material behavior needs to be introduced. The energy formulation for a purely electrostrictive material is simplified by the material symmetry. Due to the crystal center of symmetry in the perovskite structure, all odd-rank permittivity terms in the Gibbs energy expansion are necessarily zero. Additionally, $m_{ijmn}=m_{mnij}$. As a result, the piezoelectric terms, d and g, the elastostriction terms, u and n, and many of the electrical energy terms are zero. Neglecting these, the constitutive relationships for an electrostrictor become

$$\begin{aligned} D_m &= \varepsilon_{mn}E_n + \varepsilon_{mnop}E_nE_oE_p + 2r_{mnijkl}E_nT_{ij}T_{kl} + \cdots \text{h.o.t.} \\ &\quad + 2m_{mnij}E_nT_{ij} + 4h_{mnopij}E_nE_oE_pT_{ij} + \cdots \text{h.o.t.} \\ S_{ij} &= s_{ijkl}T_{kl} + s_{ijklmn}T_{kl}T_{mn} + 2r_{mnijkl}E_mE_nT_{kl} + \cdots \text{h.o.t.} \\ &\quad + m_{mnij}E_mE_n + h_{mnopij}E_mE_nE_oE_p + \cdots \text{h.o.t.} \end{aligned} \tag{3.14}$$

In the literature, the higher-order terms typically are dropped from the electrostrictive constitutive relationships. This yields

$$\begin{aligned} D_m &= \varepsilon_{mn}E_n + 2m_{mnij}E_nT_{ij} \\ S_{ij} &= s_{ijkl}T_{kl} + 2r_{mnijkl}E_mE_nT_{kl} + m_{mnij}E_mE_n \end{aligned} \tag{3.15}$$

The dielectric permittivity, ε^T, indicates the charge stored in the capacitive element of the electrostrictor at constant stress. The electrostriction term, m, is the electromechanical coupling term. The compliance, s^E, relates stress and strain at constant (zero) electric field. The elastostriction term, r, can be thought of as either an electric field induced correction to the compliance or a stress induced correction to the electrostrictive coefficient. The electric field varying compliance, s^*, is given by

$$s^*_{ijkl} = s^E_{ijkl} + 2r_{mnijkl}E_mE_n \tag{3.16}$$

The stiffness variation and importance of the elastostriction term is addressed in detail in chapter 4.

Neglecting the elastostriction term, the electrostrictive constitutive relations can be simplified to the quadratic model.

$$\boxed{\begin{aligned} D_m &= \varepsilon^T_{mn} E_n + 2m_{mnij} E_n T_{ij} \\ S_{ij} &= m_{pqij} E_p E_q + s^E_{ijkl} T_{kl}. \end{aligned}} \tag{3.17}$$

The quadratic model is the form most often quoted in the electrostrictive literature. The limitations of equation (3.17) are addressed in more detail during the experimental section of this thesis.

The form of the constitutive relationships given in equation (3.17) is the forms most easily measured experimentally. For example, the m constants are found by applying an electric field on an unconstrained (i.e. zero stress) material. However, letting strain and electric field be the independent variables eases the development of the equations of motion using variational principles and allows for simpler and intuitive assumed modes of displacement and voltage. Rewriting the quadratic constitutive equation (3.17),

$$\begin{aligned} D_m &= \varepsilon^T_{mn} E_n - 2m_{mnij} C^E_{ijkl} m_{klpq} E_n E_p E_q + 2m_{mnij} E_n C^E_{ijkl} S_{kl} \\ T_{ij} &= -C^E_{ijkl} m_{klpq} E_p E_q + C^E_{ijkl} S_{kl}. \end{aligned} \tag{3.18}$$

where $C^E_{ijkl} = \left(s^E_{ijkl}\right)^{-1}$. This form could also have been found by evaluating a different thermodynamic form, such as the electric enthalpy or the electric Gibbs energy.

3.2.2 Matrix algebraic form

It is possible to express the quadratic electrostrictive constitutive relationships in matrix notation,

$$\begin{Bmatrix}\mathbf{D}\\ \mathbf{S}\end{Bmatrix}=\begin{Bmatrix}D_1\\D_2\\D_3\\S_1\\S_2\\S_3\\S_4\\S_5\\S_6\end{Bmatrix}=\begin{Bmatrix}D_1\\D_2\\D_3\\S_{11}\\S_{22}\\S_{33}\\2S_{23}\\2S_{13}\\2S_{12}\end{Bmatrix}=\left[\begin{array}{c|c}\varepsilon^T & 2\mathbf{m}^*\\ \hline \mathbf{m}^{*t} & \mathbf{s}^E\end{array}\right]\begin{Bmatrix}E_1\\E_2\\E_3\\T_1\\T_2\\T_3\\T_4\\T_5\\T_6\end{Bmatrix}=\begin{Bmatrix}\mathbf{E}\\ \mathbf{T}\end{Bmatrix} \tag{3.19}$$

where $\mathbf{m}^*$ varies with the electric field. The m values in the tensor notation and in the expanded matrix are material constants. Most of the electrostrictive literature reduces the fourth order tensor notation on the electrostriction term to two indexes; $m_{mnij}=m_{mi}$. Expanding the matrices, the electrostrictive constitutive relationships in engineering notation are

$$\varepsilon^T=\begin{bmatrix}\varepsilon_1^T & 0 & 0\\ 0 & \varepsilon_2^T & 0\\ 0 & 0 & \varepsilon_3^T\end{bmatrix}, \tag{3.20}$$

$$\mathbf{m}^*=\begin{bmatrix}m_{11}E_1 & m_{12}E_1 & m_{12}E_1 & 0 & m_{44}E_3 & m_{44}E_2\\ m_{12}E_2 & m_{11}E_2 & m_{12}E_2 & m_{44}E_3 & 0 & m_{44}E_1\\ m_{12}E_3 & m_{12}E_3 & m_{11}E_3 & m_{44}E_2 & m_{44}E_1 & 0\end{bmatrix}, \text{ and} \tag{3.21}$$

$$\mathbf{s}^E=\begin{bmatrix}s_{11}^E & s_{12}^E & s_{12}^E & 0 & 0 & 0\\ s_{12}^E & s_{11}^E & s_{12}^E & 0 & 0 & 0\\ s_{12}^E & s_{12}^E & s_{11}^E & 0 & 0 & 0\\ 0 & 0 & 0 & s_{44}^E & 0 & 0\\ 0 & 0 & 0 & 0 & s_{44}^E & 0\\ 0 & 0 & 0 & 0 & 0 & s_{44}^E\end{bmatrix}. \tag{3.22}$$

Equation (3.19) illustrates the similarities between the simplest form of the constitutive relationships for electrostrictors and piezoelectrics. For example, the form of $\mathbf{m}^*$ with electric field only in the 3-direction is similar in form to the **d** electromechanical coupling matrix for piezoceramics.

However, there are some strong dissimilarities. Electrostrictors are isotropic materials when there is no applied electric field. Piezoceramics are orthotropic due to their poling. In addition, a factor of two is needed in the electromechanical coupling between stress and charge but this factor is not needed in the coupling between electric field and strain.

Electrostrictors are most often described in terms of index notation because the matrix form of the electromechanical coupling buries part of the electric field dependence in $\mathbf{m}^*$. The superscript star indicates that electric field terms are buried within. Index notation does not obscure the extra electric field term. When matrix notation is utilized in this document, the matrix forms are those described in this subsection.

3.2.3 Hyperbolic tangent form

In the previous subsection a very general form of the electrostrictive constitutive relationships was given in equation (3.14). This relationship was simplified to the form given in equation (3.15) by neglecting higher-order terms. As an alternate simplification, the higher-order terms can be combined into hyperbolic tangent formulation. This is an empirical simplification that is introduced solely because it works well.

To ensure compatibility between the electrical and mechanical constitutive relationships, the hyperbolic form should be introduced into the Gibbs energy formulation. The polynomial expansions of the electrostriction coupling terms can be combined into a hyperbolic tangent formulation. In other words, let

$$-m_{mnij}E_mE_nT_{ij} - h_{mnopij}E_mE_nE_oE_pT_{ij} - \cdots \text{h.o.t.} \Rightarrow -\frac{1}{k^2}m_{mnij}T_{ij}\tanh^2(k|E|)\frac{E_mE_n}{|E|^2} \quad (3.23)$$

where k is a relaxation factor. Similarly, the polynomial expansions of the elastostriction terms can be combined into a hyperbolic tangent formulation;

$$-r_{mnijkl}E_mE_nT_{ij}T_{kl} - t_{mnopijkl}E_mE_nE_oE_pT_{ij}T_{kl} - \cdots \text{h.o.t.}$$
$$\Rightarrow -\frac{1}{k^2}r_{mnijkl}T_{ij}T_{kl}\tanh^2(k|E|)\frac{E_mE_n}{|E|^2} \quad (3.24)$$

Incorporating the transcendental electrostriction term into equation (3.11), the Gibbs energy formulation becomes

$$\begin{aligned} dG = &-\tfrac{1}{2}\varepsilon_{mn}E_mE_n - \tfrac{1}{3}\varepsilon_{mno}E_mE_nE_o - \tfrac{1}{4}\varepsilon_{mnop}E_mE_nE_oE_p - \cdots \text{h.o.t.} \\ &-\tfrac{1}{2}s_{ijkl}T_{ij}T_{kl} - \tfrac{1}{3}s_{ijklmn}T_{ij}T_{kl}T_{mn} - \cdots \text{h.o.t.} \\ &-\tfrac{1}{k^2}r_{mnijkl}T_{ij}T_{kl}\tanh^2(k|E|)\frac{E_mE_n}{|E|^2} - \tfrac{1}{k^2}m_{mnij}T_{ij}\tanh^2(k|E|)\frac{E_mE_n}{|E|^2}. \end{aligned} \tag{3.25}$$

Evaluating the derivatives of the energy formulation yields the material constitutive relationships. The higher-order dielectric terms are zeroed as well as the higher-order stress-strain coupling. The resulting equations of motion become

$$\boxed{\begin{aligned} D_m &= \varepsilon^T_{mn}E_n + \frac{2}{k}m_{mnij}T_{ij}\frac{\sinh(k|E|)}{\cosh^3(k|E|)}\frac{E_n}{|E|} + \frac{2}{k}r_{mnijkl}T_{ij}T_{kl}\frac{\sinh(k|E|)}{\cosh^3(k|E|)}\frac{E_n}{|E|} \\ S_{ij} &= s^E_{ijkl}T_{kl} + \frac{1}{k^2}m_{mnij}\tanh^2(k|E|)\frac{E_mE_n}{|E|^2} + \frac{2}{k^2}r_{mnijkl}T_{kl}\tanh^2(k|E|)\frac{E_mE_n}{|E|^2} \end{aligned}} \tag{3.26}$$

These equations represent the nonlinear electrostrictive constitutive relationships at constant temperature. This form of the constitutive equations will be called the hyperbolic model.

The hyperbolic form of the constitutive relationships given in equation (3.26) also need to be reformulated so that strain is an independent variable.

$$\begin{aligned} T_{kl} &= C^*_{ijkl}S_{ij} - \tfrac{1}{k^2}C^*_{ijkl}m_{mnij}\tanh^2(k|E|)\frac{E_mE_n}{|E|^2} \\ D_m &= \varepsilon_{mn}E_n + \frac{2}{k}m_{mnij}C^*_{tuij}S_{tu}\frac{\sinh(k|E|)}{\cosh^3(k|E|)}\frac{E_n}{|E|} - \frac{2}{k^3}m_{mnij}m_{vwtu}C^*_{tuij}\frac{\sinh^3(k|E|)}{\cosh^5(k|E|)}\frac{E_nE_vE_w}{|E|^3} \\ &\quad + \frac{2}{k}r_{mnijkl}C^*_{tuij}C^*_{pqkl}\frac{\sinh(k|E|)}{\cosh^3(k|E|)}\frac{E_n}{|E|}\left(S_{pq}S_{tu} - \frac{2}{k^2}m_{vwtu}S_{pq}\tanh^2(k|E|)\frac{E_vE_w}{|E|^2}\right. \\ &\quad \left. + \frac{1}{k^4}m_{rspq}m_{vwtu}\tanh^4(k|E|)\frac{E_rE_sE_vE_w}{|E|^4}\right) \end{aligned} \tag{3.27}$$

The fourth and higher-order electric field terms and will be neglected in subsequent analysis. The star superscript on the stiffness matrix indicates that

electric field terms are buried within. The variable stiffness matrix is defined as

$$C^{*}_{ijkl} = \left(s^{E}_{ijkl} + \frac{2}{k^2} r_{mnijkl} \tanh^2(k|E|) \frac{E_m E_n}{|E|^2} \right)^{-1} \tag{3.28}$$

3.3 Electrical Polarization Expansion

The constitutive relationships can be derived for cases where polarization is used as the dependent variable instead of electric field (Hom and Shankar, 1994a) (Namboodri, 1993). These researchers have preferred to expand the constitutive properties where stress is a resultant instead of strain. As a result, the Helmholtz free energy function is used. As given in equation (3.7), the Helmholtz free energy function is given by

$$dA = -sd\Theta + T_{ij}dS_{ij} + E_m dD_m \tag{3.29}$$

Electrical displacement can be converted to electrical polarization by noting $D=\varepsilon_o E+P$. In the case of electrostrictors, the relative dielectric permittivity is very large. The polarization term depends on the total dielectric, $\varepsilon_o\varepsilon_r$, and will be much larger than the $\varepsilon_o E$ term. As a result, electrical displacement is approximately equal to electrical polarization. Since electrical polarization is preferred in the material science community instead of electrical polarization, electrical polarization will be used in this section.

The relationships between the Helmholtz free energy function and the other state variables are given by

$$T_{ij} = \left(\frac{\partial A}{\partial S_{ij}} \right)^{E} \quad \text{and} \quad E_i \cong \left(\frac{\partial A}{\partial P_i} \right)^{S} \tag{3.30}$$

The thermal dependence has been dropped from the thermodynamic formalism. The thermal terms could be included as extra terms in the thermodynamic formalism or as a parameterization of the material constants.

A form of the Helmholtz free energy function needs to be found which will describe the constitutive behavior of electrostrictive materials. The first assumption is that the electrically induced strain is proportional to the square

of the electrical polarization. Linear material behavior of strain with relation to stress is assumed. The last major assumption is that the change in polarization with respect to electric field at constant stress is given by

$$P_k = P^s \tanh(kE_k) \tag{3.31}$$

or

$$E_k = \frac{1}{k}\operatorname{arctanh}\left(\frac{P_k}{P^s}\right) \tag{3.32}$$

where P^s is the spontaneous polarization and k is the relaxation factor. With a bit of head-scratching, the Helmholtz free energy function is given by

$$\begin{aligned} A = {} & \tfrac{1}{2}C_{ijkl}\left(S_{ij} - Q_{ijpq}P_pP_q\right)\left(S_{kl} - Q_{klmn}P_mP_n\right) + \\ & \frac{1}{2k}\left[P_i \operatorname{arctanh}\left(\frac{P_i}{P^s}\right) + \tfrac{1}{2}P^s \ln\left(P^{s2} - P_iP_i\right)\right] \end{aligned} \tag{3.33}$$

Once the Helmholtz free energy has been formed, the constitutive relationships are easily found. Substituting equation (3.33) into the definition of the constitutive relationships, equation (3.30), the electrostrictive constitutive relationships become

$$\begin{aligned} T_{ij}^E &= C_{ijkl}Q_{klmn}P_mP_n + C_{ijkl}S_{ij} \\ E_m &= -2C_{ijkl}Q_{klmn}P_nS_{ij} + 2C_{ijkl}Q_{klmn}P_iP_jP_n + \frac{1}{k}\operatorname{arctanh}\left(\frac{P_m}{P^s}\right) \end{aligned} \tag{3.34}$$

In summary, the constitutive relationships can be derived in terms of electrical field or electrical polarization. Additionally, the relationship between strains and electric field can be modeled as an even powered polynomial or as a hyperbolic tangent. Although there are subtle variations between them, the different forms are equivalent. This report will utilize an even powered function and hyperbolic function of the electrical field as the base of the constitutive relationship due to the engineering ease of this form.

3.4 Temperature Variation

The variation of mechanical properties with respect to temperature is the Achilles heel of electrostrictors. The electrostriction term can vary by as much as one percent per degree Centigrade (Blackwood and Ealey, 1993). Additionally, the dielectric permittivity is strongly temperature dependent. The extreme temperature dependence arises from operating the material in or near its Curie range.

Temperature produces a diffuse phase change in electrostrictors between paraelectric and ferroelectric states. Below the Curie range, electrostrictors behave like a standard ferroelectric. As a result, the material exhibits significant hysteresis and large strains in this region. As the Curie range is passed, the hysteresis as well as the large strains diminish.

Temperature dependence is typically included in the thermodynamic formalism from which the constitutive relationships were derived. (It is a *thermo*dynamic formalism!) However, the thermal dependence was dropped from the constitutive relationships in favor of including a thermal dependence on the material constants.

When the constitutive relationships are parameterized in terms of the polarization, then the relaxation factor, k, the electrostrictive coefficient, Q, and the dielectric permittivity, ε, need to be characterized. The spontaneous polarization, P^s, is assumed constant. Parameterization in terms of the electric field requires characterization of the relaxation factor, k, the electrostrictive coefficient, m, and the dielectric permittivity, ε.

The variation of the electrostrictive effect with respect to temperature has been modeled with a modified Curie-Weiss law. Based on the work by Namboodri (Namboodri, 1993), the electrostrictive gain can be expressed as

$$m_{ijkl} = \left(q^{m}_{ijkln}(\Theta)^{n-1}\right)^2. \qquad (3.35)$$

where q^m is the temperature factor pertaining to the electrostrictive parameter. Θ is the absolute temperature and is raised to the n-1^{th} power. The

modified polarization factors in equation (3.35) are determined by curve fitting the model to the experimental results.

An identical formulation can be used to express the temperature variation of the relaxation parameter, k. At the risk of being redundant, the relaxation parameter can be expressed as

$$k = \left(q_n^k(\Theta)^{n-1}\right)^2. \tag{3.36}$$

where q^k is the temperature factor pertaining to the relaxation parameter.

Chapter 4

MATERIAL TESTS

Shivering electrostrictors
struggling to keep warm,
to reach their Curie temperature
for their optimal form.

Shivering electrostrictors
in great electric fields,
as the voltage grows higher
a size change they yield.
-Anne-Evan Kale

This chapter presents experimental verification of the constitutive relationships derived in chapter 3. The material behaviors are characterized in terms of electrostriction, elastostriction, and temperature effects.

4.1 Experimental Setup

4.1.1 Physical setup

Experiments were conducted on relaxor ferroelectric ceramic wafers manufactured by AVX corporation. The 0.27 mm thick, 2.5 mm square wafers were composed of PMN-PT, $0.9(Pb[Mg_{1/3}Nb_{2/3}]O_3)$-$0.1PbTiO_3$. The maximum relative dielectric of this electrostrictor occurred near 40°C. Unless otherwise specified, all of the experiments were conducted with the wafer temperature near 28°C. As a result, the experimental data will feature larger hysteresis

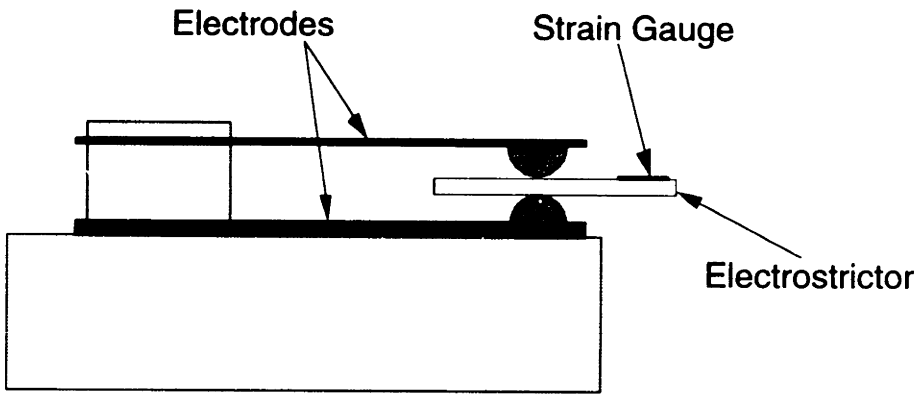

Figure 4.1: Experimental setup for measuring the transverse and longitudinal expansion of the unconstrained electrostrictive wafer. The strain gage finds the transverse expansion.

than the classic curves of an electrostrictor and will feature larger strains. This temperature trend also has been found in characterizations of pure PMN (Blackwood and Ealey, 1993) (Uchino et al, 1981).

The electrostrictive wafer was excited with a Kepco model BOP 1000M voltage amplifier which was fed a sinusoidal signal from a Phillips model PM 5191 function generator. The resulting size change of the electrostrictor was measured with a strain gauge. A model CEA-13-125UW-350, 350Ω strain gauge manufactured by Micro-Measurements Division was used for this purpose. The experimental setup is shown in figure 4.1. Strain and voltage data were collected on a Macintosh Quadra 950 using LabView software running at 1 kHz.

4.1.2 Data reduction

As with any strain-based experiment, noise reduction is at the root of any data reduction technique. A frequency-domain windowing and a time-domain averaging was used for this end. Each channel of data was windowed with an eleven point Hamming window. In this process, a Hamming shaped window is passed over the data. Points on each side raw data point are weighted and averaged together to create the windowed data point, as shown

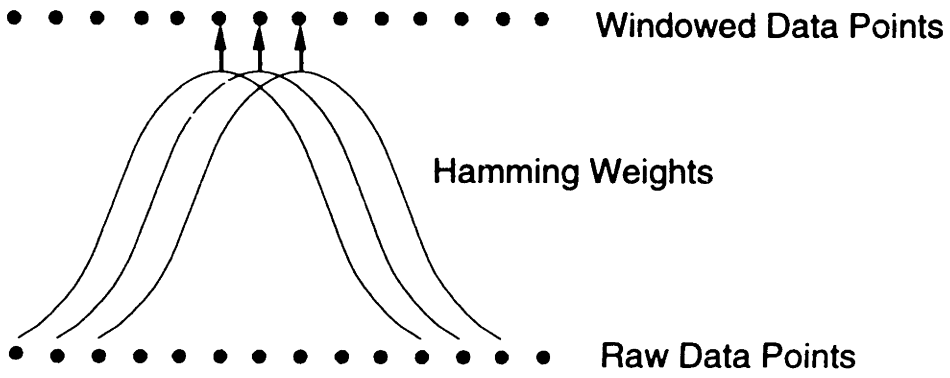

Figure 4.2: Hamming windowing low-pass filters the raw data by averaging several points together according to the Hamming weighting function.

in figure 4.2. In the case of an eleven point Hamming window, eleven raw data points are used to produce each windowed data point. This process filters high frequency signals. Windowing was performed on each channel of data in order to eliminate the possible effects of added phase.

The strain data also was averaged in the time domain. In this case, the voltage signals were matched different cycles. The overlaid strain signals were averaged together. A long enough time record was obtained so that at least four cycles were averaged together.

The material parameters were found by curve-fitting the model to the experimental data. In these cases, a direct search algorithm was used to find the local functional minimum. Such algorithms are also known as unconstrained nonlinear optimizations. MATLAB software was used in these cases. Once a parameter has been determined, the same value was used in all subsequent calculations.

4.2 Electrostrictive Effect

Electrostriction is a second-order coupling between the electrical and mechanical energies. This effect marks the principle electromechanical coupling exhibited by electrostrictive materials. The electrostrictive effect is characterized by placing a slowly varying electric field across an unconstrained

sample. The resulting curve gives the unadulterated effect of the electromechanical coupling. In Chapter 3, two models were derived to described the electromechanical coupling: a quadratic model and a hyperbolic model. As given in equation (3.17), the quadratic model expresses the induced strain as a function of the electric field squared. The hyperbolic model, given in equation (3.26), expresses the induced strain as a function of the square of the hyperbolic tangent of the electric field. Removing all but the direct electrostriction terms for the induced strain and requiring the electric field to be only in the 3-direction, the models are expressed as

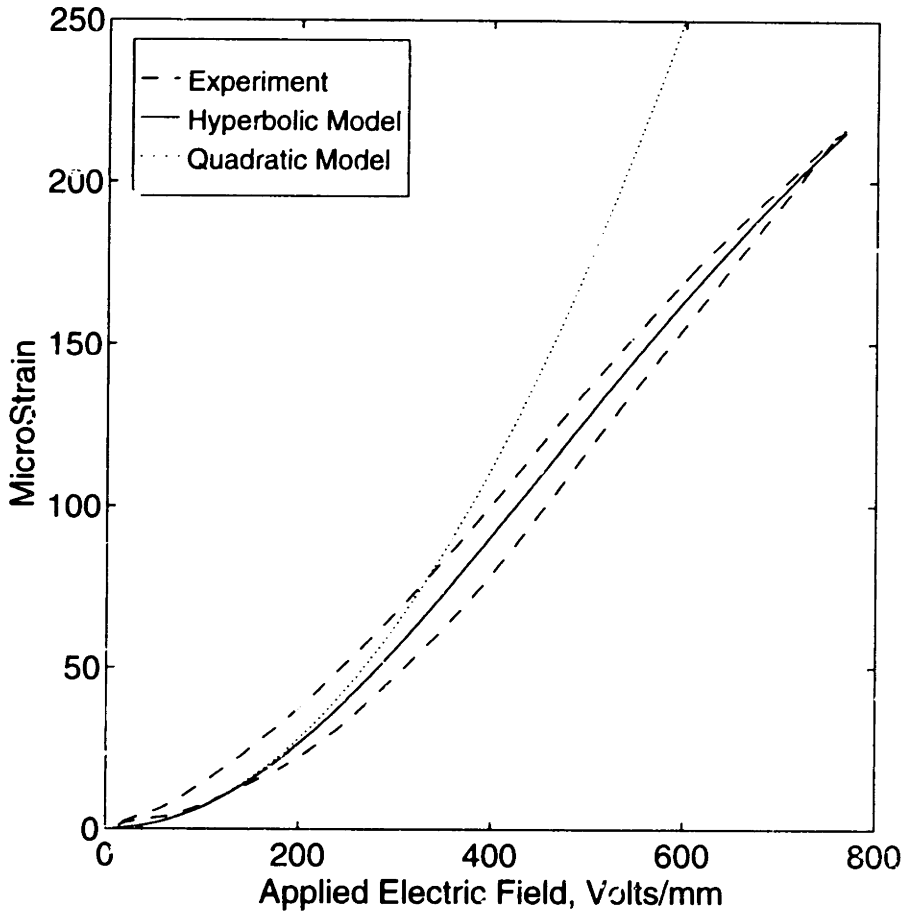

Figure 4.3: Unconstrained transverse expansion of an electrostrictive wafer. Curve fitting the hyperbolic model, equation (4.1), to the data gives the electrostrictive constant, m_{1122}=6.6e-16 m^2/V^2 and the relaxation parameter, k=1.6e-6 V/m. The same m value was used in the quadratic model and gives good low field correlation.

$$\begin{aligned} S_{ij} &= m_{33ij}E_3E_3 && \text{quadratic model} \\ S_{ij} &= \frac{1}{k^2} m_{33ij} \tanh^2(kE_3) && \text{hyperbolic model} \end{aligned} \tag{4.1}$$

Notice that at low field levels, the hyperbolic model reduces to the form of the quadratic model. As a result, the m value used in the hyperbolic model is the same value that will be used in the quadratic model.

The material parameters were obtained by fitting the hyperbolic model to the experimental data as described in subsection 4.1.2. Experimental data was from electric fields ranging from DC to 800 V/mm and the form of the hyperbolic equation was given in equation (4.1). The resulting material values are m_{3311}=6.6e-16 m^2/V^2 for the transverse electrostrictive constant and k=1.6e-6 V/m for the relaxation parameter. The electrostrictive constant scales the magnitude of the strain and the relaxation parameter dictates when the strain tends to "bend over" or relax with increasing electric field. Since the quadratic model is a low-field simplification of the hyperbolic model, the same electrostrictive constant is used in both models.

As indicated in figure 4.3, the hyperbolic model provides a close correlation between the experiment and the model through out the range of electric field levels. The quadratic model forms a good approximation of the experiment in the low and moderate electric field regions. Above 300 V/mm, the quadratic model will over predict the response. Thus, the quadratic model is valid only in the region less than 300 V/mm for PMN-PT.

4.3 Elastostrictive Effect

Elastostriction describes the stress-based correction to the induced strain. As indicated in Chapter 3, the elastostriction term can also be interpreted as an electric field based correction to the compliance of the material. In particular, from equation (3.28), the compliance of an electrostrictor can be expressed in terms of the hyperbolic model as

$$s^*_{ijkl} = s^E_{ijkl} + \frac{2}{k^2} r_{mnijkl} \tanh^2(k|E|) \frac{E_m E_n}{|E|^2} \tag{4.2}$$

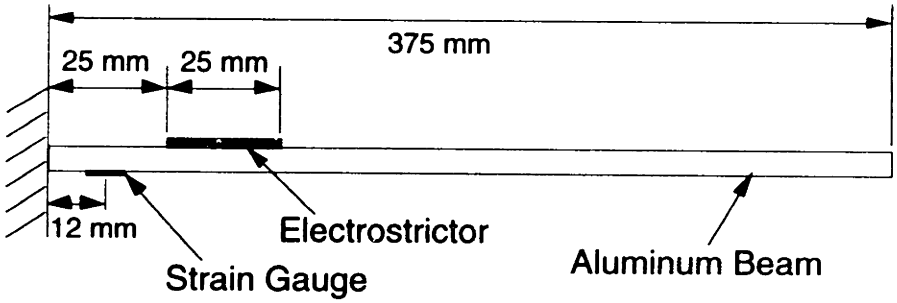

Figure 4.4: Experimental setup to calculate the elastostriction of the electrostrictor by measuring the change in the natural frequency of the system as a function of electric field.

At low and moderate field levels, the compliance can be simplified to a quadratic form. As given in equation (3.16),

$$s^{*}_{ijkl} = s^{E}_{ijkl} + 2r_{mnijkl}E_mE_n \tag{4.3}$$

The first term in the equations represents the compliance at zero electric field and the second term is the elastostriction correction. This section seeks to define the magnitude of the elastostriction term. Notice that the hyperbolic model reduces to the quadratic model at low field levels, thus the same value will be used in both models.

Measuring the elastostriction term is difficult. There are two possible techniques for measuring stiffness as a function of electric field: measuring the actuation potential or measuring the natural frequency. By far the simplest technique would be to measure the actuation potential. The actuation potential gives the amount of deformation that the electrostrictor can produce when its expansion is constrained. Thus, the deformation of an electrostrictor sandwiched between layers of metal would change based on the relative thickness of the metal and actuator. This would be an easy method from which to find the actuator stiffness if the material nonlinearity was an electric field-based nonlinearity. However, if the nonlinearity of an electrostrictor was a strain-based nonlinearity, then the reduced strain from the constraint would give erroneous results. For example, measuring the induced strain of a piezoceramic would give incorrect results since the

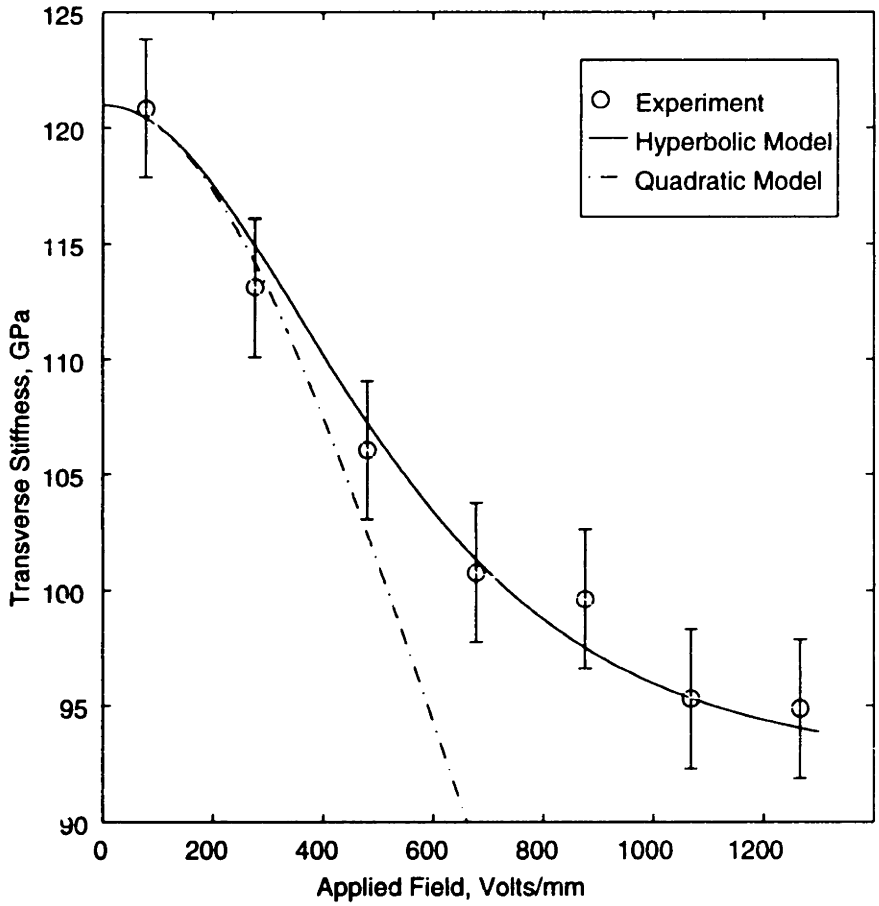

Figure 4.5: Transverse stiffness variation as a function of electric field in 0.9PMN-0.1PT. The hyperbolic model reflects the best fit of equation (4.2). This gives an r_{113311}=3.25e-24 $m^2/(V^2\ Pa)$. The quadratic model uses equation (4.3) and the same elastostriction value.

nonlinearity of a piezoceramic is a strain-based nonlinearity (Anderson, 1989). Measuring the natural frequency of the electrostrictor does not infringe upon the electric field-based versus strain-based debate.

The natural frequency of an individual electrostrictor is not easily measured. Instead, the natural frequency of an electrostrictive system needs to be measured. The simplest system is that of an electrostrictor upon a cantilevered beam. The stiffness of the electrostrictor will affect the natural frequency of the beam system. An illustration of the beam is given in

figure 4.4. By measuring the natural frequency at different bias fields across the electrostrictor, the stiffness of the electrostrictor can be calculated.

The first natural frequency was experimentally measured by applying a small sinusoidal signal, 0.5 V/mm in addition to a large DC electric field. In order to translate the natural frequencies into an actuator stiffness, the methodology developed in chapter 5 (in particular equation (5.66)) was used to calculate the natural frequency as a function of the material stiffness. The stiffness at different electric fields was obtained by matching the natural frequency versus electric field from the experiment with the natural frequency versus stiffness from the simulation.

The measured material stiffness versus electric field is shown in figure 4.5. Error bars reflect the frequency resolution of the fourier analyzer. The effective transverse stiffness decreased by roughly 20% as the electric field increased from 0 to 1300 V/mm. The elastostriction factor, r, was curve fit from the hyperbolic model given in equation (4.2). The calculated elastostriction constant, r_{113311}, equals 3.25e-24 $m^2/(V^2\,Pa)$. The relaxation parameter, k, is the same as that which was calculated from figure 4.3. The hyperbolic model closely matches the experimental values over the entire field range. The quadratic model, equation (4.3), accurately predicts the stiffness only in the low to moderate electric field range. Other investigators have seen a similar variation in the longitudinal material stiffness (Hom and Shankar, 1994b)

4.4 Temperature Effect

The variation of mechanical parameters with respect to temperature has been a perennial problem pertaining to electrostrictors. As seen in figure 4.6, the field-strain curves for an unconstrained electrostrictor changes dramatically over the range of temperatures. As the Curie range is passed, the hysteretic ferroelectric behavior transforms into a non-hysteretic non-linear relaxor ferroelectric behavior. Although the magnitude of the strain changes dramatically with temperature, the constitutive relationships for induced strain are still applicable. At each temperature, the strain-field curve was fit

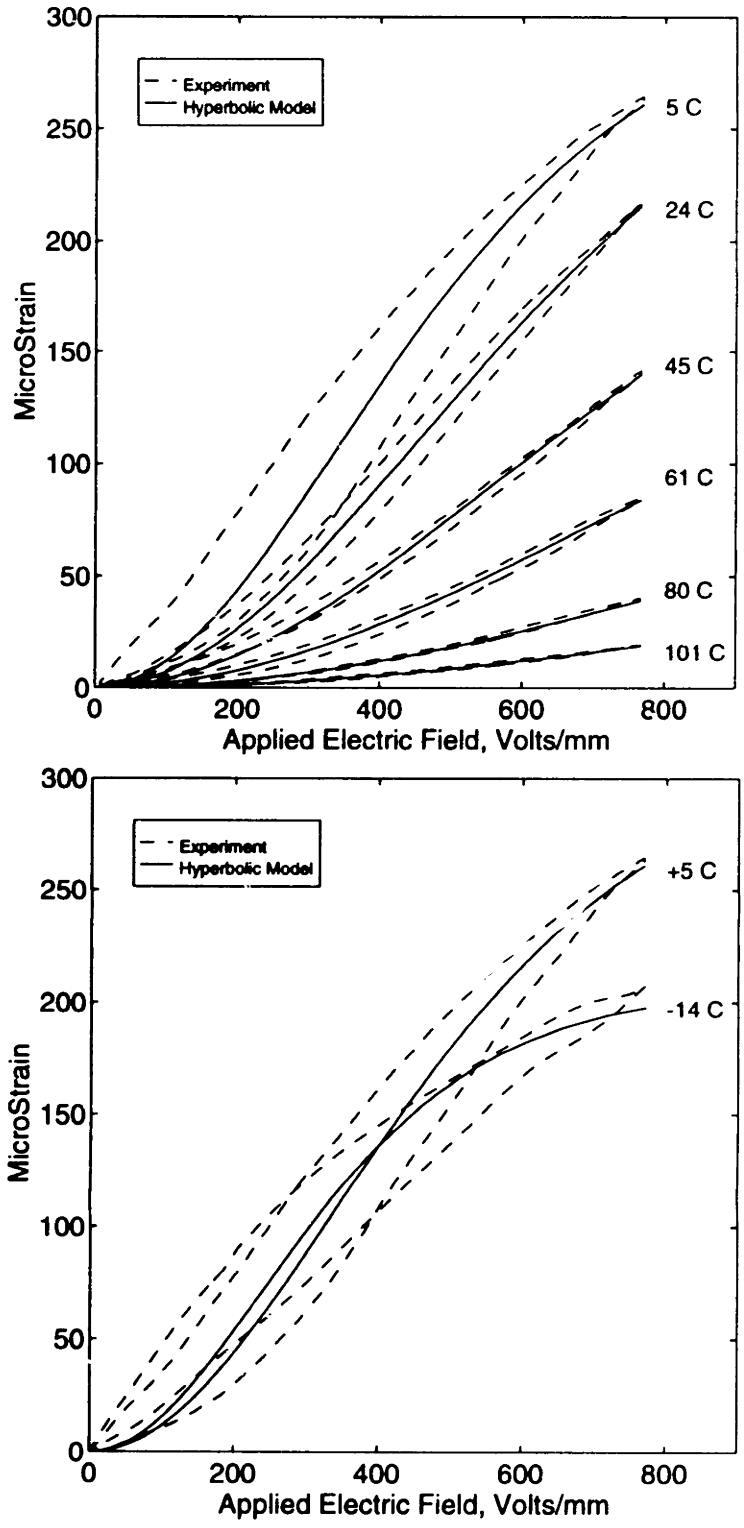

Figure 4.6: The electro-mechanical coupling of electrostrictors is strongly temperature dependent. As temperature increases, the hysteresis and the electrostriction effect decrease. The transverse expansion is shown here.

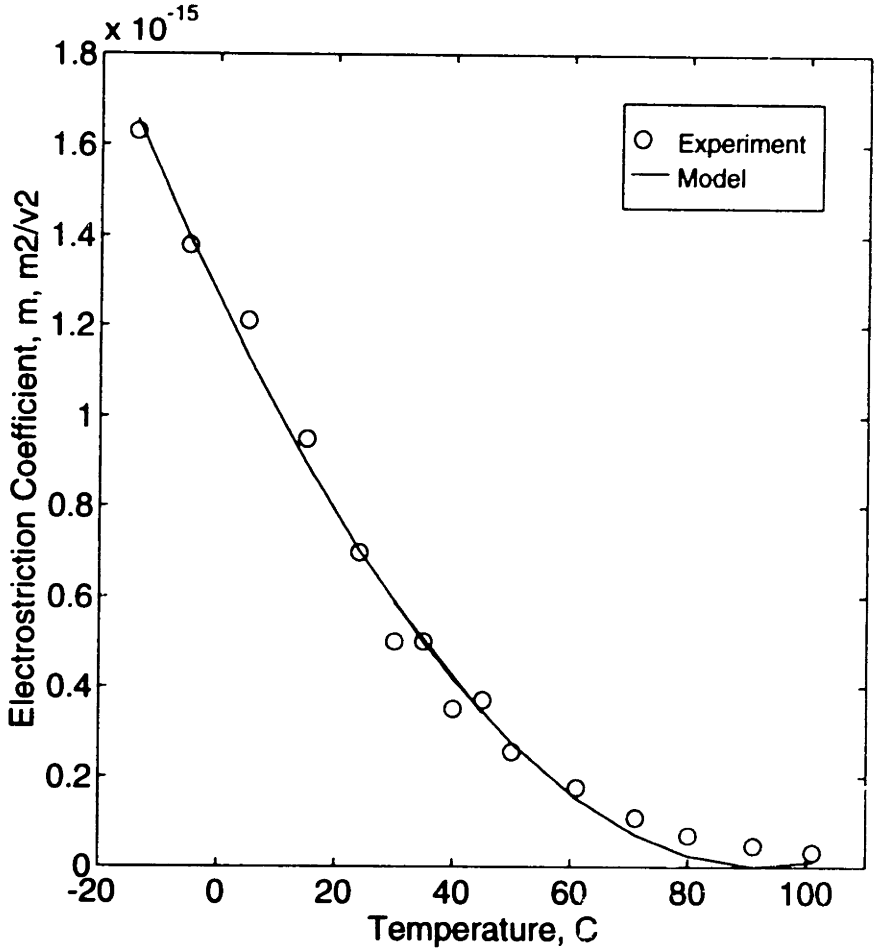

Figure 4.7: The electrostriction constant, m_{1122}, decreases as the temperature increases. The temperature variation can be curve-fit with equation (4.4). The temperature factors are $q^m{}_{11221}$=2.56e-7 m^2/V^2, $q^m{}_{11222}$=-1.21e-9 $m^2/(°K\ V^2)$, and $q^m{}_{11223}$=1.43e-12.$m^2/(°K^2\ V^2)$.

with equation (4.1) in order to give the m and k values for that temperature. As seen in figure 4.6, the form of the constitutive equation describes the behavior of the electrostrictor across a wide range of temperatures. The maximum strain is provided at 5°C. The model gives a better fit to the data a temperatures above 0°C than at temperatures below 0°C. As the material becomes increasingly ferroelectric at lower temperatures, the material strain becomes increasingly linear with respect to electric field. The inherently quadratic nature of the hyperbolic model does not provide as close of a fit to the increasingly linear data at these reduced temperatures.

The behavior of the electrostrictive constant and the relaxation parameter can be described by the thermal model developed in chapter 3. As given in equations (3.35) and (3.36), the m and k parameters can be expressed as a even-powered polynomial expansion of the absolute temperature.

$$m_{ijkl} = \left(q^{m}_{ijk\,ln}(\Theta)^{n-1}\right)^2. \tag{4.4}$$

$$k = \left(q^{k}_{n}(\Theta)^{n-1}\right)^2 \tag{4.5}$$

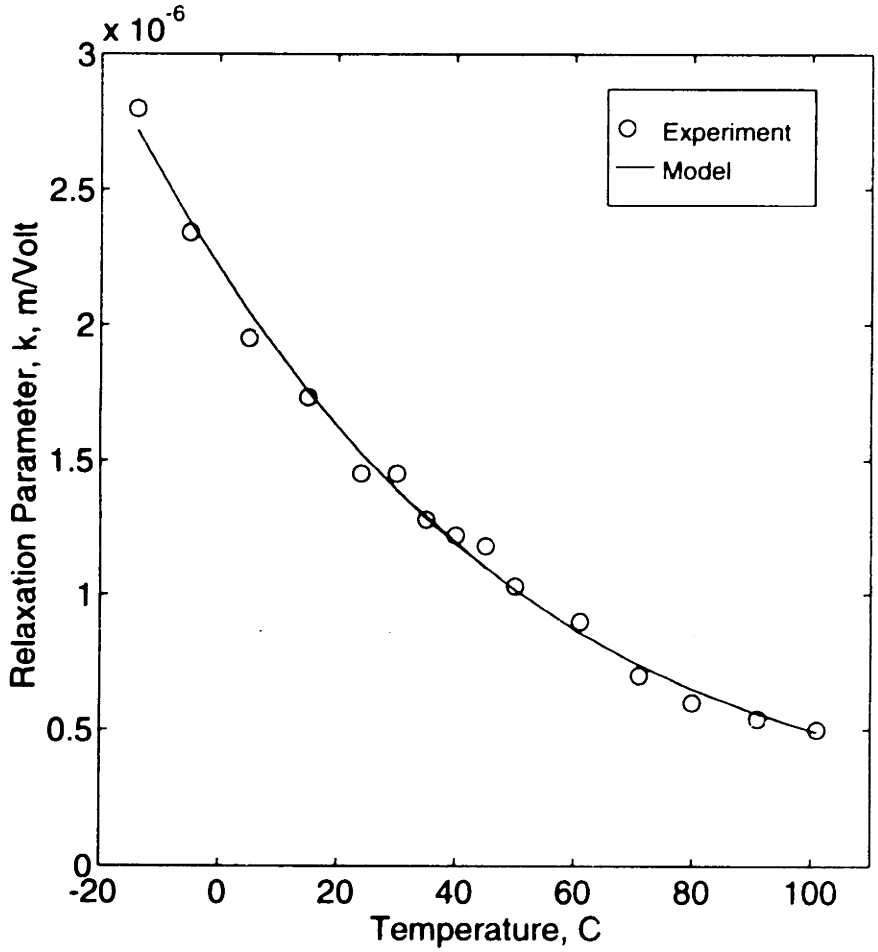

Figure 4.8: The relaxation parameter, k, decreases as the temperature increases. The temperature variation can be curve-fit with equation (4.5). The temperature factors are q^{k}_{1}=8.0e-3 m/v, q^{k}_{2}=-3.46e-5 m/(°K v), and q^{k}_{3}=4.04e-8.m/(°K² v).

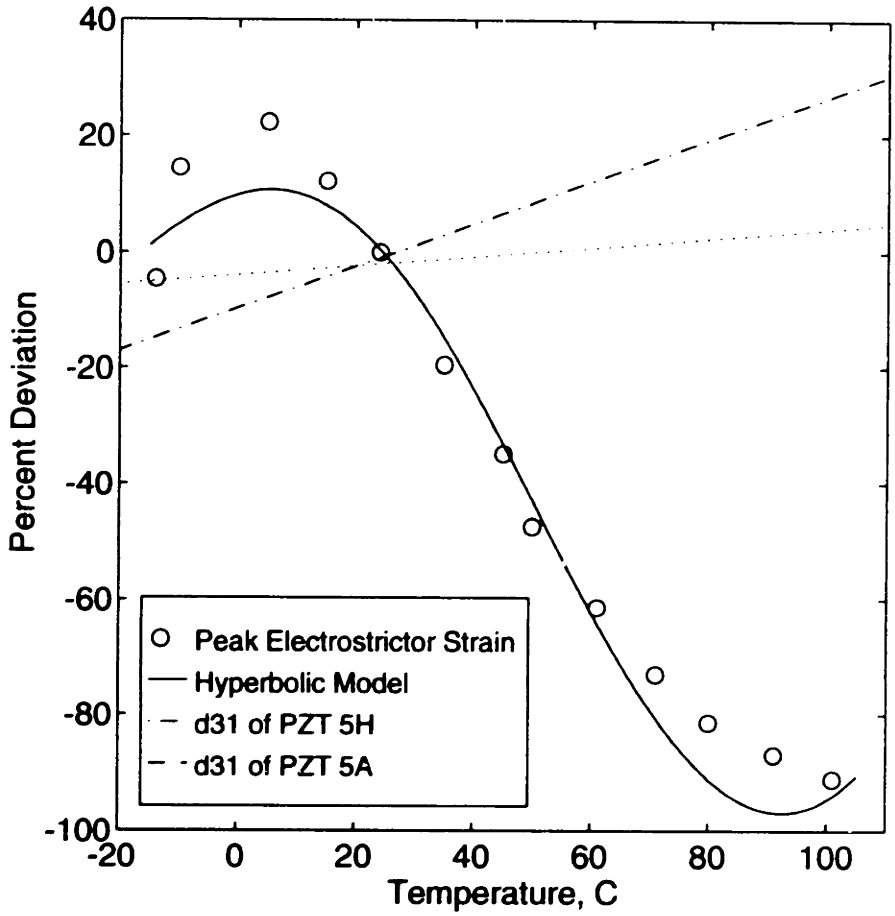

Figure 4.9: Comparison of the temperature dependence of electrostrictors and piezoceramics. Peak strain is the transverse strain occurring at 780 V/mm. The hyperbolic model is a combination of equation (4.1) and the temperature compensation of equations (4.4) and (4.5). The piezoceramic coupling is taken from Piezo Systems, Inc. product catalog (Piezo Systems, 1993).

Figures 4.7 and 4.8 illustrate the temperature dependence of the electrostrictive and relaxation parameters. These parameters were determined by curve fitting the field-strain curves at each temperature. In figure 4.7, the electrostrictive coupling coefficient, m, decreases as the temperature increases. As a result, the actuation potential of an electrostrictor correspondingly decreases. Equation (4.4) is curve fit to the data. Using three

terms in the expansion, close agreement is achieved between the model and the experiment. The resulting temperature factors are q^m_{11221}=2.56e-7 m^2/v^2, q^m_{11222}=-1.21e-9 $m^2/(^oK\ v^2)$, and q^m_{11223}=1.43e-12.$m^2/(^oK^2\ v^2)$.

In figure 4.8, the relaxation parameter, k, is shown decreasing with temperature. The relaxation or "bend over" of electrostrictors is delayed through the application of temperature. This means that the quadratic model is applicable at larger field levels during higher temperatures. Conversely, this trend also indicates that the material becomes increasingly ferroelectric at lower temperatures. Equation (4.5) is curve fit to the data and provides close agreement of model and experiment. The resulting temperature factors are q^k_1=8.0e-3 m/v, q^k_2=-3.46e-5 m/(°K v), and q^k_3=4.04e-8.m/($°K^2$ v).

In brief, electrostrictors exhibit a marked change in the coupling behavior as a function of temperature. However, figure 4.9 illustrates that other active materials, such as piezoceramics, also exhibit a significant change in the coupling parameters. The values are normalized in terms of percent deviation from room temperature. The peak strain of the electrostrictor is the transverse strain occurring at 780 V/mm. The model of the peak strain is a combination of the hyperbolic model given in equation (4.1) and the temperature corrections given in equation (4.4) and (4.5). The electromechanical coupling constant for the piezoceramics, d_{31}, is taken from Piezo Systems, Inc. product catalog (Piezo Systems, 1993). PZT-5H is the industry standard soft piezoceramic and PZT-5A is a hard piezoceramic.

Electrostrictors exhibit a larger variation of strain as a function of temperature than the piezoceramics. The peak strain varies from +22% at 5°C to -93% at 101°C. The models of the peak strain provide good correlation for temperatures ranging from 15°C to 70°C, but under predict the response for temperatures outside of the region. The piezoceramic material also exhibit a significant change with respect to temperature. The soft piezoceramic varies by -18% to +30% from -20°C to 110°C. The hard piezoceramic varies by ±5% over the same temperature range. At room temperature, the 0.4%/°C variation of the soft piezoceramic is almost a quarter of the 1.5%/°C slope of the electrostrictor. Nevertheless, the

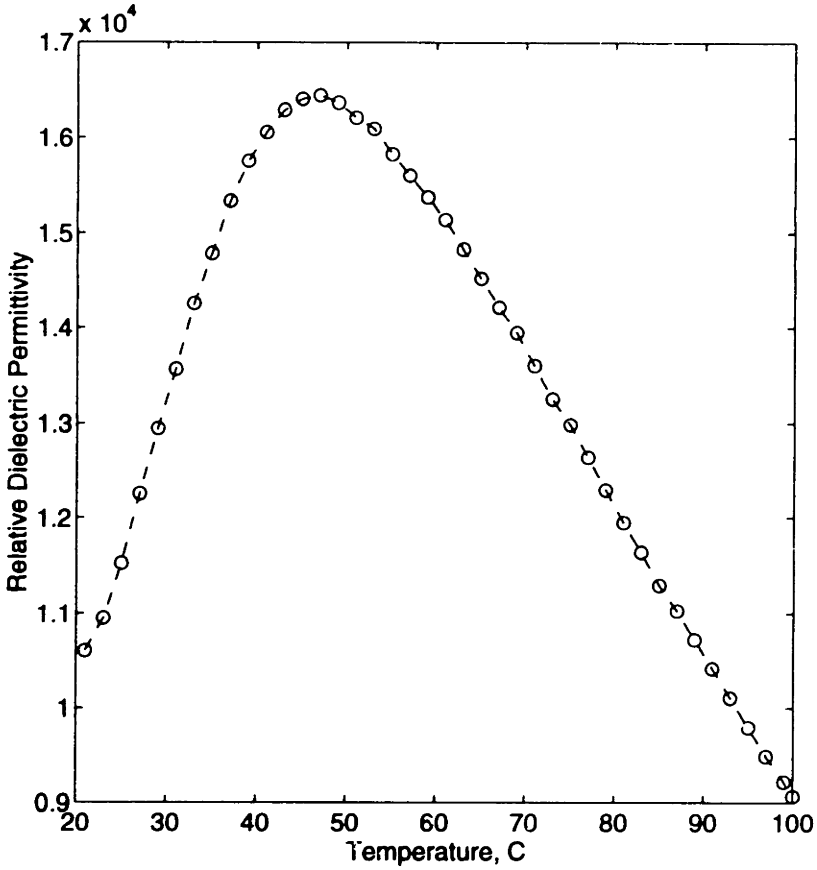

Figure 4.10: The dielectric permittivity of an electrostrictor is a strong function of temperature. The peak in the permittivity occurs during the Curie range. The permittivity was measured at 400 Hz.

temperature dependence of the piezoceramic needs to be kept in context with the significant variations of soft piezoceramics.

The Curie range coincides with dramatic changes in the dielectric permittivity, as indicated in figure 4.10. The changes in the dielectric permittivity are consistent for a ferroelectric near its Curie temperature.

4.5 Stress-Loading Effects

The previous sections have examined the behavior of an unconstrained electrostrictive wafer. This section describes the quasi-static behavior of the material when it is constrained by another structure. First,

the model of the induced strain is derived by noting the material equilibrium. Then, the theory is applied to the geometry of a electrostrictor sandwiched between plates of aluminum.

4.5.1 Linear induced strain model

The total strain in a structure containing an active material is a function of the balance of forces between the active material and the constraint. In the most general case, this balance needs to be evaluated through the use of plate theory. For such cases the reader referred to the numerous texts on plate theory, such as (Timoshenko and Woinowsky-Krieger, 1959). For the simple sandwich geometry presented in figure 4.11, the induced strain can be computed more directly. In this analysis, the epoxy layer provides a "perfect" bond between the components and, thus, shear-lag effects are ignored.

The interface force at the boundary between the structure and the actuator must balance in order for the structure to be in equilibrium. In other words

$$F^{constraint} = F^{actuation} \tag{4.6}$$

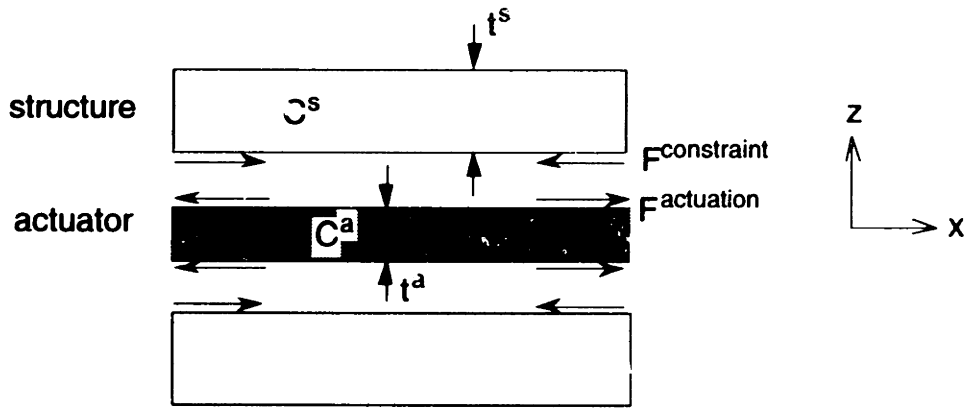

Figure 4.11: Free-body diagram of the cross section of a sandwich structure.

The force that the constraining structure and the actuator provides is a function of the cross-sectional area, the material stiffness, and the difference between the free strain and the induced strain. In other words

$$\begin{aligned} F^{constraint} &= -2t^s w^s C^s \left(0 - S^{induced}\right) \\ F^{actuation} &= t^a w^a C^a \left(S^{free} - S^{induced}\right) \end{aligned} \tag{4.7}$$

where a superscript 's' refers to the structure and a superscript 'a' refers to the actuator. The factor of two for the constraining force arises from having a constraint on the top and on the bottom. The negative sign comes from the force being in negative direction. Substituting equation (4.7) into equation (4.6), the induced strain can be found. Assuming that the width of the actuator equals the width of the structure, $w^s=w^a$, the induced strain is

$$S^{induced} = \frac{C^a t^a}{C^a t^a + 2C^s t^s} S^{free} \tag{4.8}$$

In other words, the induced strain is proportional to the unconstrained motion of the wafer. The proportionality is given by the stiffness ratios and thickness ratios of the actuator and the host structure. This ratio is often defined as the relative stiffness, Ψ.

$$\Psi = \frac{2C^s t^s}{C^a t^a} \tag{4.9}$$

Introducing the relative stiffness into equation (4.8) gives

$$S^{induced} = \frac{1}{1+\Psi} S^{free} \tag{4.10}$$

4.5.2 Nonlinear induced strain

The strain-field relationship for electrostrictors is nonlinear. Similarly, the relationship for piezoceramics is also nonlinear at moderate field levels. By looking at induced strain of unconstrained wafers, constitutive relationships can be derived. However, it is not clear whether the fundamental constitutive relationship features strain as a function of electric field or whether electric field is a function of strain. In other words, which is true,

$$S = f(E) \quad \text{electric field-based nonlinearity} \tag{4.11}$$

or

$$E = f(S) \quad \text{strain-based nonlinearity} \tag{4.12}$$

When unconstrained actuation is considered, there is no effective difference between the forms. Similarly, if the electromechanical coupling is linear, then considering the form of the nonlinearity is silly. However, for constrained actuation of nonlinear active materials, the difference can become significant.

The form of the nonlinearity is a fuzzy yet fundamentally important concept. The form of the nonlinearity dictates at which point the nonlinearity will manifest itself. The case is illustrated in figure 4.12 for a hypothetical example of constrained expansion. In the free case, a particular nonlinearity exists at a specific electric field level and strain level. When the actuator is constrained, will the nonlinearity manifest itself at the same strain level or the same electric field level? If the nonlinearity is an electric field-based nonlinearity, then the nonlinearity will exist at the same field level. If the nonlinearity is strain-based, then the nonlinearity will exist at the same magnitude in strain.

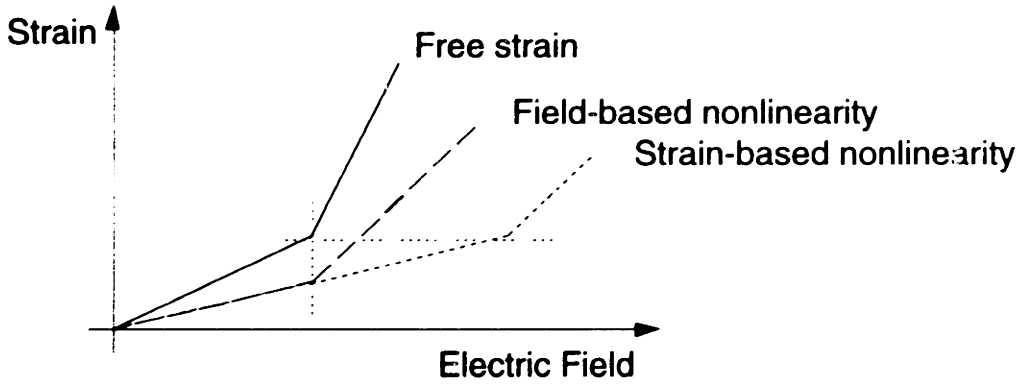

Figure 4.12: The form of the nonlinearity indicates whether the nonlinearity will manifest at a particular value of strain or at a particular electric field. A hypothetical example of constrained expansion is presented.

4.5.2.1 Electric field-based nonlinearity

Constitutive relationships generally assume that nonlinearities are a function of electric field and that equation (4.11) is true. The strain is a direct function of the applied electric field. As a result, the linear relationship for constraint given in equation (4.10) scales the magnitude of the free strain. In other words, the slope at a electric field level is a linear scale of the slope of the free strain. Using the definition of free strain expressed in the hyperbolic model, equation (4.1), and allowing electric field only in the 3-direction, the induced strain is expressed as

$$S_{ij}^{induced} = \frac{1}{1+\Psi}\frac{1}{k^2} m_{33ij} \tanh^2(kE_3) \tag{4.13}$$

4.5.2.2 Strain-based nonlinearity

If the nonlinearity is a function of the strain in the material, then equation (4.12) is the fundamental relationship between strain and electric field. In this case, the fundamental nonlinearity depends more on the deformation of the microstructure than on the externally applied stimulus. The scaling factor given in the linear relationship in equation (4.10) scales the electric field instead of the strain. Thus, the slope at any strain level is a linear scale of the slope of the free strain. Using the definition of free strain expressed in the hyperbolic model in equation (4.1) and allowing electric field only in the 3-direction, the induced strain for a strain-based nonlinear system is

$$S_{ij}^{induced} = \frac{1}{k^2} m_{33ij} \tanh^2\left(\frac{1}{1+\Psi} kE_3\right) \tag{4.14}$$

The closed form solution given in equation (4.14) is available only because the nonlinearity of electrostrictors is an algebraic function. In general, finding the strain in this case is difficult. For instance, with piezoceramics the easiest method is to assume a value for the strain and then iterate to find the correct strain (Anderson, 1989).

4.5.2 Sandwich experiment

The induced strain of an electrostrictive wafer sandwiched between two pieces of aluminum was examined. As shown in figure 4.13, a 0.27 mm thick electrostrictive wafer was bonded between two pieces of 25 mm wide, 0.50 mm thick aluminum. For comparison, the induced strain of a piezoceramic sample was taken from Anderson (Anderson, 1989) where a 0.25 mm thick piezoceramic wafer was bonded between two pieces of 25 mm by 64 mm by 0.25 mm thick aluminum wafers. In both cases, the induced strain was measured with a strain gauge mounted on the aluminum.

The measured and calculated induced strain of the electrostrictor are presented in figure 4.14. The induced strain was predicted with the model developed for electric field-based nonlinearities, equation (4.13), and with the free strain given in figure 4.3. If a constant stiffness is assumed, then the predicted strain will exceed the measured strain. If the variable stiffness given in figure 4.5 is included, then the predicted and measured strain agree. As a result, *the nonlinearity of an electrostrictor is a electric field-based nonlinearity*. This fact simplifies the treatment of electrostrictive actuation.

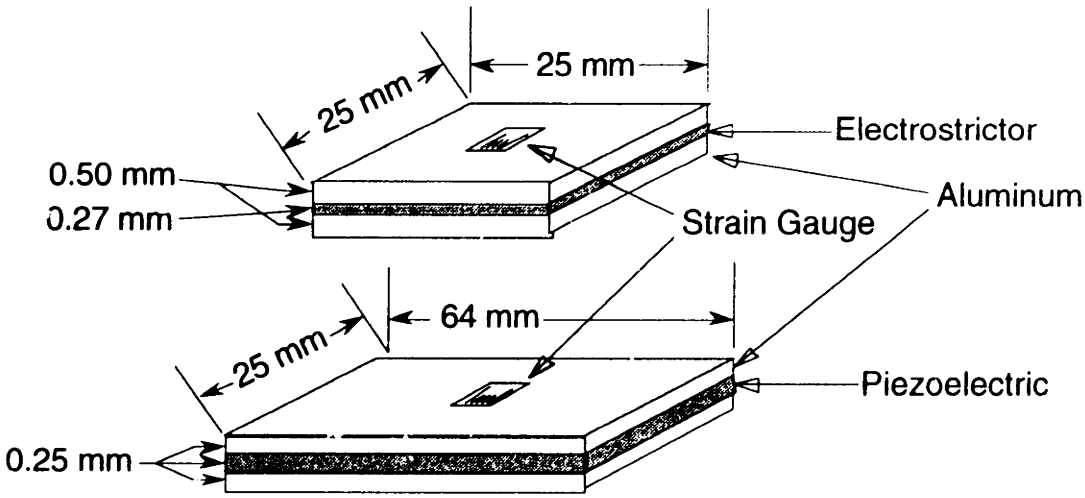

Figure 4.13: Experimental setups to measure the transverse strain of an electrostrictive wafer and a piezoceramic wafer constrained between two pieces of aluminum.

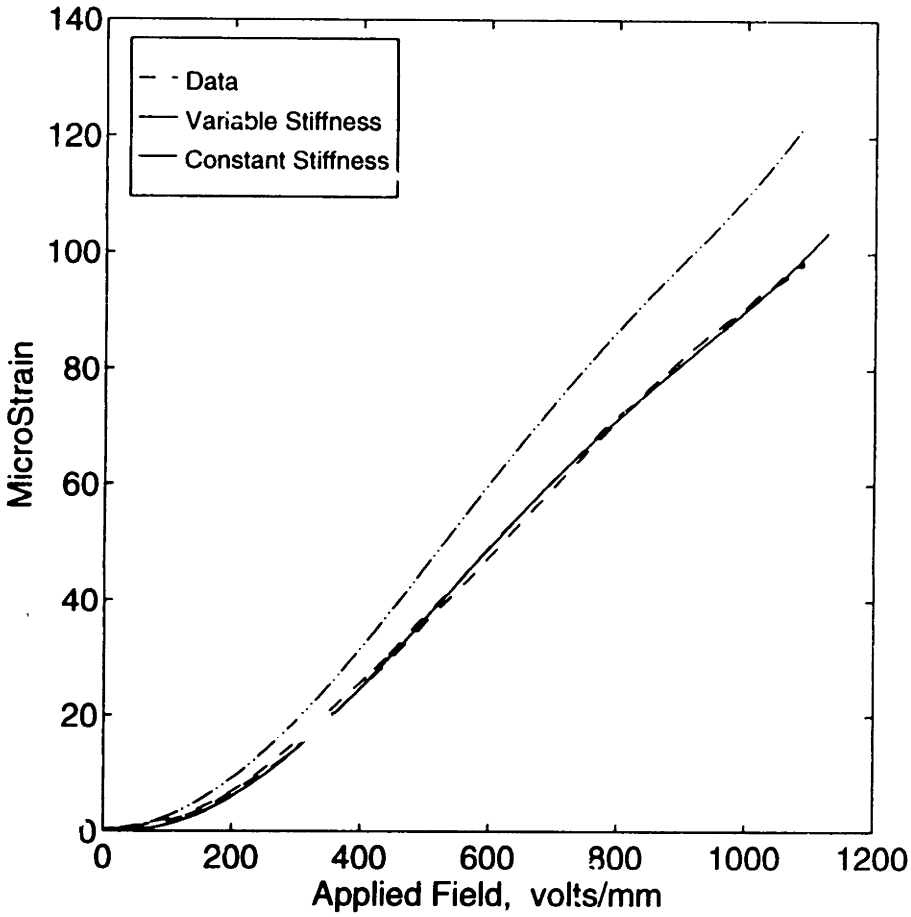

Figure 4.14: Effect of the stiffness variation on the induced strain on an electrostrictor sandwiched between two pieces of aluminum. The models assume that the electrostrictor exhibits an electric field-based nonlinearity.

The measured and calculated induced strain of the piezoceramic sandwich are presented in figure 4.15. A strain-based model and a electric field-based model are presented. Since a closed-form algebraic expression of piezoceramic nonlinearity have not been found simple expressions of the form given in equations (4.13) and (4.14) are unavailable. As a result, equation (4.8) was used in both models to calculate the induced strain. The free strain in the strain-based model was taken from the unconstrained expansion of a piezoceramic wafer. The free strain in the field-based model was determined through iteration. The process is described in Anderson (Anderson, 1989). At low field levels, piezoceramics are linear elements and

the two models yield identical results. At higher field levels the nonlinear behavior of piezoceramics becomes more significant and the two models diverge. The strain-based model closely correlates to the experimental results. As a result, *the nonlinearity of piezoceramics is a strain-based nonlinearity.* This fact complicates the treatment of piezoceramic actuation.

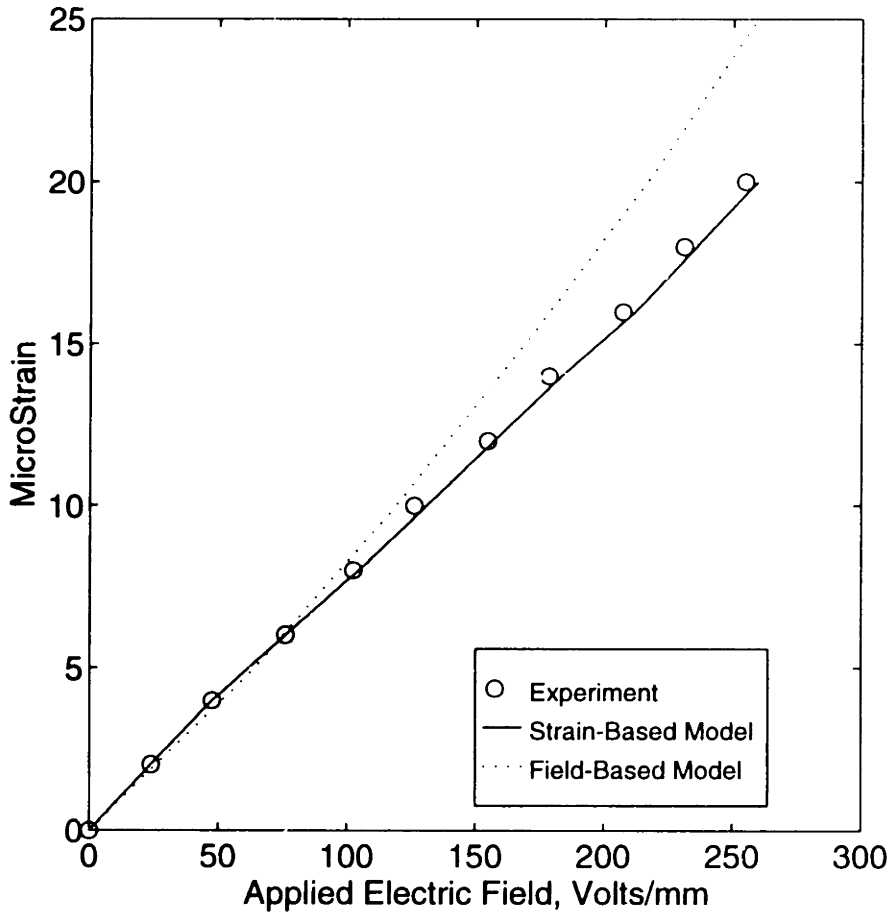

Figure 4.15: The induced strain of a piezoceramic sandwiched between layers of aluminum shows that the fundamental nonlinearity of piezoelectrics is a strain-based nonlinearity. Data is taken from Anderson (Anderson, 1989).

4.5 Material Properties

Figure 4.16 summarizes the material properties of 0.9PMN-0.1PT. Where it is possible, the parameters have been experimentally measured. When experiments are difficult, the values are taken from the literature.

Stiffness	$c^{a\,E}_{1111} = 120$ GPa from figure 4.5
Poisson's ratio	$\nu^a = 0.38$ from (Nomura and Uchino, 1982)
Dielectric constant	$\varepsilon_3^T = 17000\varepsilon_o$ from figure 4.9
m constant	$m_{12} = 6.6e\text{-}16\ m^2/v^2$ from figure 4.3
k constant	$k = 1.6e\text{-}6\ V/m$ from figure 4.3
r constant	$r_{113311} = 3.25e\text{-}24\ m^2/(v^2\ Pa)$ from figure 4.5
q^m constant (thermal effects on the electrostrictive term)	$q^m{}_{11221} = 2.2e\text{-}7\ m^2/v^2$ $q^m{}_{11222} = -1.0e\text{-}9\ m^2/(^oK\ v^2)$ $q^m{}_{11223} = 1.2e\text{-}12\ m^2/(^oK^2\ v^2)$ from figure 4.7
q^k constant (thermal effects on the relaxation parameter)	$q^k{}_1 = 8.0e\text{-}3\ \sqrt{m/v}$ $q^k{}_2 = -3.46e\text{-}5\ \sqrt{m/v}\ /^oK$ $q^k{}_3 = 4.04e\text{-}8\ \sqrt{m/v}\ /^oK^2$ from figure 4.8
Thermal expansion	$\alpha < 1e\text{-}6\ /^oC$ from (Nomura and Uchino, 1982)
Thermal conductivity	$4.3\ W/(m\ ^oC)$ from (Blackwood and Ealey, 1993)
Fracture toughness	$K_{1c} = 0.9\ MPa\sqrt{m}$ from (Freiman and White, 1994)
Ultimate strength	$\sigma_u = 24$ MPa from (Ealey and Davis, 1990)

Figure 4.16: Summary of material properties for PMN-PT.

Chapter 5

COUPLED MODELING

Actuating electrostrictor
a changing chameleon of voltage
quivering into heated blurs
as if just from a frozen fridge

Electric fields and strains
undulating temperatures
shock them with high frequency
to make them constant and tame-
while the engineer is under pressure
-Denille Marion

The until this chapter, the object has been to describe the material behavior of electrostrictor material. This chapter switches the attention to the behavior of a continuous system with a distributed active material. In such a system, the behavior of each component strongly influences the behavior of the global structure. This chapter starts by deriving the governing equations for an arbitrary nonlinear electromechanical system. These equations are then focused on the behavior of an electrostrictively coupled system. For simple geometry, the general equations of motion are simplified. The theoretical development of this chapter is based upon previous work of the authors (Fripp, Hagood, and Luoma, 1994) and upon (Hagood, Chung, and von Flotow, 1990).

5.1 Variational Principles for Nonlinear Systems

This section describes the use of variational principles to model the dynamics of nonlinear systems. First, the application of Hamilton's principle to nonlinear systems is reviewed. Particular attention is given to describe the energy terms when the state variables are coupled. Then, an electric enthalpy function is introduced in order to simplify the equations.

5.1.1 Hamilton's principle for coupled nonlinear systems

Hamilton's principle is a common variational principle in dynamics. The generalized form of Hamilton's principle for a coupled electromechanical system with a quasi-static electric field is

$$\int_{t_1}^{t_2}\left[\delta T^* - \delta U + \delta W_e^* - \delta W_m + \delta W\right]dt = 0 \tag{5.1}$$

where T^* is the complimentary kinetic energy, U is the potential energy, W_e^* is the complimentary electrical energy, W_m is the magnetic energy, and W represents the externally applied work.

For linear systems, the energy terms can be stated explicitly. With nonlinear materials, the energy terms must be integrated as the system changes. From Crandall (Crandall et al, 1968), the integral forms of the energy terms are

$$T^* = \int_V \int_0^{\dot{u}} \rho \dot{u}_j d\dot{u}_j dV \tag{5.2}$$

$$U = \int_V \int_0^S T_{ij} dS_{ij} dV \tag{5.3}$$

$$W_e^* = \int_V \int_0^E D_m dE_m dV \tag{5.4}$$

$$W_m = \int_V \int_0^B H_m dB_m dV \tag{5.5}$$

$$\delta W = \int_A f_i \, \delta u_i \, dA - \sum_j \delta \varphi_j \, q_j \tag{5.6}$$

where u represents the mechanical displacements, φ is the electric potential, f is the surface force, and q is the externally supplied charge. S is the strain, T is the stress, E is the electric field, D is the electrical displacement, B is the magnetic flux density, and H is the magnetic field.

The expressions of the energy terms given in equations (5.2) through (5.5) do not exactly express the dynamics of a system that has external constraints placed upon it. For active materials, these constraints come in the form of constitutive relationships. In these cases, it is easier to think of the energy terms as depending on a single dummy variable, ξ, which reflects the state of the system along the arbitrarily varying path. As a result, the single state variable reflects an instant in the progression of the system. The variation in energy still needs to be examined as the system changes. Substituting the dummy variable into the energy expressions changes the integrations with respect to the state variables, S, E, and B, into a integration with respect to ξ. By chain rule, equations (5.2) through equation (5.5) become

$$T^* = \int_V \int_0^{\bar{\xi}} d\dot{u}_j \rho \dot{u}_j \, dV \tag{5.7}$$

$$U = \int_V \int_0^{\bar{\xi}} S'_{ij}(\xi) T_{ij}\big(S(\xi), E(\xi)\big) \, d\xi \, dV. \tag{5.8}$$

$$W_e^* = \int_V \int_0^{\bar{\xi}} E'_m(\xi) D_m\big(S(\xi), E(\xi)\big) \, d\xi \, dV \tag{5.9}$$

$$W_m = \int_V \int_0^{\bar{\xi}} B'_m\big(S(\xi), H(\xi)\big) H_m(\xi) \, d\xi \, dV \tag{5.10}$$

The prime indicates a derivative with respect to ξ.

For electrically actuated active materials, such as electrostrictors, the magnetic energy terms are negligible. Substituting the potential energy and

the electrical energy terms from equations (5.8) and (5.9) into Hamilton's principle, equation (5.1), yields

$$\int_{t_1}^{t_2}\left[\delta T^{*} - \delta\int_V\int_0^{\bar{\xi}} \frac{\partial S_{kl}}{\partial \xi} T_{kl}\, d\xi\, dV + \delta\int_V\int_0^{\bar{\xi}} \frac{\partial E_n}{\partial \xi} D_n\, d\xi\, dV + \delta W\right] dt = 0 \quad (5.11)$$

The variation of each energy term needs to be examined with respect to each the state variables. As a result, the variations are defined as

$$\delta\int_V\int_0^{\bar{\xi}} (\cdot)\, d\xi\, dV = \int_V\int_0^{\bar{\xi}} \left\{\frac{\partial(\cdot)}{\partial E}\delta E + \frac{\partial(\cdot)}{\partial S}\delta S + \frac{\partial(\cdot)}{\partial E'}\delta E' + \frac{\partial(\cdot)}{\partial S'}\delta S'\right\} d\xi\, dV. \quad (5.12)$$

The variations are indicated by δ. Hamilton's equation states that the variation of state variables must integrate to zero. No claims are made about the variations of a derivative of a state variable, such as $\delta E'$ or $\delta S'$. As a result, the variations with respect to a derivative of a state variable, $\delta E'$ or $\delta S'$, will need to be transformed into a variation of the state variable, δE or δS, through an integration by parts with respect to ξ.

The form of Hamilton's principle given in equations (5.6-5.11) places minimal restrictions on the system. There are no constraints on the constitutive relationships; the relationships need not even be smooth. Similarly, there are no restrictions about the nature of the external forcing. The only requirement is that the strain and the electric field be continuous functions of ξ. Because of the generality of the frame work, Hamilton's principle will be utilized later in this chapter in order to derive the variational principle for an electrostrictively coupled system.

5.1.2 Thermodynamic simplification of Hamilton's principle

The derivation of the system dynamics can be simplified when the constitutive relationships are derived from a thermodynamic relationship. The thermodynamic formalism instills a compatibility between the electrical and mechanical equations. For simplicity let us examine the behavior of a system that can be described in terms of an electric enthalpy function. As

given in equation (4.7), the constitutive relationships can be defined in terms of electric enthalpy, H_2, as

$$T_{ij} = \frac{\partial H_2}{\partial S_{ij}} \qquad \text{and} \qquad D_m = -\frac{\partial H_2}{\partial E_m}. \tag{5.13}$$

Introducing the definition of electric enthalpy into Hamilton's principle, equation (5.11), yields

$$\int_{t_1}^{t_2}\left[\delta T^* - \delta\int_V\int_0^{\bar{\xi}} \frac{\partial S_{kl}}{\partial \xi}\frac{\partial H_2}{\partial S_{kl}}\,d\xi\,dV - \delta\int_V\int_0^{\bar{\xi}} \frac{\partial E_n}{\partial \xi}\frac{\partial H_2}{\partial E_n}\,d\xi\,dV + \delta W\right]dt = 0. \tag{5.14}$$

Realizing that the integrand is a chain rule expansion of H_2 allows the two integrals of H_2 to be combined. Equation (5.14) can be expressed as

$$\int_{t_1}^{t_2}\left[\delta T^* - \delta\int_V\int_0^{\bar{\xi}} \frac{\partial H_2}{\partial \xi}\,d\xi\,dV + \delta W\right]dt = \int_{t_1}^{t_2}\left[\delta T^* - \delta\int_V H_2\Big|_0^{\bar{\xi}}\,dV + \delta W\right]dt = 0 \tag{5.15}$$

where the value at $\xi = \bar{\xi}$ reflects the current state of the system and $\xi = 0$ reflects the null state of the system, i.e. $H_2(\bar{\xi})=H_2$ and $H_2(0)=0$.

Evaluating the enthalpy function in equation (5.15) produces the variational indicator of a system described by an enthalpy function as given by Tiersten (Tiersten, 1969);

$$\int_{t_1}^{t_2}\left[\delta T^* - \delta\int_V H_2\,dV + \delta W\right]dt = 0 \tag{5.16}$$

Bringing the variation on the electric enthalpy inside the integral gives

$$\int_{t_2}^{t_1}\left[\delta T^* + \int_V\left(-\frac{\partial H_2}{\partial E_n}\delta E_n - \frac{\partial H_2}{\partial S_{kl}}\delta S_{kl}\right)dV + \delta W\right]dt = 0. \tag{5.17}$$

Substituting the definitions of electric enthalpy from equation (5.13) into equation (5.17) yields the final form of the variational principle for a system which can be described by an electric enthalpy function

$$\int_{t_2}^{t_1}\left[\delta T^* + \int_V\left(D_n\delta E_n - T_{kl}\delta S_{kl}\right)dV + \delta W\right]dt = 0. \tag{5.18}$$

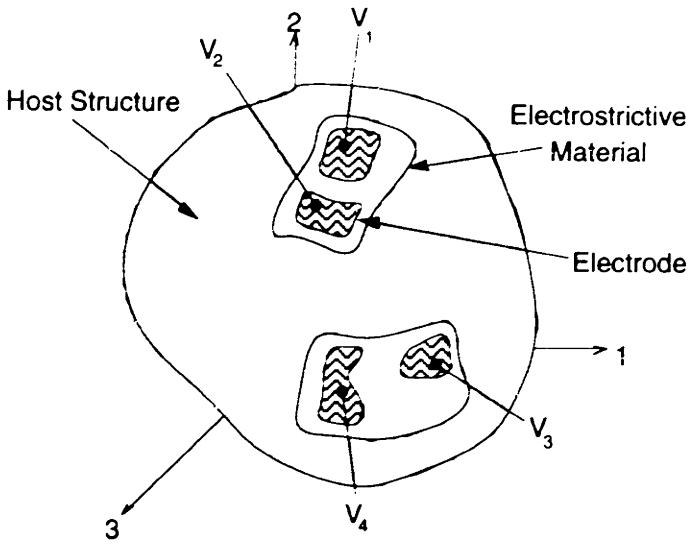

Figure 5.1: Electroelastic continuum geometry illustrating inclusions of electrostrictive material which are electroded arbitrarily

For any system where the constitutive relations can be expressed in terms of an enthalpy function, equation (5.18) is a form of the variational principle that is equivalent to the full form given in equation (5.11). This proof did not employ any assumptions as to linearity or as to the nature of the coupling. All that is required is that there exists an enthalpy function for the system that is differentiable with respect to S and E. Equation (5.18) is the standard form of Hamilton's principle for a linear piezoceramic system (Hagood et al, 1990) because such systems are derived from the thermodynamic formalism. The form of the constitutive relationships that we will use would allow the use of this thermodynamic simplification. However, not all constitutive relationships are formed from thermodynamic potentials. Often higher-order terms of constitutive relationships are discarded without rederiving the thermodynamic potential. In brief, the thermodynamic simplification is not always feasible. As a result, this thesis will address variations in the work and energy terms as given in equation (5.11) instead of jumping to the simplifications offered by equation (5.18).

5.2 General Equations of Motion

In this section, the approximate equations of motion will be derived from the variational principle expressed in (5.11). The following steps provide a general framework for dealing with nonlinear systems. Although this paper describes the derivation for an electrostrictively coupled system, the basic procedure is applicable to any nonlinear system where each component can be described by a set of piece-wise continuous, nondissipative, nonlinear algebraic constitutive relationships.

The general system is represented in Figure 5.1. The electromechanical system is composed of an elastic body with inclusions of electrostrictive material which are electroded arbitrarily. The displacements within the elastic body and electric fields about the electrodes will be combined through the electrostrictive properties to form the electromechanically coupled equations of motion.

A note on notation: During the derivation, there are times when a tensor or matrix of each value squared is needed. This representation is not easily expressed with either tensors or matrices. As a result, new notation is defined. When a matrix or tensor is raised to a power, then each element is raised to that power, but the size and rank does not change.

5.2.1 Equation for quadratic system

Several forms of the constitutive relationship for electrostrictors were derived in chapter 3. This subsection will use the quadratic model which was given in equation (3.17). Repeating the model here

$$\boxed{\begin{aligned} D_m &= \varepsilon^T_{mn} E_n + 2 m_{mnij} E_n T_{ij} \\ S_{ij} &= m_{pqij} E_p E_q + s^E_{ijkl} T_{kl}. \end{aligned}} \tag{5.19}$$

The constitutive relationship will be substituted into the general form of Hamilton's principle which was described in section 5.1.1. The evaluation of the variations needs to be performed for each of the energy expressions in equation (5.11).

5.2.1.1 Variation of kinetic energy

The complimentary kinetic energy of the system was expressed in equation (5.7) as

$$T^* = \int_V \int_0^{\dot{\xi}} d\dot{u}_j \rho \dot{u}_j \, dV \tag{5.20}$$

The variation of the kinetic energy is

$$\delta T^* = \int_V \delta \int_0^{\dot{u}} d\dot{u}^t \rho \dot{u} \, dV. \tag{5.21}$$

Bringing the variation inside of the integral gives

$$\delta T^* = \int_V \delta \dot{u}^t \rho \dot{u} \, dV. \tag{5.22}$$

Integrating by parts yields

$$\int_{t_1}^{t_2} \delta T^* \, dt = \int_V \delta \mathbf{u}^t \rho \dot{\mathbf{u}} \Big|_{t_1}^{t_2} dV - \int_{t_1}^{t_2} \int_V \delta \mathbf{u}^t \rho \ddot{\mathbf{u}} \, dV \, dt \tag{5.23}$$

where the first term must be zero. Hamilton's principle allows arbitrary variation of the path between the endpoints but requires the variation at the end points to be zero. The first term in equation (5.23) takes the difference of the variations of u at the end points t_1 and t_2 which must be zero. As a result, the variation of the kinetic energy is

$$\int_{t_1}^{t_2} \delta T^* \, dt = -\int_{t_1}^{t_2} \int_V \delta \mathbf{u}^t \rho \ddot{\mathbf{u}} \, dV \, dt \tag{5.24}$$

5.2.1.2 Variation of potential energy

The potential energy of the system, as given in equation (5.8), requires more care in its evaluation than the kinetic energy terms due to the coupling between the stress, strain, and the electrical terms. Arbitrary variation of strain and electric field is allowed, but the variables are constrained by the constitutive relationships. In order to form the variation in the face of this constraint, the two variables can be thought to depend on a single dummy

variable, ξ, which reflects the state of the system along the arbitrarily varying path. Repeating equation (5.8),

$$U = \int_V \int_0^{\bar{\xi}} S'_{ij}(\xi) T_{ij}\big(S(\xi), E(\xi)\big)\, d\xi\, dV. \tag{5.25}$$

Substituting for stress from the tensor constitutive relationship in equation (5.19) gives

$$U = \int_V \int_0^{\bar{\xi}} \underbrace{\left\{-C^E_{ijkl} m_{klpq} E_p E_q S'_{ij} + C^E_{ijkl} S_{kl} S'_{ij}\right\}}_{\tilde{U}} d\xi\, dV. \tag{5.26}$$

Taking the variation yields

$$\begin{aligned}
\delta U &= \int_V \int_0^{\bar{\xi}} \left\{ \frac{\partial \tilde{U}}{\partial E_q}\delta E_q + \frac{\partial \tilde{U}}{\partial S_{kl}}\delta S_{kl} + \frac{\partial \tilde{U}}{\partial S'_{ij}}\delta S'_{ij} \right\} d\xi\, dV \\
&= \int_V \int_0^{\bar{\xi}} \left\{ \left(-2C^E_{ijkl} m_{klpq} E_p S'_{ij}\right)\delta E_q + \left(C^E_{ijkl} S'_{ij}\right)\delta S_{kl} \right. \\
&\quad \left. + \left(-C^E_{ijkl} m_{klpq} E_p E_q + C^E_{ijkl} S_{kl}\right)\delta S'_{ij} \right\} d\xi\, dV.
\end{aligned} \tag{5.27}$$

Integrating the last term in equation (5.27) by parts in order to transform the variation of S' into a variation of S and canceling the redundant strain terms yields

$$\begin{aligned}
\delta U = \int_V \left\{ \left(\int_0^{\bar{\xi}} -2C^E_{ijkl} m_{klpq} E_p S'_{ij}\, d\xi \right)\delta E_q \right. \\
\left. + \left(\int_0^{\bar{\xi}} 2C^E_{ijkl} m_{klpq} E_p E'_q\, d\xi + \left(-C^E_{ijkl} m_{klpq} E_p E_q + C^E_{ijkl} S_{kl}\right)\Big|_0^{\bar{\xi}} \right)\delta S_{ij} \right\} dV.
\end{aligned} \tag{5.28}$$

Evaluation of the first integration is not easy and will be retained in its unevaluated form since it will be canceled by a term arising in the electrical energy expression. The second integration will be evaluated directly since there is only one path dependent variable, E. Let $\xi = \bar{\xi}$ represent the present state of the system and $\xi = 0$ correspond to zero field and zero strain conditions:

$$\begin{aligned} S\left(\xi=\tilde{\xi}\right)&=S, \qquad E\left(\xi=\tilde{\xi}\right)=E,\\ S(\xi=0)&=0, \quad \text{and} \quad E(\xi=0)=0. \end{aligned} \tag{5.29}$$

Equation (5.28) simplifies to

$$\delta U=\int_V\left\{\left(\int_0^{\tilde{\xi}}-2C^E_{ijkl}m_{klpq}E_pS'_{ij}\,d\xi\right)\delta E_q+\left(C^E_{ijkl}S_{kl}\right)\delta S_{ij}\right\}dV. \tag{5.30}$$

5.2.1.2 Variation of electrical energy

The electrical energy terms can be evaluated in a manner similar to the potential energy terms. Again, the arbitrary, yet coupled, electrical displacement and electric field variables require the introduction of a dummy variable, ξ, which indicates the state of the system along the path. As given in equation (5.8), the electrical energy of the system is

$$W^*_e=\int_V\int_0^{\tilde{\xi}}E'_m(\xi)D_m\left(S(\xi),E(\xi)\right)d\xi\,dV \tag{5.31}$$

Substituting for electrical displacement from the constitutive relationship given in equation (5.19) yields

$$W^*_e=\int_V\int_0^{\tilde{\xi}}\underbrace{\left\{\left(\varepsilon^T_{mn}-2m_{mnij}C^E_{ijkl}m_{klpq}E_pE_q\right)E_nE'_m+2m_{mnij}C^E_{ijkl}S_{kl}E_nE'_m\right\}}_{\tilde{W}^*_e}d\xi\,dV. \tag{5.32}$$

Taking the variation yields

$$\begin{aligned}\delta W^*_e&=\int_V\int_0^{\tilde{\xi}}\left\{\frac{\partial\tilde{W}^*_e}{\partial E_p}\delta E_p+\frac{\partial\tilde{W}^*_e}{\partial S_{kl}}\delta S_{kl}+\frac{\partial\tilde{W}^*_e}{\partial E'_m}\delta E'_m\right\}d\xi\,dV\\ &=\int_V\int_0^{\tilde{\xi}}\left\{\left(\varepsilon^T_{mn}E'_m-6m_{mnij}C^E_{ijkl}m_{klpq}E_pE_qE'_m\right)\delta E_n+\left(2m_{mnij}C^E_{ijkl}E_nE'_m\right)\delta S_{kl}\right.\\ &\quad\left.+\left(\varepsilon^T_{mn}E_n-2m_{mnij}C^E_{klpq}m_{klpq}E_pE_qE_n+2m_{mnij}C^E_{ijkl}E_nS_{kl}\right)\delta E'_m\right\}d\xi\,dV.\end{aligned} \tag{5.33}$$

Integrate the last term in equation (5.25) by parts in order to transform the variation of E' into a variation on E. Hamilton's principle allows arbitrary

variations of the state variable, E, but does not make any statements about the derivative of the state variable, E′. The E′ terms from the integration will cancel the E′ terms shown in equation (5.33). This yields

$$\delta W_e^* = \int_V \left\{ \left(\int_0^{\tilde{\xi}} 2m_{mnij} C_{ijkl}^E E_n E'_m \, d\xi \right) \delta S_{kl} + \left(\int_0^{\tilde{\xi}} -2m_{mnij} C_{ijkl}^E E_n S'_{kl} \, d\xi \right. \right.$$
$$\left. \left. + \left(\varepsilon_{mn}^T E_n - 2m_{mnij} C_{ijkl}^E m_{klpq} E_p E_q E_n + 2m_{mnij} C_{ijkl}^E E_n S_{kl} \right) \Big|_0^{\tilde{\xi}} \right) \delta E_m \right\} dV. \tag{5.34}$$

Evaluating the first integral which has an uncoupled integrand simplifies the equation. Again, let $\xi = \tilde{\xi}$ represent the present state of the system while $\xi = 0$ corresponds to zero field and zero strain conditions, as indicated in equation (5.29).

$$\delta W_e^* = \int_V \left\{ \left(m_{mnij} C_{ijkl}^E E_n E_m \right) \delta S_{kl} + \left(\int_0^{\tilde{\xi}} -2m_{mnij} C_{ijkl}^E E_n S'_{kl} \, d\xi \right. \right.$$
$$\left. \left. + \left(\varepsilon_{mn}^T E_n - 2m_{mnij} E_n C_{ijkl}^E m_{klpq} E_p E_q + 2m_{mnij} E_n C_{ijkl}^E S_{kl} \right) \right) \delta E_m \right\} dV \tag{5.35}$$

Each of the energy variations in equation (5.11) has now been evaluated in terms of the electrostrictive constitutive relationship. Substituting for the variations in kinetic energy, potential energy, electrical energy, and external work, Hamilton's equation becomes

$$\int_{t_1}^{t_2} \left[\int_V -\rho \ddot{u}_j \delta u_j \, dV + \int_V \left(-C_{ijkl}^E S_{ij} + m_{mnij} E_n C_{ijkl}^E E_m \right) \delta S_{kl} \, dV + \int_A f_i \, \delta u_i \, dA \right.$$
$$+ \int_V \left(\varepsilon_{mn}^T E_n - 2m_{mnij} E_n C_{ijkl}^E m_{klpq} E_p E_q + 2m_{mnij} E_n C_{ijkl}^E S_{kl} \right) \delta E_m \, dV \tag{5.36}$$
$$\left. - \sum_j q_j \delta \varphi_j \right] dt = 0$$

where the unevaluated integrals in the potential energy and electrical energy terms have canceled each other due to the assumed symmetry of the m electrostrictive terms. In other words, $m_{ijmn} = m_{mnij}$ for most electrostrictors.

Comparing the terms in equation (5.36) and in constitutive relationships given in equation (5.19), Hamilton's equation for the electrostrictively coupled system can be simplified to

$$\int_{t_1}^{t_2}\left[\int_V -\rho\ddot{u}_j\delta u_j\,dV+\int_V -T_{kl}\delta S_{kl}\,dV+\int_V D_m\delta E_m\,dV+\int_A f_i\delta u_i\,dA-\sum_j q_j\delta\varphi_j\right]dt=0. \quad (5.37)$$

For the simplified dynamics of an electrostrictor, the variational principle can be formed directly from the constitutive relationships, as indicated by section 5.1.1. The full development of the governing equations from Hamilton's principle was presented for the sake of generality and thoroughness.

5.2.2 Equation for hyperbolic tangent system

The equations of motion for an electrostrictor can be found for the hyperbolic constitutive relationships. The hyperbolic model was given in equation (3.26) as

$$\boxed{\begin{aligned} D_m &= \varepsilon^T_{mn}E_n+\frac{2}{k}m_{mnij}T_{ij}\frac{\sinh(k|E|)}{\cosh^3(k|E|)}\frac{E_n}{|E|}+\frac{2}{k}r_{mnijkl}T_{ij}T_{kl}\frac{\sinh(k|E|)}{\cosh^3(k|E|)}\frac{E_n}{|E|}\\ S_{ij} &= s^E_{ijkl}T_{kl}+\frac{1}{k^2}m_{mnij}\tanh^2(k|E|)\frac{E_mE_n}{|E|^2}+\frac{2}{k^2}r_{mnijkl}T_{kl}\tanh^2(k|E|)\frac{E_mE_n}{|E|^2}\end{aligned}} \quad (5.38)$$

The hyperbolic model was derived from thermodynamic formalism, as described in section 3.2.2. It was proven in section 5.1.1 that the final equation of motion can be written directly if a thermodynamic formalism exists. Thus, instead of repeating the steps described in the previous subsection, the constitutive relationships are substituted into equation (5.18).

$$\int_{t_1}^{t_2}\left[\int_V -\rho\ddot{u}_j\delta u_j\,dV-\int_V T_{kl}\delta S_{kl}\,dV+\int_V D_m\delta E_m\,dV+\int_A f_i\delta u_i\,dA-\sum_j q_j\delta\varphi_j\right]dt=0. \quad (5.39)$$

As a result, each term in the general equation of motion for the nonlinear system can be found directly. The potential energy expression gives

$$T_{kl}\delta S_{kl}=\left(C^*_{ijkl}S_{ij}-\frac{1}{k^2}m_{mnij}C^*_{ijkl}\tanh^2(k|E|)\frac{E_mE_n}{|E|^2}\right)\delta S_{kl} \quad (5.40)$$

and the electrical energy expression gives

$$
\begin{aligned}
D_m \delta E_m = \Bigg(& \varepsilon_{mn} E_n + \tfrac{2}{k} m_{mnij} C^*_{tuij} S_{tu} \frac{\sinh(k|E|)}{\cosh^3(k|E|)} \frac{E_n}{|E|} \\
& - \tfrac{2}{k^3} m_{mnij} m_{vwtu} C^*_{tuij} \frac{\sinh^3(k|E|)}{\cosh^5(k|E|)} \frac{E_n E_v E_w}{|E|^3} \\
& + \tfrac{2}{k} r_{mnijkl} C^*_{tuij} C^*_{pqkl} \frac{\sinh(k|E|)}{\cosh^3(k|E|)} \frac{E_n}{|E|} S_{pq} S_{tu} \\
& - \tfrac{4}{k^3} r_{mnijkl} m_{vwtu} C^*_{tuij} C^*_{pqkl} S_{pq} \frac{\sinh^3(k|E|)}{\cosh^5(k|E|)} \frac{E_n E_v E_w}{|E|^3} \Bigg) \delta E_m
\end{aligned}
\tag{5.41}
$$

By deriving the constitutive relationship from a thermodynamic formalism, extensive algebra was skipped and the resulting governing equation could be succinctly expressed.

5.3 Rayleigh-Ritz Assumptions

The previous section derived the general form of Hamilton's principle for an electrostrictively coupled electromechanical system. The general equations can be solved either in a finite elements routine or with an assumed modes formulation. Finite elements are well suited for quasi-static excitation but the assumed mode formulation give quicker results for dynamic actuation. As a result, this thesis presents the Rayleigh-Ritz assumed mode formulation.

5.3.1 Modal assumptions

The assumed modes formulation finds the strain-displacement relationship and the field-potential relationship in terms of generalized coordinates relating to the mechanical and electrical displacements. The strain-displacement and field-potential relationships can be introduced as

$$
S_{ij} = L^u_{ijq} u_q(\mathbf{x},t) \qquad \text{and} \qquad E_m = L^v_m \varphi(\mathbf{x},t) = -\varphi_{,m}(\mathbf{x},t) \tag{5.42}
$$

where u is the mechanical displacement, φ is the electric potential, L^u is the linear differential operator for the particular elasticity problem, and L^v is the negative gradient operator. In indicial notation, the elasticity operator for 3-D general elasticity is

$$L^{u}_{ijq} = \frac{1}{2}\left(\delta_{iq} \frac{\partial}{\partial r_j} + \delta_{jq} \frac{\partial}{\partial r_i} \right). \tag{5.43}$$

The deflections, u, of the structure can be expressed in terms of assumed deflection shape functions, $\psi_r(\mathbf{x})$, and the vector of time varying modal amplitudes, r(t).

$$u_q(\mathbf{x},t) = \psi^r_{qr}(\mathbf{x}) r_r(t) = \left\{ \psi^r_{q1}(\mathbf{x}) \cdots \psi^r_{qa}(\mathbf{x}) \right\} \begin{Bmatrix} r_1(t) \\ \vdots \\ r_a(t) \end{Bmatrix} \tag{5.44}$$

The modal displacement vectors are restricted only so that they obey the geometric boundary conditions of the problem. Similarly, the electrical potential can be expressed in terms of a modal vector and a vector of modal voltage amplitudes

$$\varphi(\mathbf{x},t) = \psi^v_s(\mathbf{x}) v_s(t) = \left\{ \psi^v_1(\mathbf{x}) \cdots \psi^v_b(\mathbf{x}) \right\} \begin{Bmatrix} v_1(t) \\ \vdots \\ v_b(t) \end{Bmatrix} \tag{5.45}$$

where the only restriction on the modal field vecto. is that it satisfies the prescribed electrical boundary conditions. The modal field vector must be constant across a conductor and zero at ground. We can simplify the algebra by combining the differential operators and the modal vectors

$$\begin{aligned} S_{ij}(x,t) &= N^r_{ijr}(\mathbf{x}) r_r(t) \qquad && r = 1 \cdots a \\ E_m(\mathbf{x},t) &= N^v_{ms}(\mathbf{x}) v_s(t) \qquad && s = 1 \cdots b. \end{aligned} \tag{5.46}$$

5.3.2 Equation for quadratic system

Substituting these modal assumptions and the notation definition into the matrix form of the quadratic general equations of motion, equation (5.28), gives

$$\int_{t_1}^{t_2}\Bigg[\int_V \delta r_r\left(-\ddot{r}_s\psi^r_{js}\rho\psi^r_{jr} - r_s N^r_{ijs}C^E_{ijkl}N^r_{klr} + N^r_{klr}C^E_{ijkl}m_{mnij}N^v_{ns}N^v_{mp}v_s v_p\right)dV$$

$$+\int_V \delta v_r\left(N^v_{nt}\varepsilon^T_{mn}N^v_{mr}v_t - 2N^v_{mr}N^v_{nt}m_{mnij}C^E_{ijkl}m_{klpq}N^v_{pu}N^v_{qv}v_t v_u v_v\right. \tag{5.47}$$

$$\left.+2v_t N^v_{mr}m_{mnij}N^v_{nt}C^E_{ijkl}N^r_{klu}r_u\right)dV + \int_A \delta r_r\psi^r_{ri}f_i\,dA + \sum_r \delta v_r\psi^v_s(\mathbf{x}_r)q_s\Bigg]dt = 0$$

Allowing arbitrary variations of r and v, two coupled equations in the generalized coordinates are obtained. These will be called the actuator and the sensor equations of the nonlinear electroelastic system. The actuator equation describes the dynamics of the mechanical system and the sensor equation describes the dynamics of the electrical system.

$$\begin{array}{ll} M_{sr}\ddot{r}_s + K_{sr}r_s - \Theta_{rsp}v_s v_p = B^f_r & \text{Actuator Equation} \\ 2\Theta_{utr}r_u v_t - G_{rtuv}v_t v_u v_v + Q_{rt}v_t = B^q_{rs}q_s & \text{Sensor Equation} \end{array} \tag{5.48}$$

The system mass is defined so that it includes inertial components from the electrostrictive actuator and from the host structure;

$$M_{sr} = \int_V \psi^r_{js}\rho\psi^r_{jr}\,dV \tag{5.49}$$

where ρ is a function of the position within the body and the material type. The stiffness of the system is defined so that both the electrostrictor's and the structure's stiffness are included;

$$K_{sr} = \int_V N^r_{ijs}C^E_{ijkl}N^r_{klr}\,dV. \tag{5.50}$$

where C^E is a function of the position within the body and the material type. The electromechanical coupling term is defined as

$$\Theta_{rsp} = \int_V N^r_{klr}C^{a^E}_{ijkl}m_{mnij}N_{ns}N^v_{mp}\,dV. \tag{5.51}$$

the electrostrictive capacitance is

$$Q_{rt} = \int_V N^v_{nt}\varepsilon^T_{mn}N^v_{mr}\,dV, \tag{5.52}$$

and the higher-order charge storage is

$$G_{rstq} = \int_V 2N^{\prime}_{mr} m_{mnij} C^{a^E}_{ijkl} m_{klpq} N^{\prime}_{pu} N^{\prime}_{qv} N^{\prime}_{nt} \, dV. \tag{5.53}$$

The forcing matrices are defined in terms of the modal vectors evaluated over the surfaces where the external work is supplied. The effect of the distributed forcing is found by integrating the force over the mode while the application of charge is evaluated at the r^{th} electrode.

$$B^f_r = \int_A \psi^r_n f_i \, dA \qquad \text{and} \qquad B^q_{rv} = \psi^{\prime}_v(x_r). \tag{5.54}$$

The actuator and sensor equation as given in equation (5.48) contain the generalized dynamics of an electrostrictively coupled electromechanical system. The derivation started with a generalized form of Hamilton's principle and utilized Rayleigh-Ritz assumed deflection and voltage modes.

In the actuator equation, the M, K, and B^f terms are the standard terms that arise from this approximate techniques to analyze continuous systems. The M and K terms are influenced not only by the host structure but also by the actuators. The actuator also makes its presence felt in the θ electromechanical coupling term. The quadratic behavior of the electrostrictor is indicated by the quadratic voltage terms. The B^f term indicates the effect that the forcing has upon each deflection mode of the structure.

In the sensor equation, the Q and B^q terms are the standard terms that arise from placing charge on a capacitor. The Q term is directly related to the dielectric permittivity of an electrostrictor. Due to the large relative dielectric permittivity of electrostrictors, the Q term tends to dominate the sensor equation. At large actuation fields, the higher-order charge storage matrix is significant. The electromechanical coupling in the sensor equation provided by the θ term is most significant when the electrostrictor is used as a sensor. The B^q term indicates the location of the actuator electrodes being supplied with charge.

5.3.3 Equation for hyperbolic tangent system

In this subsection, the equations of motion of an electrostrictive system are derived from the hyperbolic constitutive equations. The hyperbolic equations are given in equation (5.38) and Hamilton's expression is given in equations (5.39-5.41). Substituting the modal assumptions into the full nonlinear governing equations for the full hyperbolic tangent constitutive relations quickly becomes a nightmare of index notation. Although possible, this implementation becomes a harrowing foray requiring pages of algebra. As a result, three major simplifications are introduced: 1) notational simplification, 2) a truncation of higher-order terms in the electric field varying stiffness, and 3) a truncation of higher-order terms in the electrical energy expression .

The most fundamental simplification is a notational simplification. During the derivation, there are times when a tensor of each value squared is needed. This representation is not conveniently expressed with tensors. As a result, new notation is defined. When a tensor is raised to a power, then each element is raised to that power, but the rank does not change.

The electric field varying stiffness term, C^*, needs simplification. As described in equation (3.28), electrostrictive stiffness consists of a constant term and a field varying term.

$$C^*_{ijkl} = \left(s^E_{ijkl} + \frac{2}{k^2} r_{mnijkl} \tanh^2(k|E|) \frac{E_m E_n}{|E|^2} \right)^{-1} \tag{5.55}$$

The hyperbolic tangent function in the denominator needs to be brought into the numerator if it is to be solved with standard differential equation techniques. This transformation is done with a Taylor series expansion.

$$C^*_{ijkl} = C^*_{ijkl}\Big|_{E=0} + E \frac{\partial C^*_{ijkl}}{\partial E}\Big|_{E=0} + \text{h.o.t.} = \frac{1}{s^E_{ijkl}} - 2\frac{r_{mnijkl}}{\left(s^E_{ijkl}\right)^2} E_m E_n + \text{h.o.t.} \tag{5.56}$$

Dropping the higher-order terms, the field varying stiffness becomes

$$C^{*}_{ijkl} = \frac{1}{s^{E}_{ijkl}} - 2\frac{r_{mnijkl}}{\left(s^{E}_{ijkl}\right)^{2}}E_m E_n = C^{E}_{ijkl} - \tilde{C}_{ijklmn}E_m E_n \qquad (5.57)$$

The simplified stiffness term, equation (5.57) is substituted into the electrical energy term for the hyperbolic system which was given in equation (5.41).

$$\begin{aligned} D_m \delta E_m = \Bigg(& \varepsilon_{mn}E_n + \tfrac{2}{k} m_{mnij}\left(C^{E}_{tuij} - \tilde{C}_{tuijxy}E_x E_y\right)S_{tu}\frac{\sinh(k|E|)}{\cosh^3(k|E|)}\frac{E_n}{|E|} \\ & - \tfrac{2}{k^3} m_{mnij}m_{vwtu}\left(C^{E}_{tuij} - \tilde{C}_{tuijxy}E_x E_y\right)\frac{\sinh^3(k|E|)}{\cosh^5(k|E|)}\frac{E_n E_v E_w}{|E|^3} \\ & + \tfrac{2}{k} r_{mnijkl}\left(C^{E}_{tuij} - \tilde{C}_{tuijxy}E_x E_y\right)\left(C^{E}_{pqkl} - \tilde{C}_{pqklvw}E_v E_w\right)\frac{\sinh(k|E|)}{\cosh^3(k|E|)}\frac{E_n}{|E|}S_{pq}S_{tu} \\ & - \tfrac{4}{k^3} r_{mnijkl}m_{vwtu}C^{*}_{tuij}C^{*}_{pqkl}S_{pq}\frac{\sinh^3(k|E|)}{\cosh^5(k|E|)}\frac{E_n E_v E_w}{|E|^3}\Bigg)\delta E_m \end{aligned} \qquad (5.58)$$

Neglecting any terms that include any combination of strain and electric field that is higher than third order, the electrical energy expression becomes

$$\begin{aligned} D_m \delta E_m = \Bigg(& \varepsilon_{mn}E_n + \tfrac{2}{k} m_{mnij}C^{E}_{tuij}S_{tu}\tanh(k|E|)\frac{E_n}{|E|} \\ & - \tfrac{2}{k^3} m_{mnij}m_{vwtu}C^{E}_{tuij}\frac{\sinh^3(k|E|)}{\cosh^5(k|E|)}\frac{E_n E_v E_w}{|E|^3} \\ & + \tfrac{2}{k} r_{mnijkl}C^{E}_{tuij}C^{E}_{pqkl}S_{pq}S_{tu}\frac{\sinh(k|E|)}{\cosh^3(k|E|)}\frac{E_n}{|E|}\Bigg)\delta E_m \end{aligned} \qquad (5.59)$$

By restricting the system to a maximum of third-order coupling, the variations in the electric field are removed from the electrical energy expression.

The simplified stiffness term, equation (5.57), is also substituted into the mechanical energy term for the hyperbolic system which was given in equation (5.40).

$$T_{kl}\delta S_{kl} = \Big(\big(C^E_{ijkl} - \tilde{C}_{ijklmn}E_mE_n\big)S_{ij} - \\ - \tfrac{1}{k^2} m_{mnij}\big(C^E_{ijkl} - \tilde{C}_{ijklmn}E_mE_n\big)\tanh^2(k|El)\frac{E_mE_n}{|El|^2}\Big)\delta S_{kl} \tag{5.60}$$

Neglecting terms that are higher than third-order simplifies the mechanical energy terms to

$$T_{kl}\delta S_{kl} = \Big(C^E_{ijkl}S_{ij} - \tilde{C}_{ijklmn}E_mE_nS_{ij} - \tfrac{1}{k^2} m_{mnij}C^E_{ijkl}\tanh^2(k|El)\frac{E_mE_n}{|El|^2}\Big)\delta S_{kl} \tag{5.61}$$

The total coupled equations of motion are found by substituting the electrical energy, equation (5.59), and the mechanical energy, equation (5.61), into the expression of Hamilton's principle given in equation (5.39).

The system of equations can be expressed in the simplified Rayleigh-Ritz formulation through the modal assumptions given in subsection (5.3.1). Substituting the modal assumptions and allowing arbitrary variations of displacements and voltage, two coupled equations of motion are obtained in the generalized coordinates. For the hyperbolic model, the actuator and sensor equations become

$$\begin{array}{ll} M_{ps}\ddot{r}_p + K_{ps}r_p + \tilde{K}_{pqrs}r_pv_qv_r + \Theta_{tus}F^*_tF^*_u + \tilde{\Theta}_{tuvws}F^*_tF^*_uv_vv_w = B^f_s & \text{Actuator Equation} \\ Q_{rs}v_r + 2\Theta_{prs}F^*_pr_r + G_{klps}\beta^*F^*_kF^*_lF^*_p + R_{rvws}\beta^*F^*_wr_rr_v = B^q_s & \text{Sensor Equation} \end{array} \tag{5.62}$$

The hyperbolic electric field dependence has been incorporated into two terms

$$F^*_n = \int_V \tfrac{1}{k}\tanh\Big(k\sqrt{N^v_{ij}N^v_{ik}v_jv_k}\Big)\frac{v_n}{\sqrt{N^v_{pq}N^v_{pr}v_qv_r}}\,dV \tag{5.63}$$

and

$$\beta^* = \int_V \operatorname{sech}^2\Big(k\sqrt{N^v_{ij}N^v_{ik}v_jv_k}\Big)dV \tag{5.64}$$

The mass matrix does not change with the additional of higher-order material nonlinearities. As given in equation (5.49)

$$M_{ps} = \int_V \psi^r_{jp}\rho\psi^r_{js}\,dV \tag{5.65}$$

Similarly, the stiffness of the system has been divided into two terms. The zero field stiffness is the same as that used in the previous subsection. As given in equation (5.50)

$$K_{ps} = \int_V N^r_{ijp} C^E_{ijkl} N^r_{kls} \, dV \tag{5.66}$$

However, the addition of the elastostriction term introduces a stiffness term that is electric field dependent. In this case, the stiffness correction is

$$\tilde{K}_{pqrs} = \int_V \tilde{C}_{ijklmn} N^r_{ijp} N^r_{kls} N^v_{mq} N^v_{nr} \, dV \tag{5.67}$$

The electromechanical coupling term changes mildly by changing from the quadratic to the hyperbolic tangent formulation:

$$\Theta_{tus} = \int_V m_{mnij} C^E_{ijkl} N^r_{kls} N^v_{mt} N^v_{nu} \, dV \tag{5.68}$$

As with the stiffness term, the electromechanical coupling is strongly dependent on the stiffness of the electrostrictor. Since the stiffness varies with electric field, there is an electric field based correction to the electromechanical coupling term

$$\tilde{\Theta}_{tuvws} = \int_V m_{mnij} \tilde{C}_{ijklpq} N^r_{kls} N^v_{mt} N^v_{nu} N^v_{pv} N^v_{qw} \, dV \tag{5.69}$$

The electrostrictive capacitance does not change from the form given in equation (5.50)

$$Q_{rt} = \int_V N^v_{nt} \varepsilon^T_{mn} N^v_{mr} \, dV, \tag{5.70}$$

The higher-order charge storage is changed to

$$G_{klps} = \int_V 2 m_{mnij} m_{vwtu} C^E_{tuij} N^v_{ms} N^v_{nk} N^v_{vl} N^v_{wp} \, dV \tag{5.71}$$

The inclusion of the elastostriction term introduces a elastostriction charge storage term

$$R_{rvws} = \int_V 2 r_{mnijkl} C^E_{tuij} C^E_{pqkl} N^r_{pqr} N^r_{tuv} N^v_{nw} N^v_{ms} \, dV \tag{5.72}$$

5.3.4 Rayleigh-Ritz and finite-elements

The dynamic equations of motion for a distributed electrostrictively coupled system are given in equations (5.48) and equation (5.62). These equations are presented in terms of a Rayleigh-Ritz formulation. This presentation has been a misnomer because the same equations can be used in the same form in a finite-elements formulation. This is because *Rayleigh-Ritz and finite-element methods are fundamentally the same thing.* In finite-elements methods, FEM, each node introduces another degree-of-freedom. In Rayleigh-Ritz formulation, RRF, shape functions represent each degree-of-freedom. With either scenario, the resulting dynamics are formed from the available degrees-of-freedom. As a result, the same governing equations are used in either formulation technique. A shift between RRF and FEM only requires a redefinition of the mechanical and electrical shape functions, ψ^r and $\psi^\wedge$.

RRF require more engineering insight than FEM. In FEM every possible degree-of-freedom is considered for possible motion. RRF limits the possible motions to those which are probable for the system. Engineering intuition is needed to select the proper shape functions. Two advantages result from applying good engineering judgment in a RRF: 1) speed and 2) more intuition into the system.

RRF dramatically reduce the number of available degrees-of-freedom. A typical RRF uses 5 shape functions while a moderate FEM routine will use a thousand nodes and, hence, a thousand degrees-of-freedom for the same structure. The reduction in computation time and in computer memory requirements is tremendous.

If good judgment is used in the determination of the shape functions used in the RRF, then extra insight is gathered about the system. By seeing the relative importance of physically meaningful shape functions, a better understanding of the behavior of the system is gleaned. For complicated systems where engineering insight fails or for systems which are too

complicated for a simple set of shape functions, then RRF will fail while FEM will still succeed. However, for the systems considered in this thesis, RRF will provide quicker and more meaningful solutions.

5.4 Simplifications of General Equations

In the most general form, the constitutive relationships for electrostrictors and the governing equations for an electrostrictively coupled electromechanical system are best described in index notation. However, index notation requires thirteen indices for the quadratic model and even more for the hyperbolic model, which is rather cumbersome. The general equations can be transformed into simpler forms for the case when there is only one prescribed voltage source or for the case when the voltages are in only one direction. For this case, the equations can be placed in state-space form when the voltage is a prescribed function. Both forms are presented in this section.

A note on notation: During the derivation, there are times when a tensor or matrix of each value squared is needed. This representation is not easily expressed with either tensors or matrices. As a result, new notation is defined. When a matrix or tensor is raised to a power, then each element is raised to that power, but the size and rank does not change.

5.4.1 Matrix form of quadratic model

This simplification of the quadratic equations for an electrostrictively coupled electromechanical system assumes that there is only one prescribed voltage source (i.e. v is scalar). In this case, equation (5.48) reduces to

$$\boxed{\begin{array}{ll} \mathbf{M}\ddot{\mathbf{r}} + \mathbf{K}\mathbf{r} - \Theta^{*}\mathrm{v} = \mathbf{B}^{\mathrm{f}} & \text{Actuator Equation} \\ 2\Theta^{\mathrm{t}}\mathrm{v}\mathbf{r} - \mathrm{G}^{*}\mathrm{v} + \mathrm{Q}\mathrm{v} = \mathrm{B}^{\mathrm{q}}\mathrm{q} & \text{Sensor Equation.} \end{array}} \tag{5.73}$$

where the θ^{*} matrix and the G^{*} term include voltage dependencies. The matrix form of the system mass, system stiffness, and the electrostrictive capacitance remain essentially unchanged from the form given in equations (5.49), (5.50), and (5.52). The mass matrix is

$$\mathbf{M} = \int_V \psi^{r^t} \rho \psi^r \, dV. \tag{5.74}$$

Similarly, the stiffness matrix is

$$\mathbf{K} = \int_V \mathbf{N}^{r^t} \mathbf{C}^E \mathbf{N}^r \, dV. \tag{5.75}$$

The electrostrictive capacitance matrix is

$$\mathbf{Q} = \int_V \mathbf{N}^{v^t} \varepsilon^T \mathbf{N}^v \, dV, \tag{5.76}$$

and influence matrices are

$$\mathbf{B}^f = \int_A \psi^{r^t} \mathbf{f} \, dA \qquad \text{and} \qquad B^q = \psi^{v^t}(\mathbf{x}). \tag{5.77}$$

The electrostrictive term, m, necessitates a rearrangement of the electromechanical coupling term and the higher-order charge storage term. The electromechanical coupling matrix becomes

$$\theta^* = \int_V \mathbf{N}^{r^t} \mathbf{C}^{a^E} \mathbf{m}^{*^t} \mathbf{N}^v \, dV \tag{5.78}$$

and the higher-order charge storage matrix is

$$\mathbf{G}^* = \int_V 2\mathbf{N}^{v^t} \mathbf{m}^* \mathbf{C}^{a^E} \mathbf{m}^{*^t} \mathbf{N}^v \, dV. \tag{5.79}$$

The matrix form of the terms used in equations (5.74-5.79) are the expansions of the tensors previously defined in this chapter. The matrix form of the electric field varying electrostriction term was given in equation (3.21) as

$$\mathbf{m}^* = \begin{bmatrix} m_{11}E_1 & m_{12}E_1 & m_{12}E_1 & 0 & m_{44}E_3 & m_{44}E_2 \\ m_{12}E_2 & m_{11}E_2 & m_{12}E_2 & m_{44}E_3 & 0 & m_{44}E_1 \\ m_{12}E_3 & m_{12}E_3 & m_{11}E_3 & m_{44}E_2 & m_{44}E_1 & 0 \end{bmatrix} \tag{5.80}$$

The dielectric coupling terms was defined in equation (3.20) as

$$\varepsilon^{T} = \begin{bmatrix} \varepsilon_1^{T} & 0 & 0 \\ 0 & \varepsilon_2^{T} & 0 \\ 0 & 0 & \varepsilon_3^{T} \end{bmatrix}, \tag{5.81}$$

The stiffness terms of the symmetric electrostrictor at constant electric field are

$$\mathbf{C}^{E} = \begin{bmatrix} C_{11}^{E} & C_{12}^{E} & C_{12}^{E} & 0 & 0 & 0 \\ C_{12}^{E} & C_{11}^{E} & C_{12}^{E} & 0 & 0 & 0 \\ C_{12}^{E} & C_{12}^{E} & C_{11}^{E} & 0 & 0 & 0 \\ 0 & 0 & 0 & C_{44}^{E} & 0 & 0 \\ 0 & 0 & 0 & 0 & C_{44}^{E} & 0 \\ 0 & 0 & 0 & 0 & 0 & C_{44}^{E} \end{bmatrix}. \tag{5.82}$$

The mechanical displacement shape function is a matrix of the deformation shapes of all of the shape functions. The mechanical displacement is given by the product of the shape function with their time varying amplitudes.

$$\mathbf{u}(\mathbf{x},t) = \psi^{r}(\mathbf{x})\mathbf{r}(t) = \begin{bmatrix} \psi_{11}^{r}(\mathbf{x}) & \psi_{12}^{r}(\mathbf{x}) & \cdots \\ \psi_{21}^{r}(\mathbf{x}) & \psi_{22}^{r}(\mathbf{x}) & \cdots \\ \psi_{31}^{r}(\mathbf{x}) & \psi_{32}^{r}(\mathbf{x}) & \cdots \end{bmatrix} \begin{Bmatrix} r_1(t) \\ r_2(t) \\ \vdots \end{Bmatrix} \tag{5.83}$$

The strains in the structure are product of the linear differential operator for the particular elasticity problem and the vector of mechanical displacements.

$$\mathbf{S}(\mathbf{x},t) = \mathbf{N}^{r}(\mathbf{x})\mathbf{r}(t) = \begin{bmatrix} \frac{\partial}{\partial x} & 0 & 0 \\ 0 & \frac{\partial}{\partial y} & 0 \\ 0 & 0 & \frac{\partial}{\partial z} \\ 0 & \frac{1}{2}\frac{\partial}{\partial z} & \frac{1}{2}\frac{\partial}{\partial y} \\ \frac{1}{2}\frac{\partial}{\partial z} & 0 & \frac{1}{2}\frac{\partial}{\partial x} \\ \frac{1}{2}\frac{\partial}{\partial y} & \frac{1}{2}\frac{\partial}{\partial x} & 0 \end{bmatrix} \begin{bmatrix} \psi_{11}^{r}(\mathbf{x}) & \psi_{12}^{r}(\mathbf{x}) & \cdots \\ \psi_{21}^{r}(\mathbf{x}) & \psi_{22}^{r}(\mathbf{x}) & \cdots \\ \psi_{31}^{r}(\mathbf{x}) & \psi_{32}^{r}(\mathbf{x}) & \cdots \end{bmatrix} \begin{Bmatrix} r_1(t) \\ r_2(t) \\ \vdots \end{Bmatrix} \tag{5.84}$$

The electrical potentials correspond to the voltages at the electrodes.

$$\varphi(\mathbf{x},t) = \psi^{v}(\mathbf{x})v(t) \tag{5.85}$$

The electrical field comes from the variation of the electrical potential;

$$\mathbf{E}(\mathbf{x},t) = \mathbf{N}^{v}(\mathbf{x})v(t) = -\nabla\psi^{v}v \tag{5.86}$$

where ∇ is the gradient operator.

The form of the actuator and sensor equation as given in equation (5.59) represent a simplification when only one actuator is present on the structure. The general form of the actuator and sensor equations, equation (5.39), can also be readily translated to matrix form for other actuation scenarios, such when as the electric field is present in only one direction.

5.4.2 State-space representation of quadratic system

Although electrostrictors are nonlinear elements, actuation with electrostrictors can be modeled as a linear plant with a nonlinear input for the case when there is only one actuator. In other words, the nonlinear system given in equation (5.48) can be placed in a state-space form when the voltages are prescribed functions of time. The system can be described as

$$\begin{Bmatrix} \dot{\mathbf{x}} \\ \mathbf{y} \end{Bmatrix} = \begin{bmatrix} \mathbf{A} & \mathbf{B} \\ \mathbf{C} & \mathbf{D} \end{bmatrix} \begin{Bmatrix} \mathbf{x} \\ \mathbf{u} \end{Bmatrix} \tag{5.87}$$

where

$$\mathbf{x} = \begin{Bmatrix} \mathbf{r} \\ \dot{\mathbf{r}} \end{Bmatrix}, \qquad \mathbf{u} = \begin{Bmatrix} \mathbf{f} \\ \mathbf{v} \end{Bmatrix} \tag{5.88}$$

$$\mathbf{A} = \begin{bmatrix} \mathbf{0} & \mathbf{I} \\ -\mathbf{M}^{-1} & -\mathbf{M}^{-1}\mathbf{C}^{\mathrm{d}} \end{bmatrix}, \quad \text{and} \quad \mathbf{B} = \begin{bmatrix} \mathbf{0} & \mathbf{0} \\ \mathbf{M}^{-1}\mathbf{B}^{\mathrm{f}} & \mathbf{M}^{-1}\Theta^{*} \end{bmatrix}. \tag{5.89}$$

$\mathbf{C}^{\mathrm{d}}$ is a possible viscous damping matrix and the electromechanical coupling θ^{*} includes a factor of electric field. The output equations depend on which variables are desired. Let us assume that the strain values at some discrete location are desired, then the other parts of equation (5.87) become

$$\mathbf{y} = \mathbf{S}(\mathrm{x}_{\mathrm{i}}), \qquad \mathbf{C} = \left[\mathbf{N}^{\mathrm{r}}(\mathrm{x}_{\mathrm{i}}) \quad \mathbf{0}\right], \qquad \text{and} \qquad \mathbf{D} = \left[\mathbf{0} \quad \mathbf{0}\right]. \tag{5.90}$$

Although the voltage-driven case readily lends itself to state-space format, the charge-driven couplings would require significant algebraic effort in order to place them in a similar format.

5.4.3 State-space representation of hyperbolic system

5.4.3.1 Without elastostriction

The general equations of motion which involve hyperbolic trigonometry can also be placed in a state-space representation. For this simplification, it is assumed that the elastostriction term is zero. Also, it is assumed that the voltages are prescribed functions of time. In other words, it is assumed that the active materials are actuators. But there are no restrictions on the number of active elements. As a result, equation (5.62) can be described as

$$\begin{Bmatrix} \dot{\mathbf{x}} \\ \mathbf{y} \end{Bmatrix} = \begin{bmatrix} \mathbf{A} & \mathbf{B} \\ \mathbf{C} & \mathbf{D} \end{bmatrix} \begin{Bmatrix} \mathbf{x} \\ \mathbf{u} \end{Bmatrix} \tag{5.91}$$

where

$$\mathbf{x} = \begin{Bmatrix} \mathbf{r} \\ \dot{\mathbf{r}} \end{Bmatrix}, \qquad \mathbf{u} = \begin{Bmatrix} \mathbf{f} \\ \left(\frac{1}{k} \tanh\left(k\sqrt{\mathbf{v}^t \mathbf{N}^{v^t} \mathbf{N}^v \mathbf{v}} \right) \frac{\mathbf{N}^v \mathbf{v}}{\left(\mathbf{v}^t \mathbf{N}^{v^t} \mathbf{N}^v \mathbf{v} \right)} \right)^2 \end{Bmatrix} \tag{5.92}$$

$$\mathbf{A} = \begin{bmatrix} \mathbf{0} & \mathbf{I} \\ -\mathbf{M}^{-1}\mathbf{K} & -\mathbf{M}^{-1}\mathbf{C}^d \end{bmatrix}, \quad \text{and} \quad \mathbf{B} = \begin{bmatrix} \mathbf{0} & \mathbf{0} \\ \mathbf{M}^{-1}\mathbf{B}^f & \mathbf{M}^{-1}\Theta \end{bmatrix}. \tag{5.93}$$

The output equations depend on which variables are desired. Let us assume that the strain values at some discrete location are desired, then the other parts of equation (5.91) become

$$\mathbf{y} = \mathbf{S}(x_i), \qquad \mathbf{C} = \begin{bmatrix} \mathbf{N}^r(x_i) & \mathbf{0} \end{bmatrix}, \qquad \text{and} \qquad \mathbf{D} = \begin{bmatrix} \mathbf{0} & \mathbf{0} \end{bmatrix}. \tag{5.94}$$

The mass, stiffness, and influence matrices remain unchanged from the form given in equations (5.74), (5.75), and (5.77). The electromechanical coupling matrix is now defined as

$$\Theta = \int_V \mathbf{N}^{r^t} \mathbf{C}^{a^E} \mathbf{m}^t \, dV \tag{5.95}$$

5.4.3.2 With elastostriction

If only a one-dimensional investigation is required, then the reduced actuation due to the elastostriction effect can be added. Since the actuation is one-dimensional, the elastostriction term, r, the electrostriction term, m, and the stiffness term, C^E, are scalar. In this case, the forcing term given in equation (5.91) would include the $\tilde{\Theta}$ term described in equation (5.69). As a result the forcing term and the coupling term need to be redefined.

$$\mathbf{u} = \begin{Bmatrix} \mathbf{f} \\ \left(\frac{1}{k}\tanh\left(k\sqrt{\mathbf{v}^t\mathbf{N}^{v^t}\mathbf{N}^v\mathbf{v}}\right)\frac{\mathbf{N}^v\mathbf{v}}{\left(\mathbf{v}^t\mathbf{N}^{v^t}\mathbf{N}^v\mathbf{v}\right)}\right)^2 \\ \left(\frac{1}{k}\tanh\left(k\sqrt{\mathbf{v}^t\mathbf{N}^{v^t}\mathbf{N}^v\mathbf{v}}\right)\frac{\mathbf{N}^v\mathbf{v}}{\left(\mathbf{v}^t\mathbf{N}^{v^t}\mathbf{N}^v\mathbf{v}\right)}\right)^2 \mathbf{v}^t\mathbf{N}^{v^t}\mathbf{N}^v\mathbf{v} \end{Bmatrix} \tag{5.96}$$

and

$$\mathbf{B} = \begin{bmatrix} 0 & 0 & 0 \\ \mathbf{M}^{-1}\mathbf{B}^f & \mathbf{M}^{-1}\Theta & -\mathbf{M}^{-1}\tilde{\Theta} \end{bmatrix}. \tag{5.97}$$

The elastostriction coupling matrix is defined as

$$\tilde{\Theta} = \int_V \mathbf{N}^{r^t}\tilde{C}m^t dV = \int_V 2\mathbf{N}^{r^t}C^{E^2}r\mathbf{N}^v\mathbf{N}^{v^t}m^t dV \tag{5.98}$$

Only one of the elastostriction coupling terms is included in this state-space representation. This elastostriction term describes how the decreasing stiffness and higher electric fields produces decreasing actuation potential. The term that is neglected describes how the decreasing stiffness produces varying natural frequencies.

Chapter 6

STRUCTURAL EXPERIMENTS

Ceramic devices that shiver
Structural deflectors that quiver
The end to man's vices
Lies in these devices
Electrostrictors .. they deliver!
-Eric Wobells

Experiments were conducted to test the validity of the analytical models of the electrostrictively coupled electromechanical system that were derived in chapter 5. In these tests, the electrostrictor was driven by a prescribed voltage and both the strain and the induced charge were measured.

6.1 Experimental Setup

6.1.1 Physical setup and data reduction

The experiments were conducted on a cantilevered aluminum beam with a surface-bonded electrostrictive wafer, as indicated in figure 6.1. The beam is 37.8 cm long, 2.7 cm wide, and 0.16 cm thick. An electrostrictor was bonded to one side of the beam 2.1 cm from the base and extends 2.7 cm. The electrostrictor is a 0.027 cm thick 0.9 PMN-0.1 PT ceramic wafer manufactured by AVX. The surfaces were electroded with aluminum and the transverse properties of the wafers (i.e. m_{1122} values) were utilized. The wafer was bonded to one side of the beam. Transverse motion of the wafer induced not only a moment, but also stretching in the beam. The maximum relative

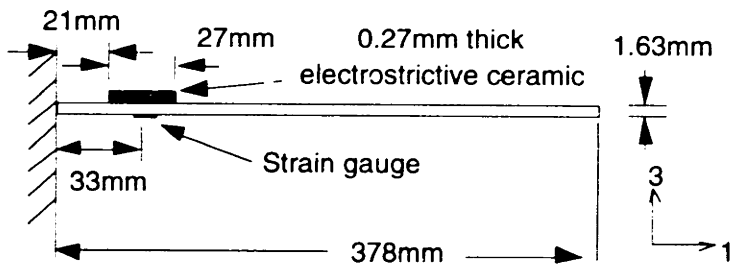

Figure 6.1: Cantilevered beam test article

dielectric of this electrostrictor occurred at a temperature of 40°C. Unless otherwise noted, all of the experiments were conducted with the wafer temperature at 28°C. As a result, the experimental data will feature larger hysteresis than the classic curves of an electrostrictor and will feature larger strains (Blackwood and Ealey, 1993) (Uchino et al, 1982).

The basic material properties of the beam and the electrostrictive actuator are given in figure 6.2. A more complete summary of the electrostrictive material properties are given in figure 4.9. The damping ratio of the beam was measured with a ring-down test for the first three dynamic modes of the beam, the dielectric permittivity was measured with an Omega multimeter, and the electromechanical coupling terms were obtained from free wafer tests as described in section 4.

The electrostrictive wafer was excited with a Kepco model BOP 1000M voltage amplifier which was fed a sinusoidal signal from a Phillips model PM 5191 function generator. The modal displacements were measured with a strain gauge located on the reverse side of the beam from the electrostrictive wafer, 3.3 cm from the base. Data was collected on a Macintosh Quadra 950 using LabView software running at 4 kHz. The electrical displacement was measured by integrating the current applied to the actuator.

The strain data was windowed in the frequency domain with an eleven point Hamming window and then averaged in the time domain over four cycles. A similar process was performed on the voltage data in order to eliminate the possible effects of added phase. A more detailed description of

Beam:	Stiffness	$C^{s}_{111.} = 68$ GPa
	Poisson's ratio	$\nu^{s} = 0.33$
	Damping ratio	
	- First mode	$\zeta = 0.6\%$
	- Second mode	$\zeta = 0.4\%$
	- Third mode	$\zeta = 0.3\%$
Electrostrictor:	Stiffness	$C^{a^{E}}_{1111} = 120$ GPa
	Dielectric constant	$\varepsilon_3^{T} = 17000\varepsilon_{\circ}$
	m constant	$m_{12} = 6.6e\text{-}16\ m^2/v^2$
	k constant	$k = 1.6e\text{-}6$ V/m

Figure 6.2: Material properties of the aluminum beam and electrostrictive actuator

the data reduction was presented in subsection 4.1.2 of the chapter dealing with materials testing.

6.1.2 Model comparison and shape functions

The experimental results are compared with the models developed in chapter 5. Two expressions of the coupled structure interaction were developed: a hyperbolic model and a quadratic model. The hyperbolic model is more general than the quadratic model and expresses the electromechanical coupling in terms of hyperbolic tangent functions. The state-space form of the hyperbolic model is expressed in subsection 5.4.3.1. The quadratic model is the low field simplification of the hyperbolic model and features a quadratic electromechanical coupling. The state-space form of the quadratic model is expressed in subsection 5.4.2. The values used in the simulations of the experimental data are taken from values presented in the literature or previously calculated in this thesis. No iteration was attempted to enhance the correlation between the experiments and the model.

For all of the model simulations, the driving voltage was a single frequency sinusoid and the beam was initially at rest. The model used seven assumed deflection shape functions, $\psi_r(x)$. Five of these deflection modes

reflect the exact mode shape for a uniform cantilevered beam. The other two mode shapes represent the beam profile if there was a static electric field on the electrostrictive wafer; one mode represented bending while the other mode represented extension. These "static" mode shapes help to better represent any residual strain energy due to the discontinuous stiffness at the electrostrictor (Fleming and Crawley, 1991).

The exact mode shapes for a cantilevered beam are (Meirovitch, 1985)

$$\psi_{3r}^{r}(x) = (\cosh \lambda_r x - \cos \lambda_r x) - \alpha_r (\sinh \lambda_r x - \sin \lambda_r x) \tag{6.1}$$

where λ and α are unique for each mode of the structure. The first "static" mode shape represents the bending induced by the electrostrictive wafer. This mode has constant curvature around the actuator and zero curvature elsewhere. If a_1 and a_2 represent the endpoints of the actuator, then the static bending mode is given by

$$\psi_{3r}^{r} = \begin{cases} 0 & x < a_1 \\ \frac{1}{2}(x - a_1)^2 & a_1 < x < a_2 \\ (a_2 - a_1)\left(x - \frac{1}{2}(a_2 - a_1)\right) & a_2 < x \end{cases}. \tag{6.2}$$

The "static" mode shape associated with extension exhibits constant slope around the actuator and zero slope elsewhere.

$$\psi_{1r}^{r} = \begin{cases} 0 & x < a_1 \\ \dfrac{x - a_1}{a_2 - a_1} & a_1 < x < a_2 \\ 1 & a_2 < x \end{cases} \tag{6.3}$$

The process of applying Rayleigh-Ritz analysis to a beam with surface mounted actuators is explained in detail in other sources (Fripp, Hagood, and Luoma, 1994) (Hagood et al, 1990) and more generally in (Meirovitch, 1985).

6.2 Quasi-Static Response

The quasi-static response of the cantilevered beam system is illustrated in figure 6.3. A prescribed voltage was placed across the electrostrictive wafer and the resulting strain was measured. The applied voltage was in the form of a 0.1 Hertz sinusoid. The theoretical strain was found by numerically evaluating the state-space form of the actuator equation. The hyperbolic model is presented in equation (5.70) and the quadratic model is presented in equation (5.66). The quadratic model is the low-field simplification of the hyperbolic model.

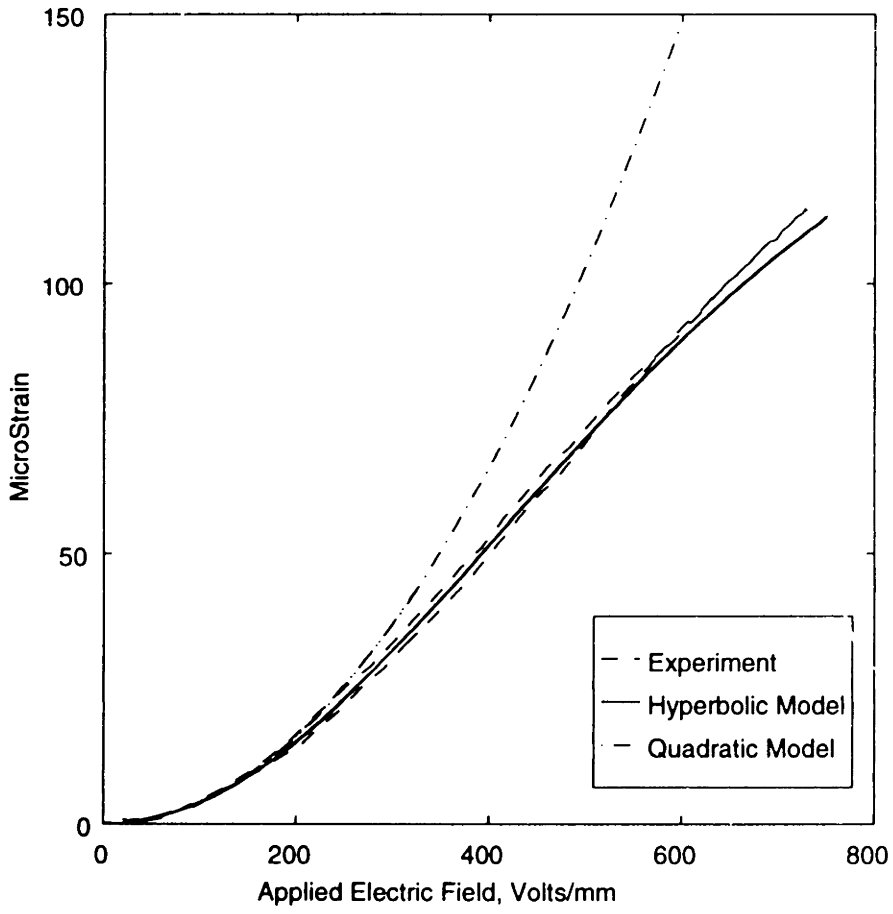

Figure 6.3: Quasi-static deflections of the cantilevered beam. The hyperbolic model used equation (5.70) to predict the response. The quadratic model used equation (5.66).

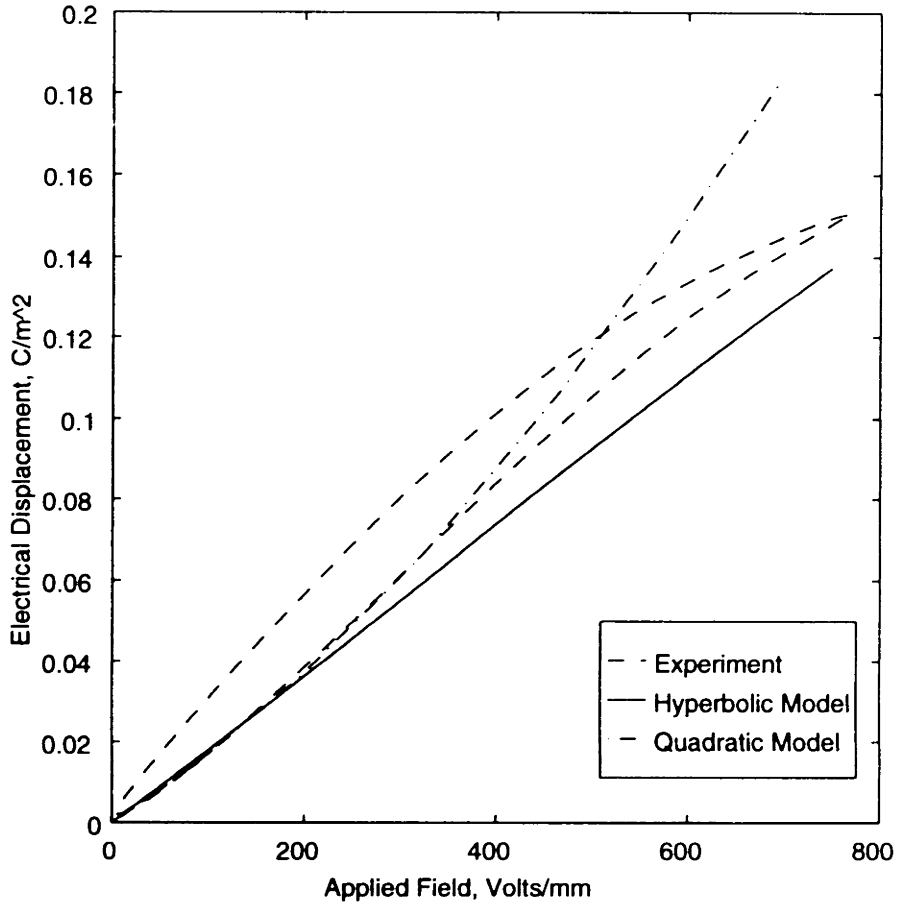

Figure 6.4: Charge variations on the electrostrictor during 6 Hz dynamic actuation. The hyperbolic model used the state-space form of the sensor equation as given by equation (5.70) and the quadratic model used equation (5.48) to calculate the response. The discrepancy between the modeled and experimental result could result from a variation in the dielectric permittivity.

At low fields, good agreement is achieved with both model and experiments when both static modes are included in the Rayleigh-Ritz approximations, as shown in figure 6.3. The quadratic model tends to break down above 300 V/mm because the initial simplifying approximations are no longer valid at the higher field levels. The hyperbolic model provides excellent agreement across the entire range of applied electric field levels.

6.3 Charge Variation

The sensor equation of an electrostrictively-coupled system can be verified by examining the charge variation on the electrostrictive wafer. In this case, a 6.00 Hertz sinusoidal voltage signal was supplied to the wafer. The charge on the electrostrictor was determined by integrating the current applied to the electrostrictor. The current supplied to the electrostrictor was measured with a sensing resistor in series with the electrostrictor. The integrating circuit featured a single pole integrator with a corner at 0.1 Hertz. The charge in the simulation was calculated through the sensor relation in the general equations of motion. The hyperbolic model is given in equation (5.62) and the quadratic model is expressed in equation (5.48).

As shown in figure 6.4, the quadratic model over predicts the charge at large electric field levels. The hyperbolic model under predicts the charge at all levels, but more closely approximates the shape of the charge-field curve. The mismatch between experimental and modeled performance in the low-field region suggests that the dielectric permittivity of the electrostrictor might have been larger than that which was used in the model. The dielectric is sensitive to changes in temperature, frequency, and electric field. The dielectric was calculated from the capacitance measured by the Omega multimeter. The multimeter measures the capacitance at 390 Hz. The capacitance of electrostrictors increases as the frequency decreases (Namboodri, 1992). The capacitance could increase by 20% in the frequency range between the 390 Hz measurement and the 6 Hz experiment. A 20% increase in the capacitance would provide a very close correlation between the experiment and the model in figure 6.4.

6.4 Frequency Response

For a linear system, the frequency response can be expressed as a transfer function. Unfortunately, a transfer function loses its meaning when referring to a nonlinear system. As a result, the RMS strain was calculated as a function of the excitation frequency at a low and a high electrical bias. The low electrical bias case, 75 V/mm, is presented in figure 6.5 and the high

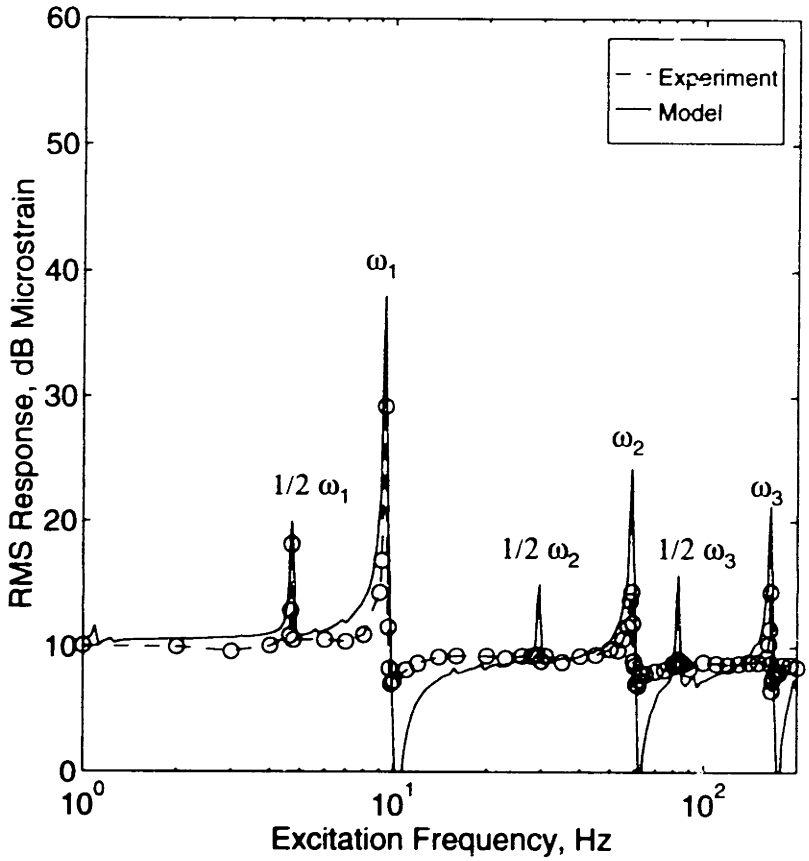

Figure 6.5: Frequency response of the cantilevered beam. There is a low DC bias of 75 V/mm. Superharmonic resonances are prevalent due to the quadratic nonlinearity inherent to electrostrictors. The quadratic model and the hyperbolic model yield identical results at this low electric field level.

electrical bias case of 400 V/mm is shown in figure 6.6. In both cases a 75 V/mm sinusoidal signal provided the excitation.

In figure 6.5, the first, second, and third modes of the beam are visible and represented by peaks in both the modeled and experimental data. There are also large responses at one half of these natural frequencies. A nonlinear system, such as an electrostrictor, is not constrained to respond at the same frequency as the excitation. An excitation at half of the natural frequency induces a resonance at the natural frequency due to the quadratic nonlinearity inherent to electrostrictors. This frequency doubling is called a

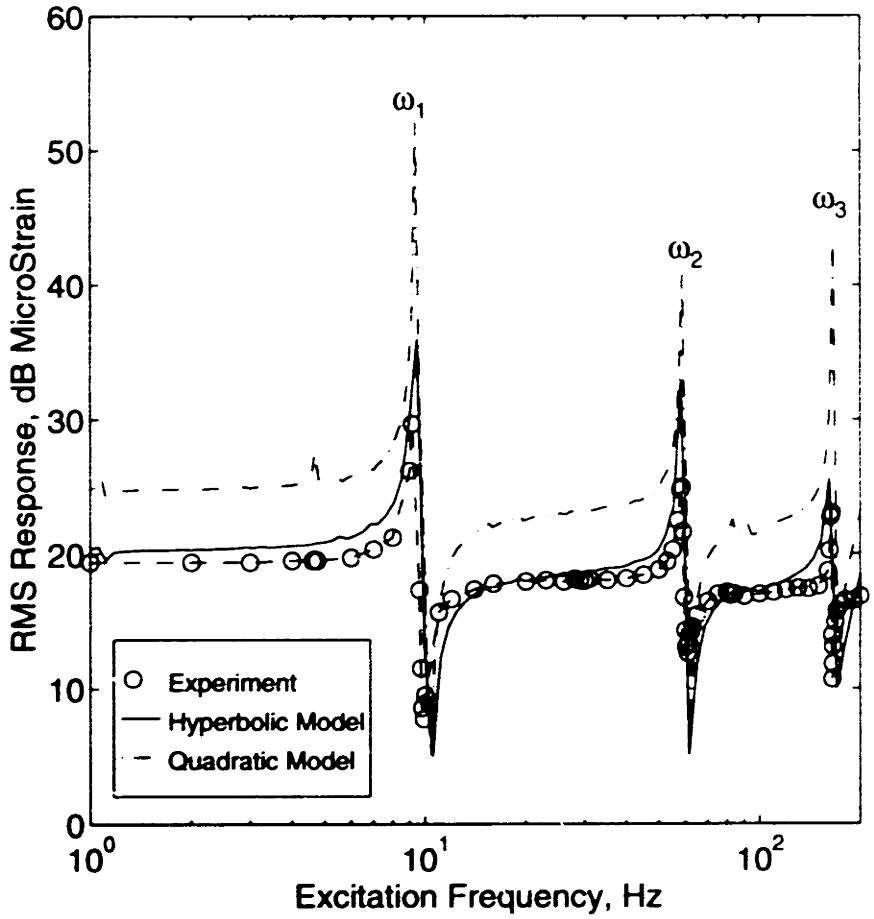

Figure 6.6: Frequency response of the cantilevered beam. There is a large DC bias of 400 V/mm. The superharmonic resonances are virtually eliminated because the high bias effectively linearizes the system.

superharmonic resonance (Nayfeh and Mook, 1979). The hyperbolic model and the quadratic model provide identical results at this field level. Additionally, the modeled and experimental results agree closely over the range of frequencies.

The superharmonic resonances are less visible in the experiment and in the simulation at the high electric bias field, as seen in figure 6.6. By going to the large bias levels, the nonlinear system essentially has been linearized. The hyperbolic model again provides close agreement over the range of frequencies. The quadratic model over predicts the response at high electric

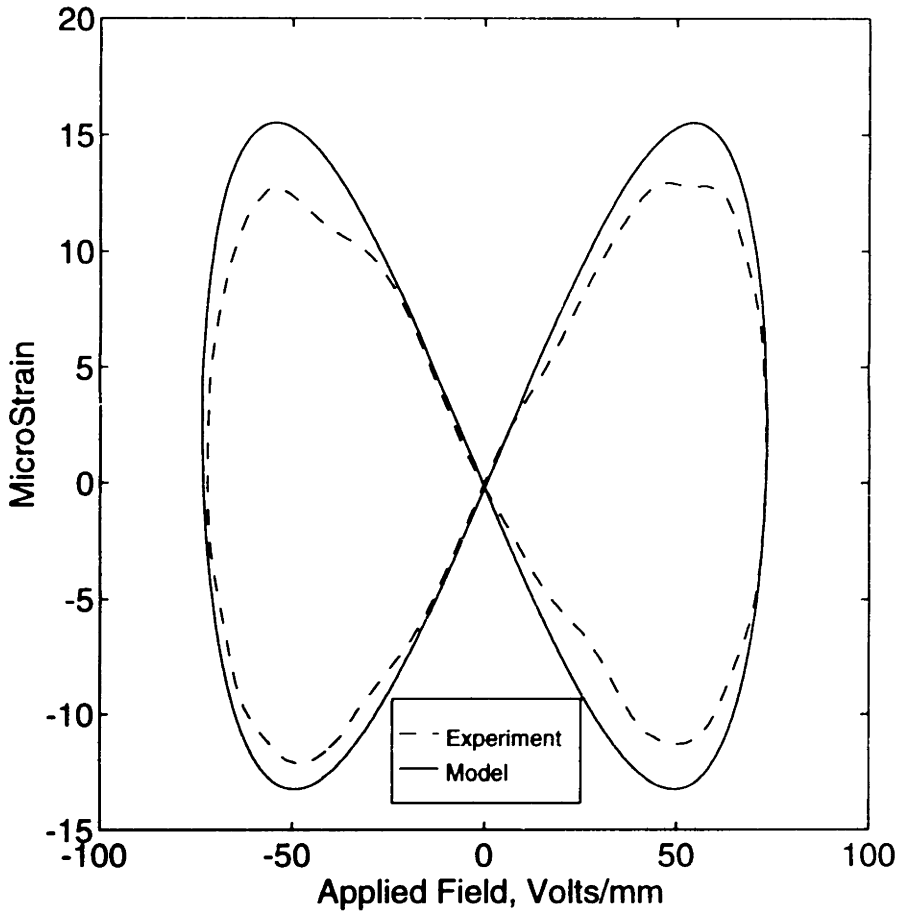

Figure 6.7: Superharmonic resonance. Excitation at one half of the first natural frequency, 4.69 Hz, excites a resonance at the natural frequency, 9.38 Hz. The quadratic model and the hyperbolic model yield identical results at this low electric field level.

field levels because the 400 V/mm DC electric bias is beyond the valid range of the reduced material constitutive relationships.

The phase portrait of the first superharmonic resonance is illustrated in figure 6.7. In this case, an excitation at one half of the first natural frequency excites the first mode of the beam. The input excitation is 4.69 Hz and the system responds at 9.38 Hz. This figure corresponds to the first peak in figure 6.5. The bow tie effect occurs because the structure (and hence the strains) are responding at twice the rate of the applied electric fields. Again, the hyperbolic model and the quadratic model yield identical results.

Chapter 7

CONTROL

Electrostriction seizes the jointed opportunity
To actively control lattices of stress
Thereby achieving greater virtues of stability.

But first the ceramic beast
Must tame its own wildness
Of careening thermal dependency
By humming a high pitched tune of constancy
To allay all fears but one-
A blizzard with a power outage
Which lends reason to its shivering.
-Dan Jobson

The previous chapters have examined the mechanical behavior of electrostrictors and the ability to model the nonlinearly coupled electromechanical behavior of an electrostrictively coupled system. This chapter applies the previous knowledge into the design and implementation of electrostrictors in feedback control. An electrostrictive actuator is used for active vibration control. A simple second-order control loop is used as well as an adaptive control algorithm. The stability of the control algorithms in the face of temperature variation is also addressed.

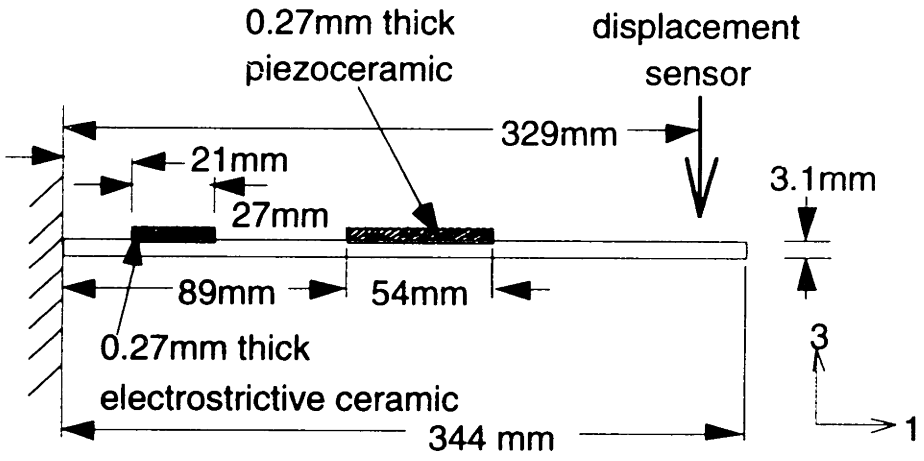

Figure 7.1: Cantilevered beam test article. The piezoceramic wafer introduces mechanical disturbances into the system. The electrostrictive wafer is used to cancel the vibrations so that the non-collocated tip displacement is minimized.

7.1 Experimental Setup

The physical setup for the controls is illustrated in figure 7.1 and the material parameters are given in figure 7.2. An electrostrictive wafer is used to cancel the disturbances introduced by a piezoceramic wafer. The vibrations measured by the displacement sensor are minimized through actuation of the electrostrictive wafer. A transfer function between the disturbance signal to the piezoceramic and the tip displacement is used to compare the effectiveness of the controllers.

7.1.1 Closed-loop setup

The basic signal diagram of the experimental setup is illustrated in figure 7.3. A Tektronix 2630 Fourier Analyzer is used to generate the transfer function. For measuring the effectiveness of the tip control, the analyzer generates a random signal and sends it to a Trek Model 663A High Voltage Power Supply and a Trek Model 662 10kV Amplifier. This amplifier magnifies the signal by a factor of 1000 before sending it to the piezoceramic

wafer. The output from this amplifier is represented by d since it is a disturbance signal.

A Bently Nevada 7200 Series Proximitor, a non-contacting inductive sensor, finds the displacement of the beam tip. The conversion factor of the sensor is 3.9 V/mm. This displacement signal is sent not only to the fourier analyzer for inclusion in the transfer function but also to the control algorithm. The digital controller is written in C, calls National Instrument input/output drivers, and runs on a Macintosh Quadra 950. The control output is passed through a Kepco model BOP 1000M voltage amplifier in route to the electrostrictive actuator. This amplifier magnifies the signal by a factor of 100 with a roll-off above 1 kHz. The controller has a cycle time of 180 Hz which is close to the second mode of the cantilevered beam system.

Piezoceramic:	Stiffness	$C^{piezo^E}_{1111} = 63$ GPa
	d constant	$d_{31} = 180\text{e-}12$ m/v
Electrostrictor:	Stiffness	$C^{a^E}_{1111} = 120$ GPa
	m constant	$m_{12} = 6.6\text{e-}16$ m^2/v^2
	k constant	$k = 1.6\text{e-}6$ v/m
	q^m constant (thermal effects on the electrostrictive term)	$q^m{}_{11221} = 2.2\text{e-}7$ m^2/v^2 $q^m{}_{11222} = -1.0\text{e-}9$ m^2/(°K v^2) $q^m{}_{11223} = 1.2\text{e-}12$ m^2/(°K^2 v^2)
	q^k constant (thermal effects on the relaxation parameter)	$q^k{}_1 = 8.0\text{e-}3\ \sqrt{m/v}$ $q^k{}_2 = -3.46\text{e-}5\ \sqrt{m/v}$ /°K $q^k{}_3 = 4.04\text{e-}8\ \sqrt{m/v}$ /°K^2
Beam:	Stiffness	$C^s_{1111} = 68$ GPa
	Poisson's ratio	$\nu^c = 0.33$
	Damping ratio	
	- First mode	$\zeta = 0.6\%$
	- Second mode	$\zeta = 0.4\%$
	- Third mode	$\zeta = 0.2\%$

Figure 7.2: Material properties of the beam, the piezoceramic disturbance source, and the electrostrictive actuator.

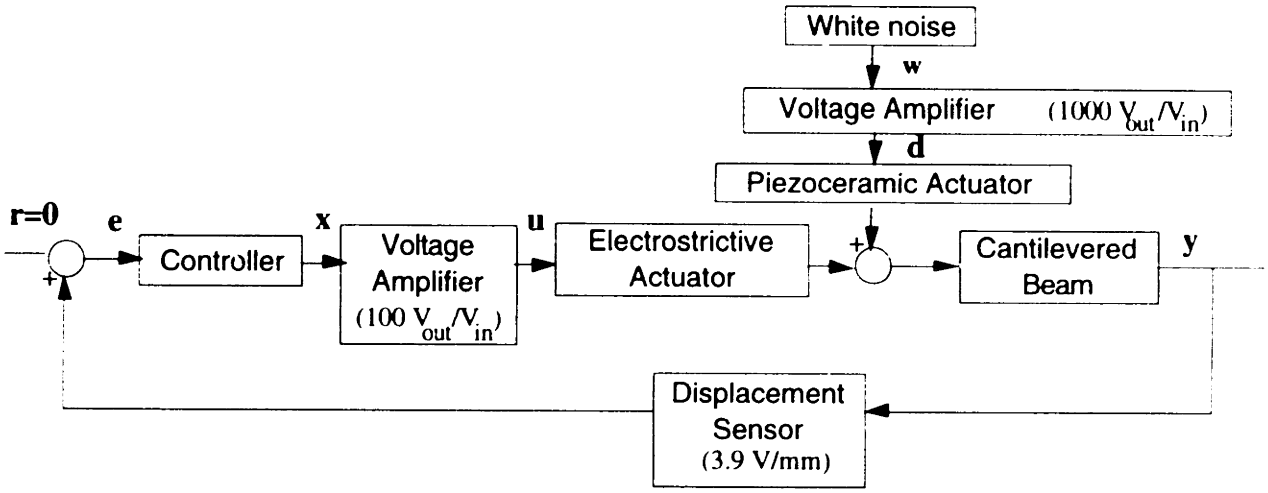

Figure 7.3: Signal diagram of the setup used to control the tip deflection of the cantilevered beam. The effectiveness of the control algorithms is determined by a transfer function between the displacement error, e, and the disturbance voltage, d.

7.1.2 Open-loop setup

The signal diagram for measuring the open-loop transfer function of the cantilevered beam system is based upon figure 7.3. The only difference is that the controller does not exist in the open-loop measurements. The transfer function between the the disturbance signal, d, and the output, y, represents the open-loop transfer function.

7.1.3 Actuator authority

The basic signal diagram for measuring the transfer function of the electrostrictive actuator is illustrated in figure 7.4. As with the open and closed-loop responses, a Tektronix 2630 Fourier Analyzer is used to generate the transfer function. The singal is amplified with the Kepco model BOP

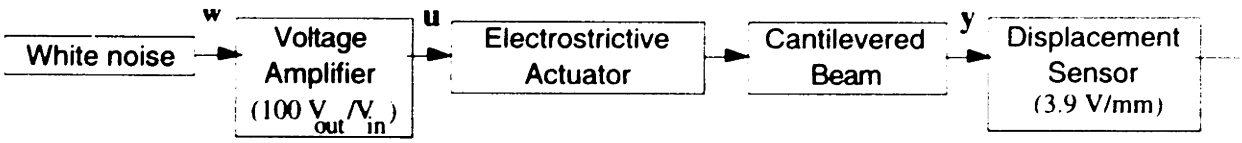

Figure 7.4: Signal diagram of the setup used to find the transfer function of the actuator.

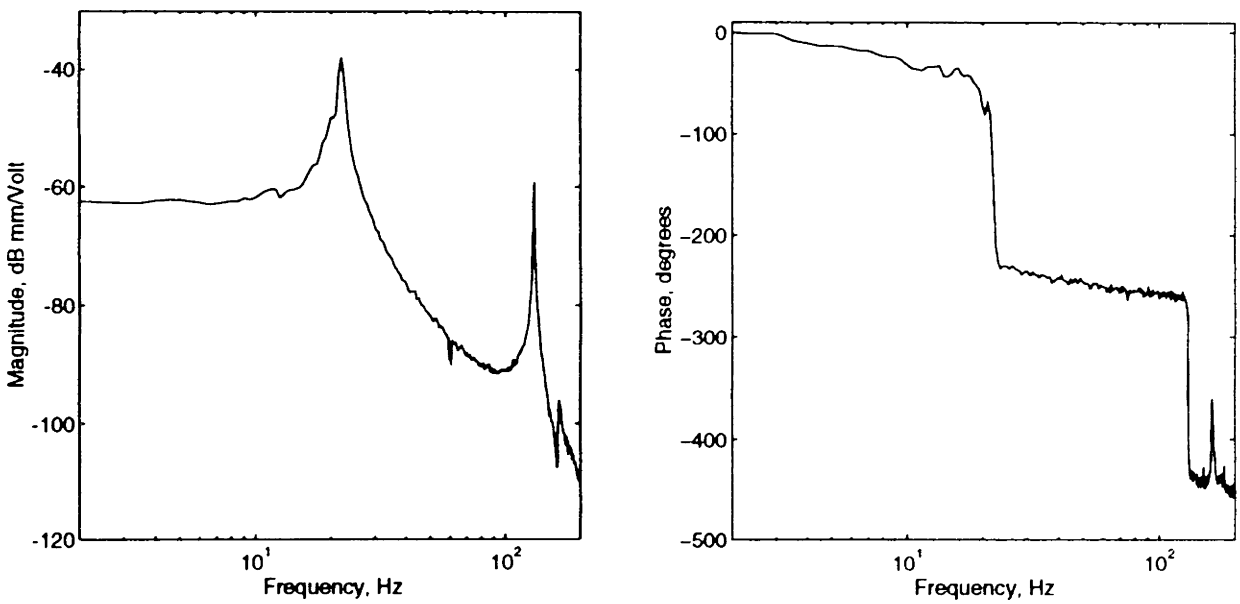

Figure 7.5: Frequency response of the electrostrictive actuator at a bias of 180 V/mm. The transfer function was taken by providing 10 V_{rms}/mm white noise at u and measuring the resulting displacement at y.

1000M voltage amplifier and then sent to the electrostrictor. The Bently Nevada 7200 Series Proximitor finds the tip displacement of the beam.

The effectiveness of the electrostrictive actuator is illustrated in figure 7.5. The wafer was biased with a 180 V/mm electric field. The Tektronix Fourier Analyzer supplied a white noise input so that the voltage at u (in figure 7.4) was 10 V_{rms}/mm. The resulting tip displacement, y, was measured. The first and second modes of the beam are clearly visible. Also of note is the lack of a zero between the two modes.

7.2 Output Linearization

The force produced by an electrostrictor is nonlinear. Until this section, the focus of this thesis has been to work with this strong material nonlinearity. This section describes a method to linearize the output from the electrostrictor. In other words, through output linearization, the electrostrictor will essentially become a linear element. As a result, with

output linearization an electrostrictor can be easily incorporated in linear control theory.

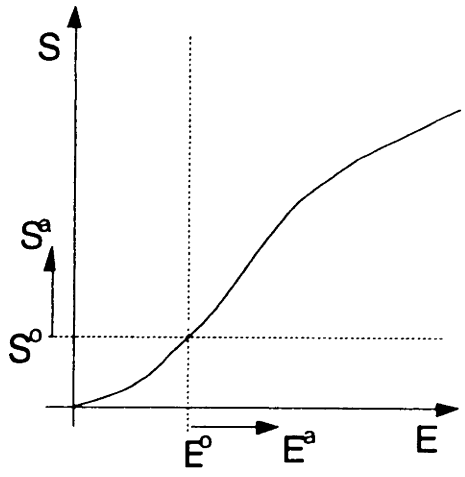

Figure 7.6: Notation for field and strain bias.

7.2.1 Output linearization model

Through output linearization, a transform is sought so that a linear input produces a linear output. In brief, the inverse of the hyperbolic strain-voltage relationship is sought. In chapter 3, the hyperbolic strain-voltage relationship was expressed in equation (3.8). Repeating the relation without the elastostriction term, the induced strain is given by

$$S_{ij} = \frac{1}{k^2} m_{mnij} \tanh^2(k|E|) \frac{E_m E_n}{|E|^2}. \tag{7.1}$$

Most applications of electrostrictives use the material in the form of a wafer. In this case, the electric field goes in only one direction. As a result, equation (7.1) can be simplified to

$$S_{ij} = \frac{1}{k^2} m_{ij} \tanh^2(k|E|). \tag{7.2}$$

Assuming that the strain is only needed in one direction transforms S and m into scalars. This allows the finding of an inverse. Inverting a scalar form of equation (7.2) gives

$$|E| = \frac{1}{k} \tanh^{-1} \sqrt{k^2 m_{ij}^{-1} S_{ij}} \tag{7.3}$$

Nominally, equation (7.3) is all that is needed for output linearization. However, for bipolar actuation an electrostrictor must be biased. The bias should be included in the formulation of the linearization. As shown in figure 7.6, define the bias point to be

$$S_{ij}^o + S_{ij}^a = S_{ij} \qquad \text{and} \qquad E_m^o + E_m^a = E_m. \tag{7.4}$$

where the superscript "o" indicates the bias point and the superscript "a" indicates the applied level after the output linearization. Substituting the strain and field bias into the inverted strain-voltage relationship becomes

$$|E^o + E^a| = \frac{1}{k}\tanh^{-1}\sqrt{k^2 m_{ij}^{-1}\left(S_{ij}^o + S_{ij}^a\right)} \tag{7.5}$$

From strain-field relationship, we can define the biased strain in terms of the electric field. Substituting equation (7.2) into equation (7.5) gives

$$|E^o + E^a| = \frac{1}{k}\tanh^{-1}\sqrt{k^2 m_{ij}^{-1}\left(\frac{1}{k^2} m_{ij}\tanh^2|kE^o| + S_{ij}^a\right)} \tag{7.6}$$

Through output linearization we are seeking a relationship where the resulting strain, S^a, is linearly proportional to the commanded field, E^c. In other words, what operation must be performed on E^c so that the applied electric field, E^a, produces a linear response. The commanded field is the response from the controller and the applied field is what is actually given to the actuator. Both the commanded field, E^c, and the resulting strain are variations around the bias point.

$$S_{ij}^a = g_{ijm} E_m^c \tag{7.7}$$

Substituting equation (7.7) into equation (7.6) yields

$$|E^o + E^a| = \frac{1}{k}\tanh^{-1}\sqrt{k^2 m_{ij}^{-1}\left(\frac{1}{k^2} m_{ij}\tanh^2|kE^o| + gE^c\right)} \tag{7.8}$$

Assuming that the biased electric field is larger than the electric field variation, i.e.. $E^c < E^o$, then we can obtain the final form of the output linearization

$$\boxed{E^a = \frac{1}{k}\tanh^{-1}\sqrt{\tanh^2(kE^o) + k^2 m_{ij}^{-1} gE^c} - E^o} \tag{7.9}$$

Equation (7.9) has incorporated several substantial assumptions. First, it is assumed that the electric field flows in only one direction which allowed the scalar for of E to be used. Similarly, unidirectional actuation was assumed which allowed the use of the scalar form of m and S. Finally, the bias in the electric field was assumed larger than the time varying component of electric field. Also, it is assumed that a linearization of the plant is desired.

Although substantial assumptions, most engineering applications will utilize these simplifications.

7.2.2 Output linearization experiment

Output linearization is meaningless unless there exists a good linear controller for the system. As a simple, yet effect linear controller, a second-order control was chosen to cancel the tip displacement of the cantilevered beam illustrated in figure 7.1. For simplicity and due to the sloth of the digital controller, damping of only the first mode was attempted.

The controller was chosen in the form of a positive position feedback (PPF) controller. A PPF controller feeds the structural position coordinate directly to the compensator and the product of the compensator position coordinate and a scalar gain positively back to the structure. This type of controller was chosen because it can pick-off modes in a dense pack and can be tuned so that it is inherently stable in the crossover region. On the downside,

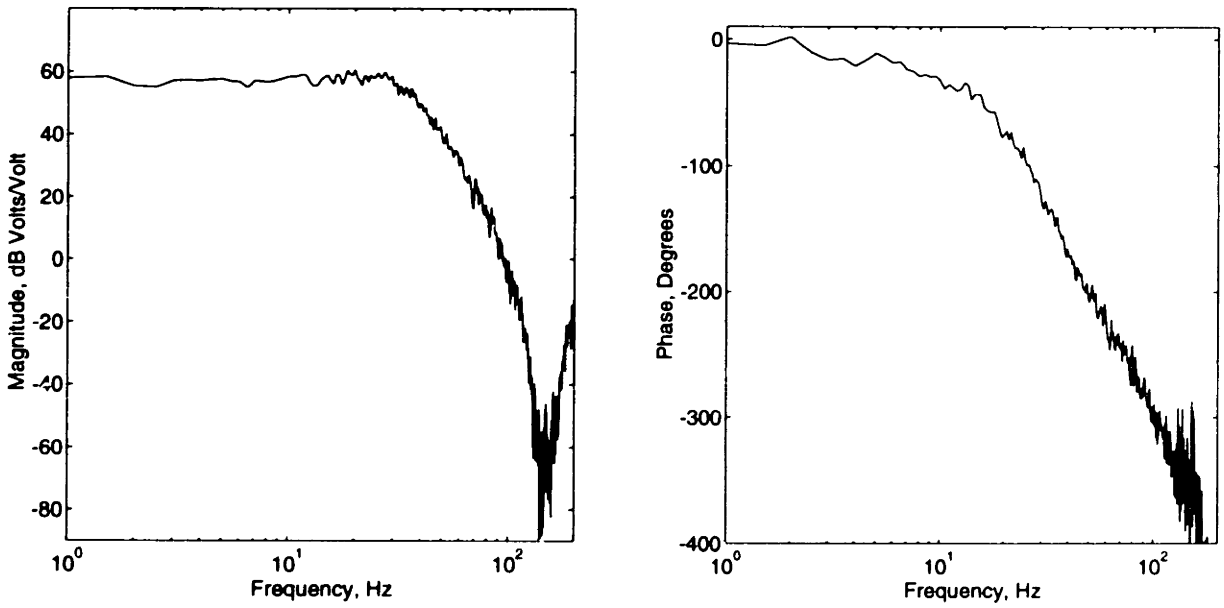

Figure 7.7: Transfer function of the PPF controller. The controller was given in equation (7.13) and the output linearization described in equation (7.9). The zero at 160 Hz corresponds to the non-minimum phase zero due to the time delay inherent to digital control.

a PPF system adds flexibility at low frequency (possible static instability) and offers only moderate damping levels.

The Laplace representation of a PPF control system is

$$H(s) = \frac{\omega^{c2}}{s^2 + 2\zeta^c\omega^c s + \omega^{c2}} \tag{7.10}$$

where ω^c is the compensator frequency, ζ^c is the compensator damping ratio, and s is the Laplace transform variable. The change from the continuous domain to the digital domain is achieved with Tustin's method in which s is replaced with its digital equivalent;

$$s \rightarrow \frac{2}{T}\frac{1-z^{-1}}{1+z^{-1}}. \tag{7.11}$$

T is the sampling interval and z is the Z transform variable. Applying Tustin's method to the PPF controller gives

$$H(z) = \frac{u(z)}{y(z)} = \omega^{c2}\left(\frac{4}{T^2}\frac{1-2z^{-1}+z^{-2}}{1+2z^{-1}+z^{-2}} + \frac{2\zeta^c\omega^c}{T}\frac{1-z^{-1}}{1+z^{-1}} + \omega^{c2}\right) \tag{7.12}$$

The Z transform is easily converted to the finite difference form. The exponent on the z indicate the delay on the variable, (i.e.. $z^{-1}u(z) \rightarrow u_{k-1}$). Writing the PPF control algorithm in the finite difference form gives

$$u_k = \frac{u_{k-1}\left(8-2\omega^{c2}\right) - u_{k-2}\left(4-4\zeta^c\omega^c T+\omega^{c2}T^2\right) + \omega^{c2}T^2\left(y_k+2y_{k-1}+y_{k-2}\right)}{4+4\zeta^c\omega^c T+\omega^{c2}T^2} \tag{7.13}$$

Control is performed by sending the output of the PPF controller given in equation (7.13) through the output linearization described in equation (7.9). The PPF controller was applied to the experimental setup described in section 7.1. The parameters were chosen to achieve roll-off quickly after the first mode the system. As a result, ζ^c=0.5, ω^c=110 rad/sec, and T=0.0062 sec. The time period is a hardware fixed parameter which is dictated by the 160 Hz cycle time. The linearization factor was chosen to be $g=15*10^{-10}$ which lies on the verge of stability. Figure 7.7 shows the PPF controller with output linearization. A representative bias voltage of 400 V/mm was used in the

linearization. The transfer function is taken between the position error, e, and the control output, x, as indicated in figure 7.3. The controller rolls-off shortly after the first natural frequency of the system. The roll-off is aided by a non-minimum phase zero which corresponds to the time delay introduced by the digital controller.

Experimentally implementing the output linearized PPF controller on the cantilevered beam produces a dramatic reduction in the disturbance of the first mode of the system. The RMS disturbance voltage to the piezoceramic, d, is 120 V/mm. The control voltage, u, is prevented from ever exceeding ±150 V/mm. Figure 7.8 shows the open-loop and closed-loop response of the system. The transfer function is between the disturbance voltage, d, and the tip displacement of the beam, y. The first mode of the system is effectively eliminated. There is also a slight softening of the low frequency behavior. In the region between 10 Hz and 100 Hz, the RMS displacement is reduced by 63%.

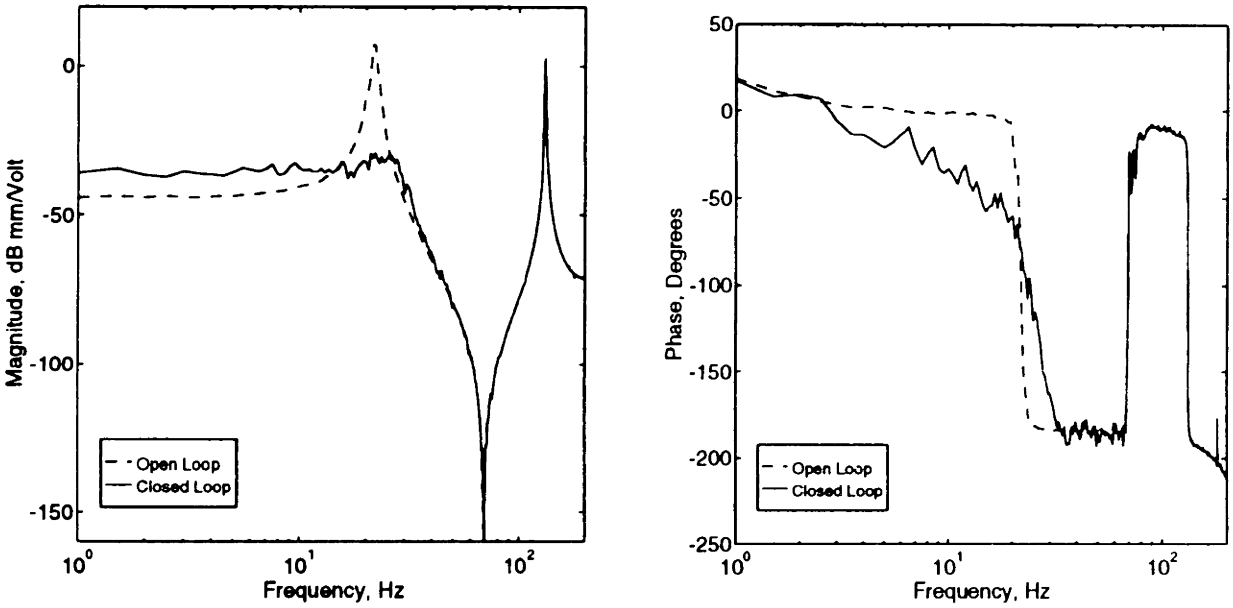

Figure 7.8: Effectiveness of the PPF controller. The electrostrictive wafer is biased to 400 V/mm. The transfer function is between the disturbance voltage, d, and the resulting displacement, y. A 63% RMS reduction is achieved between 10 Hz and 100 Hz.

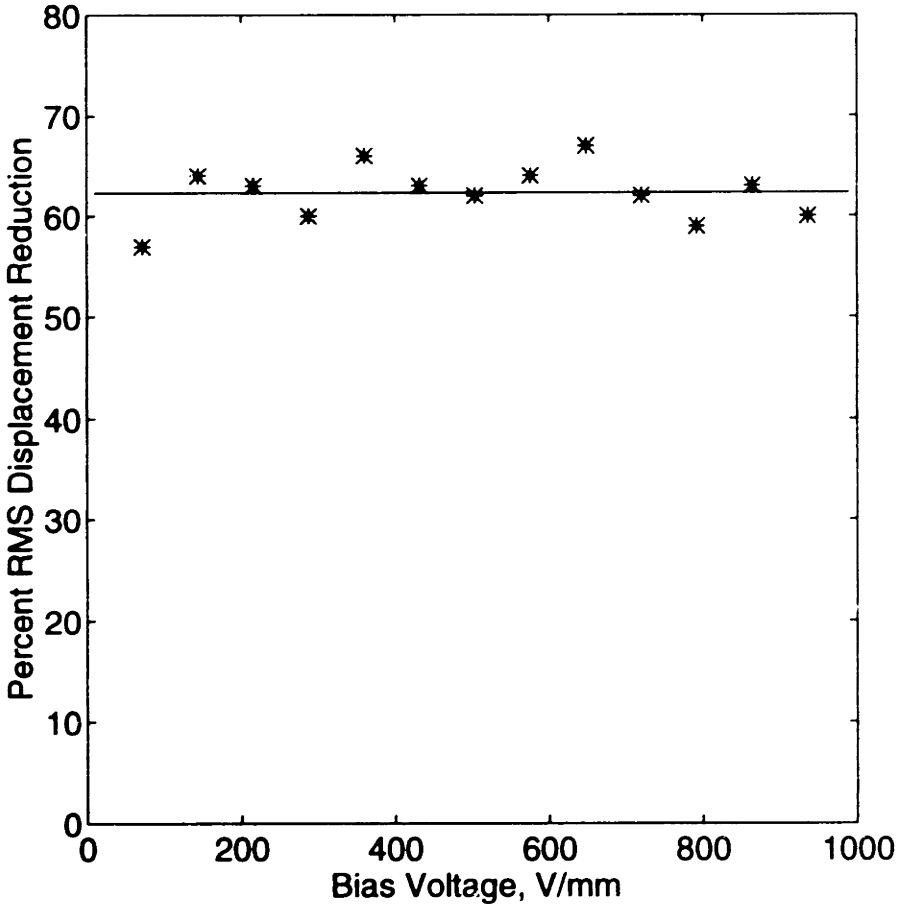

Figure 7.9: Effectiveness of the output linearization. Through output linearization, the electrostrictive actuator delivers consistent performance across a wide range of voltage amplitudes.

The purpose of the output linearization was to provide consistent performance across a wide range of voltages. As a result, the same controller was implement at different bias voltages. The reduction in the RMS displacement was noted at the different bias levels. As indicated in figure 7.9, the variation is negligible. In other words, *output linearization is a very effective method through which to obtain linear performance from an electrostrictor.*

7.3 Simple Temperature Control

Temperature sensitivity is the principle reason that electrostrictors are avoided. The electromechanical coupling changes dramatically with respect to temperature. Any design which utilizes electrostrictors must address the temperature variation.

Most engineering systems that utilize electrostrictors require temperature stability. Since the temperature does not change, the electromechanical coupling can be know very accurately. As a result, when the fix of the Hubble telescope was performed, the astronauts not only added a series of electrostrictive micropositioners but also installed a small heater.

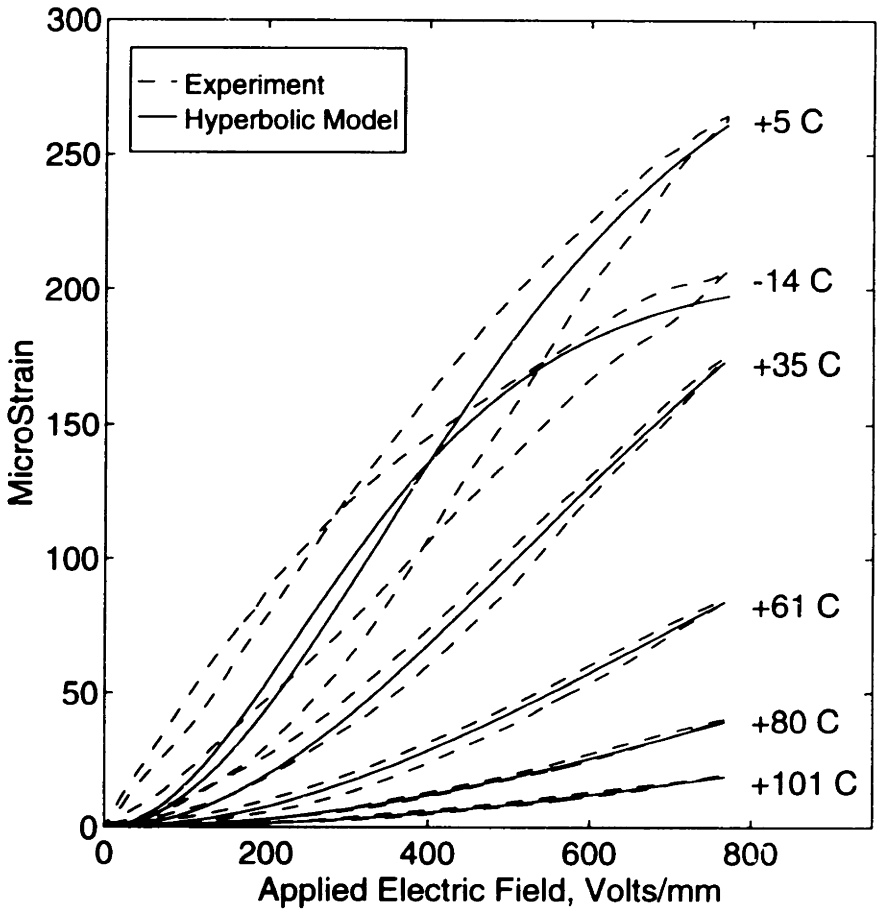

Figure 7.10: Effect of temperature variation in the transverse actuation of an electrostrictive wafer. This figure is duplicated from chapter 4.

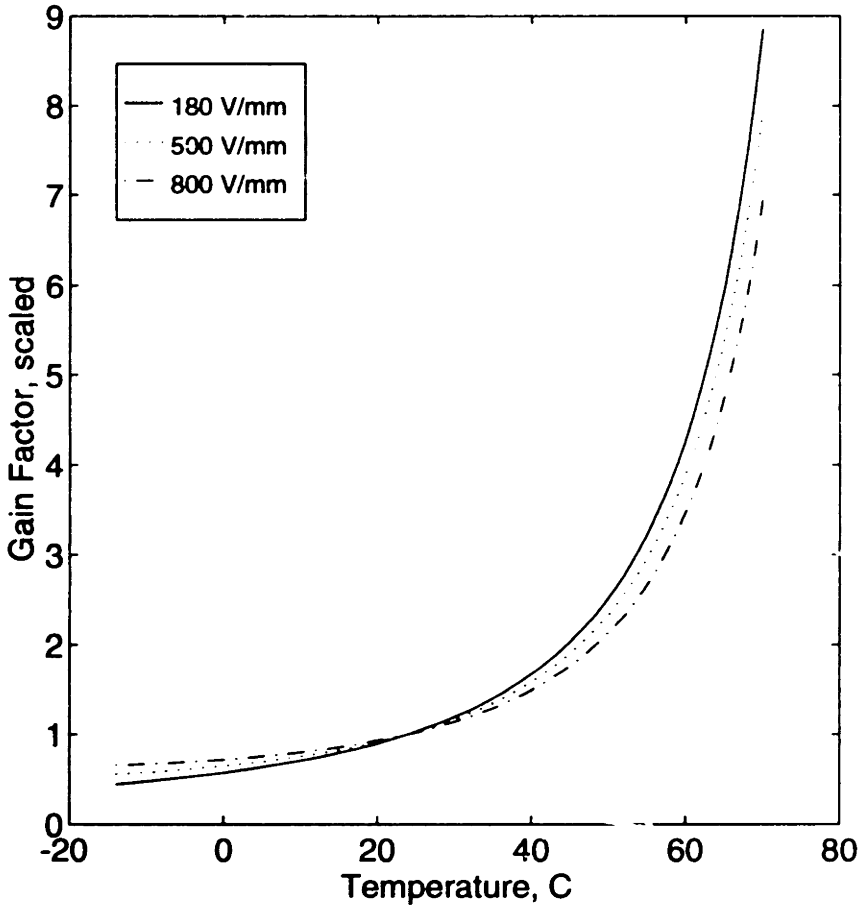

Figure 7.11: Gain factor for temperature compensation. The gain is normalized so that 25°C has unity gain.

The active vibration isolators designed by Martin Marietta require the operating temperature to be held within ±5°F (Hom and Shankar, 1994b).

Although effective, maintaining temperature stability is often an unacceptably strict requirement. This section describes two techniques to tackle the temperature troubles tied to electrostrictors: gain compensation and shivering. The gain compensation is effective and yields consistent performance over a wide range of temperatures. Shivering is essentially ineffective except for systems with very small heat capacity.

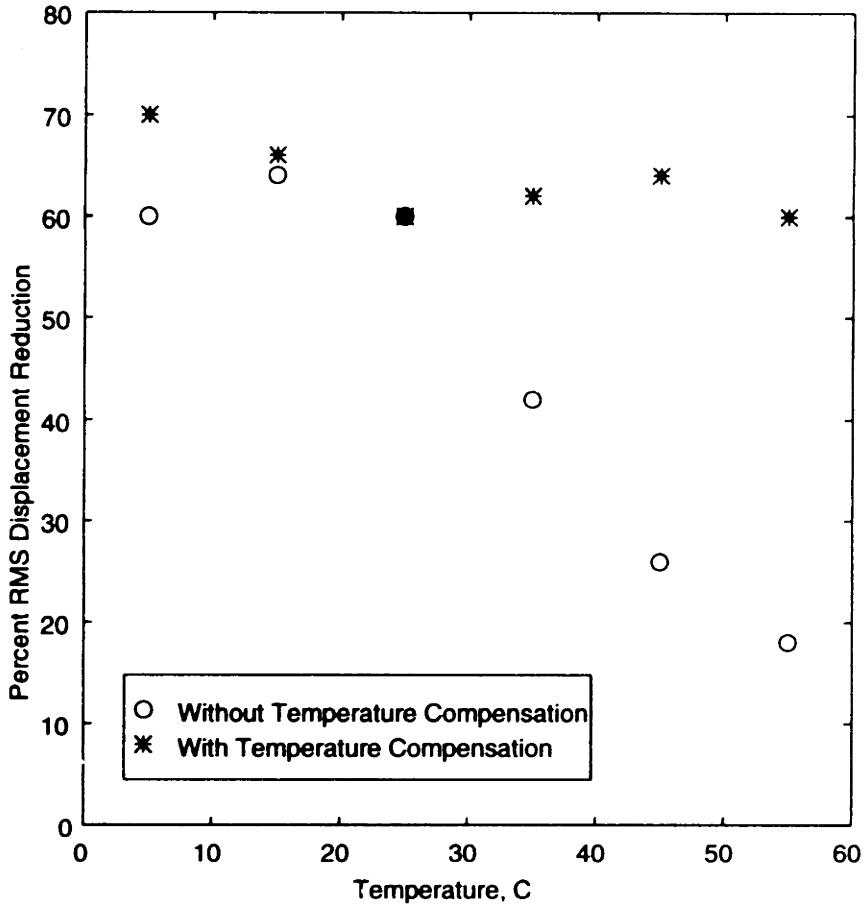

Figure 7.12: Effectiveness of electrostrictive control at different temperatures. Without any temperature compensation, the performance drops dramatically. A temperature dependent multiplicative gain allows consistent performance over a wide range of temperatures. The electrostrictor was biased by 180 V/mm.

7.3.1 Temperature gain compensation

Gain compensation is an intuitive technique to obtain uniform performance across a range of temperatures. The electr mechanical coupling of an electrostrictor decreases with temperature. As a result, if the gain of the controller is equivalently increased, then consistent performance will result. Thus, all that is needed is a temperature dependent multiplicative factor scaling the amplitude of the control signal.

The temperature variation of electrostrictors can be accurately modeled, as shown in figure 7.10. The temperature model was described in subsection 3.3.4 and experimentally validated for one dimensional actuation in section 4.4. Figure 7.10 is repeated from chapter 4.

With the models of the temperature variation given in equations (3.27) and (3.28), the electromechanical coupling can be computed at each of the temperatures. The coupling at a 180 V/mm bias field is easily found. The reciprocal of the coupling factor gives the gain needed for temperature compensation. The gain is normalized so that 25°C has unity gain. The gain as a function of temperature is presented in figure 7.11.

The tip displacement control of the cantilevered beam was attempted with the PPF controller described in equation (7.13). The parameter values remain unchanged from those given in subsection 7.2.2. The control was implemented with temperatures ranging from 5°C to 55°C. The vibration control was attempted with and without the temperature gain compensation. As seen in figure 7.12, control with temperature gain compensation delivers consistent performance across a wide range of temperatures. Control without gain compensation yields dismal performance at elevated temperatures.

7.3.2 Shivering

Hysteresis represents energy that is dissipated during a cycle. The energy is typically dissipated in the form of heat. Electrostrictors have small, but nonzero, hysteresis and, thus, will heat under a cycling electric field. The hysteresis in electrostrictors decreases with increasing temperature, as shown in figure 7.10. As a result, the heating will not significantly exceed the Curie temperature range.

The concept of small amplitude, high frequency cycling creating heat is not a revolutionary concept. This is another way of describing shivering where rapid muscle activity generates heat. Some insects vibrate their wings for a while before flight, heating the muscles to the temperature at which they

work best. The cycling of electrostrictors is simply another application of self-heating.

Unfortunately, shivering does not work very well. As seen in figure 7.13, the heat generated by the small hysteresis of the electrostrictor is small compared with the heat lost to the system. In this case, a 100 V/mm signal was applied at 1200 Hz and a DC offset of 150 V/mm. Shivering with a free wafer will increase the operating between 15°C and 5°C. This could be a significant reduction in the temperature sensitivity of the material.

However, the extra convection provided by a host aluminum structure

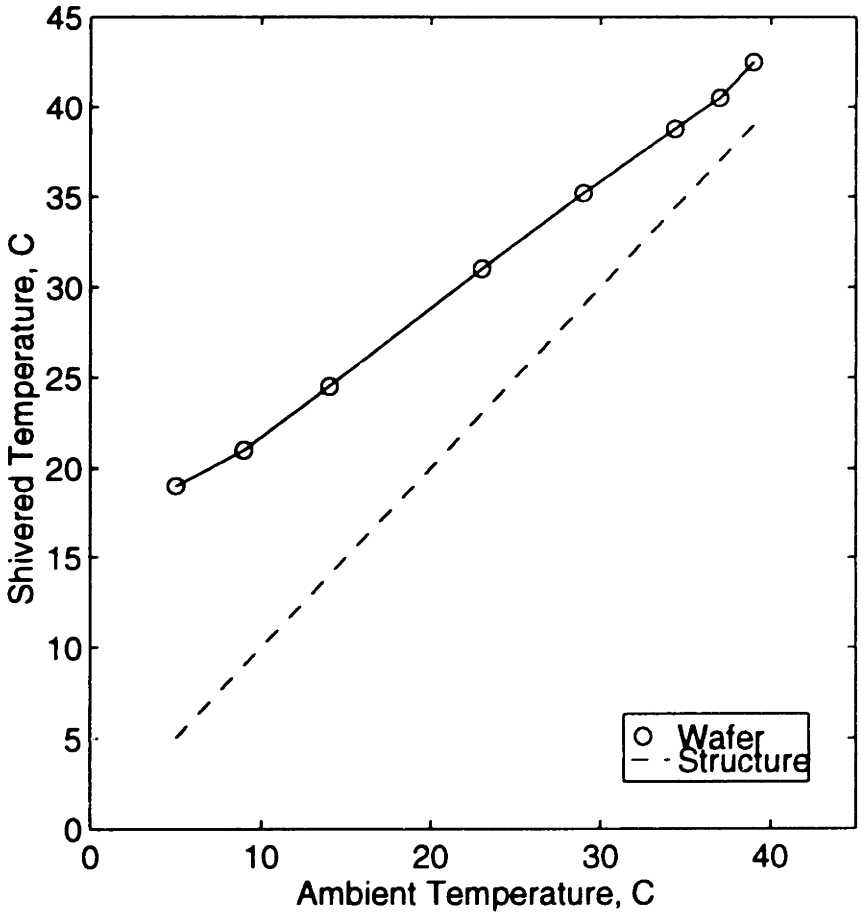

Figure 7.13: Effect of shivering (self-heating) with electrostrictors by applying a 1200 Hz, 100V/mm signal at a 150V/mm DC bias. With a free wafer, shivering significantly increases the material temperature but the heat dissipates rapidly when the wafer is applied to a structure.

completely cancels the raise in temperature. Shivering will only work when the material is well insulted.

7.4 Adaptive Control

7.4.1 Theory of adaptive control

This section applies an adaptive control algorithm to the experimental system described previously in this chapter. The theory behind adaptive control algorithms is taken from Slotine and Li (Slotine and Li, 1991).

Adaptive control differs from an ordinary controller in that the controller parameters are variable, and there is a mechanism for adjusting these parameters on-line based on signals in the system. These controllers assume that the parameters are constant or at most slowly varying. The basic approach of the adaptive controller is to estimate the uncertain system parameters based on the measured system signals, and to use the estimated parameters in the control input computation. In brief, adaptive control algorithms are control algorithms with on-line parameter estimation.

There are a variety of methods for updating the adaptation parameters. A common technique compares the output of the system with the output from a model of the system. The difference between the system output and the expected output is the basis of the adaptation. The reference model is altered so that it can accurately predict the dynamics of the system. The control output is based upon the command signal and the modeled system dynamics. As a result, adaptive controllers require a good model of the system dynamics.

Adaptive control algorithms are fundamentally different from robust control algorithms. Adaptive control algorithms are superior to the robust approach when dealing with uncertainties which are constant or slowly-varying. An adaptive control algorithm learns about its system and maximizes performance for the given set of parameters. A robust algorithm simply attempts to maximize performance over a range of possible

conditions. The adaptive control algorithm requires little or no *a priori* knowledge about the unknown parameters while the robust controller requires a reasonable estimate of the parameter bounds. The robust control algorithm is superior for dealing with disturbances, quickly varying parameters, and unmodeled dynamics.

In adaptive control, the dynamics of the system can be represented in the form

$$\mathbf{M}(\mathbf{r})\ddot{\mathbf{r}} + \mathbf{C}(\mathbf{r},\dot{\mathbf{r}})\dot{\mathbf{r}} + \mathbf{K}(\mathbf{r}) = \tau \tag{7.14}$$

where **M** represents the mass, **C** is the damping, **K** is the stiffness, and τ is the external force. At this point, the understanding of the system dynamics is introduced. It is assumed that there exists an unknown vector, **a**, which can describe the system parameters, **M**, **C**, and **K**. Although the parameter, **a**, is unknown, the relationships is know. The reference model becomes

$$\mathbf{M}(\mathbf{r})\ddot{\mathbf{r}}^{r} + \mathbf{C}(\mathbf{r},\dot{\mathbf{r}})\dot{\mathbf{r}}^{r} + \mathbf{K}(\mathbf{r}) = \mathbf{Y}(\mathbf{r},\dot{\mathbf{r}},\dot{\mathbf{r}}^{r},\ddot{\mathbf{r}}^{r})\mathbf{a} \tag{7.15}$$

where $\dot{\mathbf{r}}^{r}$ is the reference velocity. The reference velocity is formed by shifting the desired velocities according to the position error.

$$\dot{\mathbf{r}}^{r} = \dot{\mathbf{r}}^{d} - \Lambda\left(\mathbf{r} - \mathbf{r}^{d}\right). \tag{7.16}$$

The desired position is given by $\mathbf{r}^{d}$ and Λ is a relative weighting between the position error and the desired velocity components.

The unknown system parameter vector, $\hat{\mathbf{a}}$, is estimated based upon the system dynamics,

$$\dot{\hat{\mathbf{a}}} = -\Gamma\,\mathbf{Y}^{t}\mathbf{s}, \tag{7.17}$$

where the hat atop the **a** indicates the estimated value instead of the actual parameter value and Γ controls the rate of the adaptation. The velocity error, **s**, is given by

$$\mathbf{s} = \dot{\mathbf{r}} - \dot{\mathbf{r}}^{r} = \dot{\mathbf{r}} - \dot{\mathbf{r}}^{d} + \Lambda\left(\mathbf{r} - \mathbf{r}^{d}\right). \tag{7.18}$$

Combining the pieces together, the control law becomes

$$\tau = \mathbf{Y}\hat{\mathbf{a}} - \mathbf{K}^{D}\mathbf{s}. \tag{7.19}$$

The control law contains a feed forward term, $\mathbf{Y}\hat{\mathbf{a}}$, and a PD term $\mathbf{K}^D\mathbf{s}$. The PD term is exactly analogous to the form of the controller described in equation (7.10). The feed forward term incorporates the adaptive part of the control algorithm.

In summary, based upon the knowledge of the dynamics of the system, a parameter matrix $\mathbf{Y}$ is formed and initial values for the system parameters, $\hat{\mathbf{a}}$, are guessed. The output control, τ, given in equation (7.19) is based upon the system error, $\mathbf{s}$, as given in equation (7.18) and the reference model, $\mathbf{Y}\hat{\mathbf{a}}$. The system parameters are updated through equation (7.17). The loop continues by reforming the output control based upon the system error and the reference model.

7.4.2 Implementation of adaptive control

The adaptive controller described in the previous subsection can be applied to the experimental setup given in section 7.1. However, the adaptive control algorithm assumes full-state feedback. Because full-state feedback is not easily realizable for the continuous system, a single-state adaptive controller is used. The tip deflection will be used to approximate the first mode of the beam. These are bad assumptions but are the best available for the current system configuration.

For the reduced system, the gain of the system was used as the adaptation parameter. For ease in implementation, the gain was set at unity and the mass, damping, and stiffness of the reference model were varied. Thus, the reference model is

$$\mathbf{Y} = \left\{ \ddot{r}^d \quad \dot{r} \quad r \right\}. \tag{7.20}$$

The controller was used for active vibration control, so all of the desired parameter variables (variables with superscript d) were zeroed. The r value were taken from the tip displacement of the beam. The $\dot{r}$ parameter was found by differencing the current tip displacement with the previous

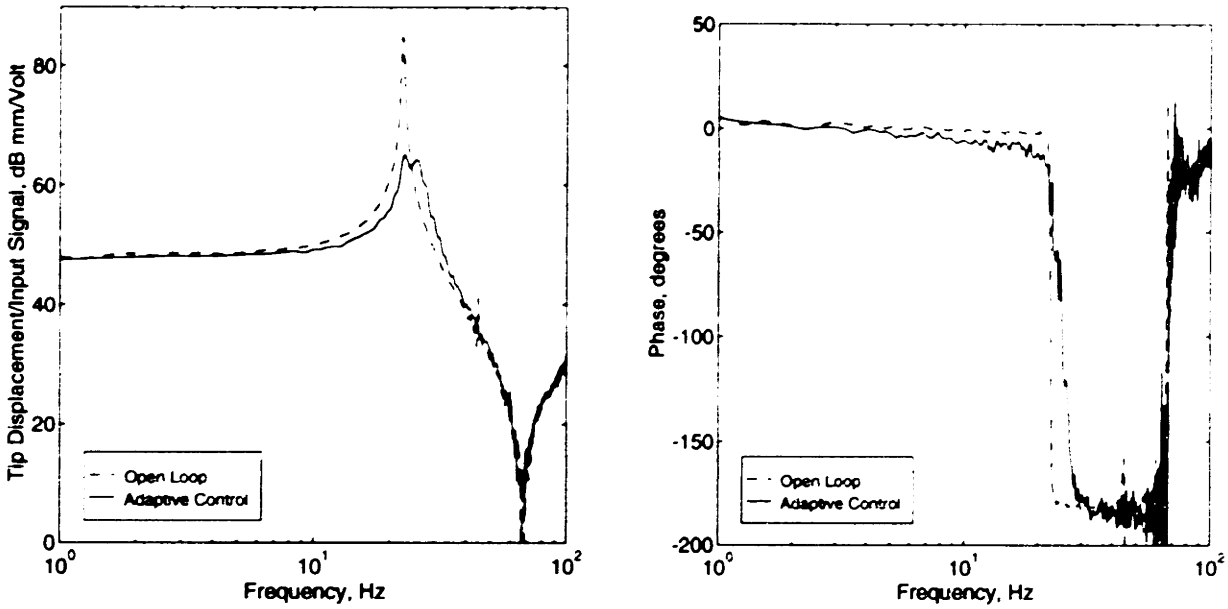

Figure 7.14: Experimental implementation of an adaptive control algorithm decreases the resonant displacement by 20%. The control algorithm was running at 150 Hz. The electrostrictive actuator was biased by 300 V/mm and the maximum signal was limited not to exceed ±70 V/mm.

displacement. During the experimental implementation, the initial values of $\hat{\mathbf{a}}$ were set to zero.

The adaptation rate was chosen to be

$$\Gamma = \begin{bmatrix} 2e-4 & 0 & 0 \\ 0 & 1e-5 & 0 \\ 0 & 0 & 1e-2 \end{bmatrix} \tag{7.21}$$

and the relative weighting was chosen to be Λ=1000. The PD gain was taken as K^D=1e-4. These parameters were experimentally chosen so as to be large enough to ensure quick convergence and effective control without inducing instability. Since these values are strongly related to the unmodeled dynamics of the system and the system noise, they are typically determined experimentally.

The experimental implementation of the adaptive control algorithm is presented in figure 7.14. The electrostrictive wafer was linearized by a bias voltage of 300 V/mm and the maximum control signal was limited to be less than 70 V/mm. With a cycle rate of 150 Hz, control was only effective on the first mode of the structure. The performance of the adaptive controller is dismal when compared with the previous controllers.

The basic experimental system doomed the adapative controller from the start. Adaptive controllers were orignially designed and work best in system that have few degrees-of-freedom, full-state feedback, moderate to large damping, and low noise levels. The cantilevered beam system has none of these attributes. The experimental setup is lightly damped continuous structure with one state of feedback through a noisy sensor. Thus, to maintain stability, low adaptation gains were required. Since low gains were used, poor performance was obtained.

Despite the poor performance, the adaptive controller holds the advantage that no knowledge of the system is required. The controller gives the 20% noise reduction regardless of the system gains. Thus, if no knowledge is available then an adaptive controller might be worth the ghastly performance that it provides.

Chapter 8

CONCLUSIONS

Shivering back and forth
Trying to be warm
Moving south then north
All in perfect form.

Vibrating still faster
Unable to stop.
Small ceramic master
Reaching for the top.
-Sarah Melton

8.1 Summary

This thesis presents the theory and the experiments describing the use of electrostrictive elements for structural actuation and control. The electromechanical behavior of the relaxor ferroelectric 0.9 PMN - 0.1 PT was categorized and presented in context of its constitutive relationships. The general form of the nonlinear constitutive relationships for an electrostrictor were reduced to a hyperbolic tangent squared relationship and even further reduced to a single quadratic relationship. The temperature dependence of the material was also presented and modeled. In this process, the 20% stiffness reduction with a 1300 V/mm electric field was measured and the material nonlinearity was shown to be an electric field-based nonlinearity.

The simplified constitutive relations were introduced into a generalized form of Hamilton's principle. Introducing an assumed mode formulation allowed these equations to be succinctly expressed in terms of an actuator equation and a sensor equation. The actuator equation describes the dynamics of the mechanical system and the sensor equation describes the dynamics of the electrical system and these equations are coupled by the electrostriction term. Although the derivation was applied to the case of an electrostrictor, the derivation is far more general and forms a framework around which the global dynamics of many nonlinear electroceramic actuated system can be derived. The equations of motion in assumed modes form could be utilized in a finite elements solution scheme or in a Rayleigh-Ritz solution since the general form of the two techniques are identical.

The general model for an electrostrictively coupled system was applied to the special case of an electrostrictive wafer (.9PMN-.1PT) mounted on a cantilevered beam. The dynamics of the electrostrictively coupled system were predicted based upon the separate dynamics of the cantilevered beam and of the electrostrictor. There was solid agreement between the predicted and experimentally measured strain and electrical displacement over a wide range of frequencies and voltages. The quadratic nonlinearity of the electrostrictor can lead to a superharmonic resonance in which case an excitation at half of the natural frequencies leads to a resonance at the natural frequency. The superharmonics greatly decreased as the bias voltage was increased.

The general model for the electrostrictively coupled system was also summoned to model the closed-loop dynamics of the electrostrictive wafer mounted on a cantilevered beam. A second-order controller and an adaptive control algorithm were implemented to cancel the tip displacements induced by a piezoceramic disturbance source. By adjusting the gains of the second-order controller according to the theory, a consistent 60% reduction of the peak displacement was achieved over a wide range of temperatures and bias voltages. The adaptive control algorithm used the gain of the electrostrictor as the adaptation parameter and succeeded in providing 20% attenuation of the tip displacement.

8.2 Contributions by Chapter

The brief summary of the conclusions from this thesis presented in the previous section is overly brief. In this section, the salient points from each chapter are presented sequentially, as appearing in the thesis. Where appropriate, section references are included so that the detailed description can be found.

8.2.1 Chapter 2: material overview

During chapter 2 the material properties of electrostrictors are placed in context with the material's crystalline structure. In section 2.1 electrostrictors are placed among the classes of crystalline materials. Additionally, the fundamental differences between electrostriction and piezoelectricity are described. The identifying characteristics of electrostriction are a diffuse phase transition and a strong material symmetry. The diffuse phase transition, which is created by microvolumes of magnesium, niobium and titanium, produces a Curie range and allows for large strains. The material symmetry causes the even powered strains-field relationships, produces a symmetric stiffness matrix, and prohibits spontaneous macroscopic polarization. The lack of spontaneous macroscopic polarization translates into the small hysteresis which is characteristic of electrostrictive devices. The temperature dependence of the gains is a function of operating the material near its Curie range. Perovskite structure is also reviewed.

During section 2.2 the applications of electrostrictive actuators are reviewed. Most applications currently involve quasi-static micro-positioning devices.

All of the information presented in chapter 2 is taken from previously published sources.

8.2.2 Chapter 3: constitutive equations

During chapter 3 the constitutive relationships for electrostrictors are derived. The chapter starts in section 3.1 with a review of the thermodynamic formalism from which constitutive relationships are derived. As with most formalisms, the thermodynamic formalism is greatly aided if the investigator knows the answer before the problem is started. In such cases the formalism then provides continuity and compatibility of the resulting equations.

One expansion of the thermodynamic formalism leads to quadratic representation of the electrostrictive constitutive relationships. In this derivation the material symmetry is utilized and higher-order terms, such as the elastostriction term, are dropped. The steps are detailed in subsection 3.2.1. The resulting relationships are dubbed the quadratic model and this is the standard representation of electrostrictors in the literature.

$$\begin{aligned} D_m &= \varepsilon^T_{mn} E_n + 2 m_{mnij} E_n T_{ij} \\ S_{ij} &= m_{pqij} E_p E_q + s^E_{ijkl} T_{kl}. \end{aligned} \tag{3.17}$$

As described in subsection 3.2.2, the quadratic model can also be expressed in matrix notation.

An alternate expansion of the thermodynamic formalisms leads to a hyperbolic tangent squared representation of the electrostrictive constitutive relationships. As detailed in subsection 3.2.3, the material symmetry is utilized and some higher-order terms are dropped. As expressed in equation (3.26) the elastostriction terms have been retained. This form of the constitutive equations is referred to as the hyperbolic model.

$$\begin{aligned} D_m &= \varepsilon^T_{mn} E_n + \frac{2}{k} m_{mnij} T_{ij} \frac{\sinh(k|E|)}{\cosh^3(k|E|)} \frac{E_n}{|E|} + \frac{2}{k} r_{mnijkl} T_{ij} T_{kl} \frac{\sinh(k|E|)}{\cosh^3(k|E|)} \frac{E_n}{|E|} \\ S_{ij} &= s^E_{ijkl} T_{kl} + \frac{1}{k^2} m_{mnij} \tanh^2(k|E|) \frac{E_m E_n}{|E|^2} + \frac{2}{k^2} r_{mnijkl} T_{kl} \tanh^2(k|E|) \frac{E_m E_n}{|E|^2} \end{aligned} \tag{3.26}$$

The last terms in equation (3.26) can be thought of as an electric field correction to the material stiffness. In this case, the variable stiffness matrix is defined as

$$C^{*}_{ijkl} = \left(s^{E}_{ijkl} + \frac{2}{k^2} r_{mnijkl} \tanh^2(k|E|) \frac{E_m E_n}{|E|^2} \right)^{-1} \qquad (3.28)$$

The previous expressions are valid only at constant temperature. The temperature dependence of the electrostrictive gains can be expressed as an algebraic expansion in terms of temperature. The form of the expansion is detailed in section 3.4.

One of the major contributions of this thesis is the introduction of the hyperbolic model and the temperature expansion of the coupling terms. Although based upon the works of Namboodri (Namboodri, 1993), this formulation is simpler and more applicable. The elastostriction term and the variable stiffness matrix were first explored by the author (Fripp, Hagood, and Luoma, 1994).

8.2.3 Chapter 4: material tests

Experiments were presented in chapter 4 that confirmed the relationships derived in chapter 3. In section 4.2 the primary coupling between electric field and strain, the electrostrictive effect, is presented. The quadratic model provides good correlation with the experiments up to 300 V/mm. The hyperbolic model continues to provide good correlation to the experiment at the maximum field level of 800 V/mm.

The elastostrictive effect is presented in section 4.3. The elastostrictive effect manifests as the electric field-based correction to the material stiffness. The stiffness was measured by examining the variation of natural frequency of a cantilvered beam as a function of bias field across the surface-bonded electrostrictor. A 20% reduction of transverse stiffness was found as the electric field increased from 0 to 1300 V/mm.

The material properties as a function of temperature are presented in section 4.4. Strain versus field curves are taken at temperatures ranging from -14°C to 100°C. The strains vary from a high of +22% at 5°C to low of -93% at

100°C of the room temperature magnitudes. Material parameters are fit to each of the curves and then the array of material parameters versus temperature are fit with an algebraic expansion. The temperature models provide a solid fit between 15°C and 70°C and a rough fit across the entire range of temperatures.

The effects of a constraint on the material properties is presented in section 4.5. The electric field-based correction to the stiffness needed to be included for good experimental agreement. Additionally it is shown that the nonlinearity of electrostrictors are an electric field-based nonlinearity.

Figure 4.16 gives a through summary of the material constants of the electrostrictor 0.9PMN-0.1PT.

One of the major contributions from this chapter is the experimental measure of the elastostrictive effect and the effect that this has upon the material stiffness. Utilization of the hyperbolic model and of the temperature models is also new. Similarly, the proof that electrostriction is a electric field-based nonlinearity is a new and fundamentally important finding.

8.2.4 Chapter 5: coupled modeling

The behavior of a continuous system with distributed active material is modeled in chapter 5. The chapter starts with a review of Hamilton's principle for coupled nonlinear systems. If the constitutive relationships are derived from a thermodynamic formalism, then the general integral nonlinear form of Hamilton's principle given in equation (5.1) can be simplified to the non-integral form given in equation (5.18).

$$\int_{t_2}^{t_1}\left[\delta T^{*}+\int_{V}\left(D_n\delta E_n-T_{kl}\delta S_{kl}\right)dV+\delta W\right]dt=0. \qquad (5.18)$$

Equation (5.18) does not impose any limitations on the material nonlinearity nor on the nature of the coupling.

Both the integral and algebraic form of Hamilton's equation are used to develop nonlinear equations of motion for electrostrictors. The process is described in detail in section 5.2. Assumed modes are introduced in section 5.3. The assumed modes are valid for Rayleigh-Ritz or for finite element solution techniques since the two techniques differ only in the number of mode shapes that are introduced. By allowing arbitrary variations in the mechanical displacements and in the voltages, coupled dynamic equations of motion result. The equations are know as the actuator equation and the sensor equation. The quadratic form is given in equation (5.48) and the hyperbolic form is given in equation (5.62).

During section 5.4 simplifications of the general equations of motion are presented. The tensor forms derived in section 5.3 are expressed in matrix form and in state-space representation.

With the exception of the general form of Hamilton's equation, everything in this chapter is new. The process of applying Hamilton's principle to coupled nonlinear systems previously had not been done. The simplification of Hamilton's principle for thermodynamic formalisms is also new. The equations of motion for arbitrarily distributed electrostrictors is the main contribution of this thesis.

8.2.5 Chapter 6: structural experiments

The models developed in chapter 5 are verified in chapter 6. Before utilizing the models, shape functions are introduced in subsection 6.1.2. The models were then used to verify the behavior of the quasi-static deflections of a cantilevered beam actuated by electrostrictors. As shown in section 6.2, the quadratic model provides correlation up until 300 V/mm while the hyperbolic model provides correlation throughout the range of field levels. The charge on the electrostrictor followed similar trends to the strain, as detailed in section 6.3.

The validity of the equations of motion at wide range of frequencies was presented in section 6.4. At low electrical bias levels, 75 V/mm, the

quadratic nonlinearity of the electrostrictor can lead to superharmonic resonances. At higher bias levels, 400 V/mm, the electrostrictor becomes more linearized and the superharmonics disappear. Both models provide good correlation at the low bias level. The hyperbolic model also provides good correlation at the higher bias level while the quadratic model over predicts the response.

This thesis is the first to illustrate the superhamonic behavior that can result from the quadratic nonlinearity inherent to electrostrictors. Models have not previously existed, and, thus, have not previously been applied to distributed actuation with electrostrictors.

8.2.6 Chapter 7: control

The knowledge developed in the previous chapter is brought to the problem of using electrostrictors to regulate the tip displacement of a cantilevered beam in chapter 7. This chapter sought to provide constant control authority at different field levels and temperatures by adjusting the control gain.

The use of output linearization is presented in section 7.2. The hyperbolic model developed in chapter 3 is inverted. As presented in equation (7.9), the applied electric field, E^a, is a direct function of the commanded electric field, E^c, and the bias electric field, E^o.

$$E^a = \frac{1}{k}\tanh^{-1}\sqrt{\tanh^2(kE^o) + k^2 m_{ij}^{-1} g E^c} - E^o \qquad (7.9)$$

A second-order control system based upon a positive position feedback controller was used in the experiment. The system was digitally implemented and provided consistent 60% signal reduction from DC to 950 V/mm.

The control of electrostrictors at different temperatures was described in section 7.3. In subsection 7.3.1 the gain of the controller is adjusted as a function of temperature to compensate for the change in the material behavior. By adjusting the gain, consistent performance is achieved between

0°C and 55°C. Without gain adjustment, the control authority and, hence, the performance drops dramatically with increasing temperature. Attempts to use self-heating or "shivering" to regulate the material temperature failed due to heat dissipation.

A nonlinear control technique known as adaptive control was introduced in section 7.4. Unlike the previous techniques where temperature and the field level must be explicitly measured, no prior knowledge is required for adaptive control. An adaptive control algorithm was implemented where the material gain was the adaptation parameter. A minor 20% signal reduction was obtained. Adaptive controllers do not work well with continuous systems or with noisy systems.

The theory of control systems was not advanced by the investigations presented in this chapter. All of the control techniques had been previously applied to other systems. This thesis simply sought to apply these techniques towards the control with electrostrictors. Dynamic control with distributed electrostrictors had not been done previously. As a result, the output linearization and the temperature stabilization are new concepts for electrostrictive control. Proving that the nonlinear behavior can be linearized and that the temperature sensitive behavior can be compensated is an exciting and important finding.

8.3 Recommendations for Future Work

Since only a single type of electrostrictive material was used in the experiments of this study (0.9PMN-0.1PT manufactured by AVX), some characteristics which were measured may be different in other materials. Even within the same batch of electrostrictors, a 10% variation in the electromechanical coupling was observed. Different formulations of electrostrictor certainly lead to different macroscopic behavior. As a result, a broader investigation into different electrostrictive types is warranted.

This study focused upon the use of electrostrictors for actuation. Little attention was paid to the use of electrostrictors as sensor. The models

developed in this thesis should be applied to the sensor applications. Also, the models should be extended and verified with magnetostrictive actuators. Applications beyond the cantilevered beam need to be investigated. More complex and more applicable structures need to be modeled and built.

The control applications presented in this study are fundamental and simple. Since digital control is required for implementation, more elaborate control should be attempted. LQR and other robust control algorithms should be used to diminish the influence of temperature.

REFERENCES

ANDERSON, E., 1989. "Piezoceramic actuation of one- and two-dimensional structures," S.M.. Thesis, Department of Aeronautics and Astronautics, Massachusetts Institute of Technology, Cambridge, Massachusetts.

ANJANAPPA, M. and BI, J., 1994. "A theoretical and experimental study of magnetostrictive mini-actuators," *Smart Materials and Structures*, Vol. 3, pp 83-91.

BAILEY, T. and J.E. HUBBARD JR., 1985. "Distributed piezoelectric-polymer active vibration control of a cantilevered beam," *Journal of Guidance, Control, and Dynamics*, Vol. 8, No. 5, pp 605-611.

BLACKWOOD, G. and M.A. EALEY, 1993. "Electrostrictive behavior in lead magnesium niobate (PMN) actuators. Part I: materials perspective," *Smart Materials and Structures*, Vol. 2, pp 124-133.

BRAITHWAITE, N. and G. WEAVER, 1990. Electronic Materials, Butterworth Scientific, Ltd., Boston.

BROADHURST, M.G., F. MICHERON, and Y. WADA, 1981. "Special issue on PVDF and associated piezoelectric polymers," *Ferroelectrics*, Vol. 32, No. 1.

BROCK, D., W. LEE, D. SEGALMAN, and W. WITKOWSKI, 1994. "A dynamic model of a linear actuator based on polymer hydrogel," *Proceedings of the Second International Conference on Intelligent Materials*, Williamsburg, Virginia, ed. Craig Rogers, pp 210-222.

BROWN, W., 1966. "Magnetoelastic Interactions," Springer-Verlag, New York, pp 62-106.

BUTLER, J.L., 1988. "Application manual for design of EXTREMA Terfenol-D magnetostrictive transducers," Edge Technologies, Inc., N. Marshfield, Massachusetts.

CADY, W.G., 1984. Piezoelectricity, Dover, New York.

CARMAN, G.P., 1994. "Nonlinear constitutive relations for magnetostrictive materials with applications to 1-D problems," *Proceedings of the Second International Conference on Smart Materials*, Williamsburg, Virginia, ed. Craig Rogers, pp. 265-277.

CHAN, K. and N. HAGOOD, 1994. "Modeling of nonlinear piezoceramics for structural actuation," *Smart Structures and Materials Conference*, Orlando, Florida, ed. Nesbitt Hagood, SPIE 2190, pp 194-205.

CHEN, P.J. and S.T. MONTGOMERY, 1980. "A macroscopic theory of the existence of the hysteresis and butterfly loops in ferroelectricity," *Ferroelectrics*, Vol 23, pp 199-208.

CHANDRA, R. and I. CHOPRA, 1991. "Experimental and theoretical analysis of composite I-beams with elastic couplings," *AIAA Journal*, Vol. 29, No. 12, pp 2197-2206.

CRANDALL, S., D. KARNOPP, E. KURTZ, and D. PRIDMORE-BROWN, 1968. *Dynamics of mechanical and electromechanical systems*. Malabar, Florida: Robert E. Krieger Publishing Company, pp 261-301.

CROSS, L. 1987. "Relaxor Ferroelectrics" *Ferroelectrics* Vol 76 pp241-267.

DEGENNES, P.G. 1982. "Pierre Curie and the role of symmetry in physical laws" *Ferroelectrics*, Vol 40, pp 125-129.

DEVONSHIRE, A.F. 1954. "Advances in Physics" *Philosophical Magazine*, Vol 3, No 10, April, pp 86-130.

EALEY, M. and P.A. DAVIS, 1990. "Standard SELECT electrostrictive lead magnesium niobate actuators for active and adaptive optical components" *Optical Engineering*, Vol 29, No 11, pp 1373-1381.

FLEMING, F. and E. CRAWLEY, 1991. "The zeroes of controlled structures: sensor/actuator attributes and structural modeling" *AIAA Journal*. .

FREIMAN, S.W. and G.S. WHITE, 1994. "Intelligent ceramic materials: Issues of brittle fracture," *Proceedings of the Second International Conference on Intelligent Materials*, Williamsburg, Virginia, ed. Craig Rogers, pp 52-62.

FRIPP, M. and N. HAGOOD, 1994. "Distributed actuation with electrostrictors," *Smart Structures and Materials Conference*, Orlando, Florida, ed. Nesbitt Hagood, SPIE 2190, pp 571-586.

GALVAGNI, J, 1990. "Electrostrictive actuators and their use in optical applications" *Optical Engineering*, Vol 29, No 11, pp 1389-1391.

GENG, Z.J. and L.S. HAYNES, 1994. "Six degree-of-freedom active vibration control using the Stewart platforms," *IEEE Transactions on Control Systems Technology*, Vol. 2, No. 1, pp 45-53.

GHANDI, K. and N.W. HAGOOD, 1994. "Shape memory ceramic actuation of adaptive structures," *Proceedings of the 35th AIAA/ASME/ASCE/AHS Structures, Structural Dynamics, and Materials Conference*, Hilton Head, South Carolina.

GOMI, M., Y. MIYAZAWA, K. UCHINO, M. ABE, and S. NOMURA, 1982. "Optical stabilizer using a bistable optical device with a PMN electrostrictor" *Applied Optics*, Vol 21, No 14, pp 2616-2619.

HAERTLING, G.H., 1986. "Piezoelectric and electrooptic ceramics" Ceramic Materials for Electronics, ed. R. Buchanan, Marcel Dekker, Inc., New York, New York.

HAGOOD, N., W. CHUNG, and A. VON FLOTOW, 1990. "Modeling of piezoelectric actuator dynamics for active structural control" *Journal of Intelligent Materials and Structures*, Vol. 1, pp 327-354.

HAGOOD, N. and E. CRAWLEY, 1988. "Development and experimental verification of damping enhancement methodologies for space structures," Space Systems Laboratory Report, SSL 18-88, Massachusetts Institute of Technology, Cambridge, Massachusetts.

HOM, C. and N. SHANKAR, 1994a. "A fully coupled constitutive model for electrostrictive ceramic materials" *Proceedings of the Second International Conference on Intelligent Materials*, Williamsburg, Virginia, ed. Craig Rogers, pp 623-634.

HOM, C. and N. SHANKAR, 1994b. Martin Marietta poster session at the Second International Conference on Intelligent Materials, Williamsburg, Virginia, June 8.

JAFFE, B., W.R. COOK, and H. JAFFE, 1971. Piezoelectric ceramics, Academic Press, New York.

JOBSON, D., 1994. "Shivering electrostrictors" NASA Langley Research Center, Hampton, Virginia.

KALE, A., 1994. "Shivering electrostrictor" York County School of the Arts, Williamsburg, Virginia.

KANNAN, K.S. and A. DASGUPTA, 1994. "Finite element scheme for modeling the magnetoelastic response of magnetostrictive smart structures," *Proceedings of the Second International Conference on Intelligent Materials*, Williamsburg, Virginia, ed. Craig Rogers, pp 719-730.

KYNAR Piezo Film Technical Manual, 1987. Pennwalt Corp., Valley Forge, Pennsylvania.

LAZARUS, K., 1989. "Induced strain actuation of anisotropic plates," S.M. Thesis, Department of Aeronautics and Astronautics, Massachusetts Institute of Technology, Cambridge, Massachusetts.

LEE, C.K., 1990. "Theory of laminated piezoelectric plates for the design of distributed sensors/actuators. Part I: Governing equations and reciprocal relationships," *Journal of the Acoustical Society of America*, Vol. 87, No. 3, pp 1144-1158.

LEE, C.K. and F.C. MOON, 1989. "Laminated piezopolymer plates for torsion and bending sensors and actuators," *Journal of the Acoustical Society of America*, Vol. 6, No. 85, pp 2432-2436.

LEVINSON, L, 1988. Electronic Ceramics: Properties, Devices, and Applications Marcel Dekker, Inc: New York pp128-144.

LINES, M. E. and A. M. GLASS, 1977. Principles and Applications of Ferroelectrics and Related Materials, Claredon Press, New York, New York.

MALONE, M., 1994. "Electrostrictor" York Country School of the Arts, Williamsburg, Virginia.

MARION, D., 1994. "Actuating Electrostrictors" York Country School of the Arts, Williamsburg, Virginia.

MASINGILL, M.V., 1994. "Ode to the Electrostrictor" York County School of the Arts, Williamsburg, Virginia.

MEIROVITCH, L., 1985. *Elements of Vibration Analysis*. New York: McGraw-Hill Book Company, pp. 223-232.

MELTON, S., 1994. "Electrostrictors" York County School of the Arts, Williamsburg, Virginia.

MOULSON, A.J. and J.M. HERBERT, 1990. Electroceramics: Materials, Properties, Applications, Chapman and Hall, New York, New York.

NAMBOODRI, C., 1992. "Experimental investigation and modeling of the electrostrictive relaxor ferroelectric lead magnesium niobate-lead titinate" M.S. thesis, Department of Mechanical Engineering, Virginia Polytechnic Institute and State University, 1992.

NAMBOODRI, C, 1993. "Temperature, frequency, and bias-field co-dependence of the electrostrictive relaxor ferroelectric lead magnesium niobate-lead titinate" *AIAA Structures, Structural Dynamics, and Materials Conference*, La Jolla, California, April 19-22, pp 3639-3648.

NAMBOODRI, C. and C. ROGERS, 1992. "Tunable vibration/strain sensing with electrostrictive materials," *Proceedings of the Conference on Recent Advances in Adaptive and Sensory Materials and their Applications*, ed. C. Rogers and R. Rogers, Blacksburg Virginia, April 27-29, pp 285-297.

NAYFEH, A. and D. MOOK, 1979. Nonlinear oscillations. New York: John Wiley and Sons, Inc.

NOMURA, S. and K. UCHINO, 1983. "Recent applications of PMN-based electrostrictors" *Ferroelectrics*, Vol 50, pp 197-202.

OGATA, K., 1990. Modern Control Engineering Prentice Hall: Englewood Cliffs, New Jersey.

Piezo Systems, Inc., 1993. Product Catalog of Piezo Systems, Inc., Cambridge, Massachusetts.

REGELBRUGGE, M., A. CARRIER, M. WRIGHT, and Y. YIU, 1994. "Performance estimates for electrostrictive vibration isolators," *Proceedings of the Second International Conference on Intelligent Materials*, Williamsburg, Virginia, ed. Craig Rogers, pp 1015-1024.

ROGERS, C.A., C. LIANG, and D.K. BARKER, 1989. "Dynamic control concepts using shape memory alloy reinforced plates," *Smart Materials, Structures, and Mathematical Issues*, Technomic, pp 39-68.

SCHETKY, K. et al., 1979. "Shape memory alloys," *Scientific American*, Vol. 241.

SLOTINE, J. and W. LI, 1991. Applied Nonlinear Control Prentice Hall: Englewood Cliffs, New Jersey. pp 311-418.

SMOLENSKII, G.A., V.A. ISUPOV, A.I. AGRANOVKAYA and S.N. POPOV, 1961. "Ferroelectrics with diffuse phase transitions," *Soviet Physics Solid State*, Vol 2, No 11, pp 2584-2594.

SOLYMAR, L. and D. WALSH, 1988. Lectures on the Electrical Properties of Materials, Oxford University Press, New York.

TAKEUCHI, T., H. MASUZAWA, C. NAKAYA, and Y. ITO, 1989. "Medical ultrasonic probe using electrostrictive-ceramic/polymer composite" *Proceedings of the IEEE Symposium on Ultrasonics*, pp 705-708.

TIERSTEN, H., 1969. *Linear piezoelectric plate vibrations* . New York: Plenum Press, pp 41-50.

TIMOSHENKO, S. and S. WOINOWSKY-KRIEGER, 1959. *Theory of Plates and Shells*. New York: McGraw-Hill, Inc.

TZOU, H. and R. HOWARD, 1992. "A piezothermoelastic shell theory applied to active structures," *Active Control of Noise and Vibration, ASME* Vol. 38, pp 205-212.

UCHINO, K., 1986. "Electrostrictive actuators: Materials and Applications," *American Ceramic Society Bulletin*, Vol. 65, No. 4, April.

UCHINO, K.,, S. NOMURA, and L. CROSS, 1982. "Anomalous temperature dependence of electrostrictive coefficients in $K(Ta_{0.55}Nb_{0.45})O_3$." *Journal of the Physical Society of Japan* , Vol 51, pp. 3242-3244.

UCHINO, K., S. NOMURA, L.E. CROSS, R.E. NEWHAM, and S.J. JANG, 1981. "Review of the electrostrictive effect in perovskites and its transducer applications" *Journal of Materials Science*, Vol 16, pp 569-578.

UPDIKE, J. "The Dance of the Solid"

WADA, B., J. FANSON, and E. CRAWLEY, 198?. "Adaptive structures"

WANG, S., 1966. *Solid-State Electronics*, McGraw-Hill Book Co., New York, pp 559-565.

WILL, G., 1994. "Electrostrictor" York County School of the Arts, Williamsburg, Virginia.

WOBELLS, E., 1994. "Shivering electrostrictors" York County School of the Arts, Williamsburg, Virginia.

YU, Y.Y., 1993. "Some recent advances in linear and nonlinear dynamical modeling of elastic and piezoelectric plates," *Adaptive Structures and Material Systems, ASME*, Vol 35, pp 185-195.

ZHANG, B. and Z.Q. ZHU, 1994. "Design of an inchworm-type linear piezomotor," *Smart Structures and Materials Conference*, Orlando, Florida, ed. Nesbitt Hagood, SPIE 2190.

Appendix A

MAGNETOSTRICTION

Magnetic Atoms, such as iron, keep
Unpaired Electrons in their middle shell,
Each one a spinning Magnet that would leap
The Bloch Walls whereat antiparallel
Domains converge. Diffuse Material
Becomes Magnetic when another Field
Aligns domains, like Seaweed in a swell.
How nicely Microscopic Forces yield,
In Units growing visible, the World we wield!
-John Updike

This chapter describes applies the models developed during the thesis to the problem of actuation with magnetostrictors. The chapter starts by describing the material behavior of magnetostrictors in general terms. Nonlinear constitutive relationships are presented. The constitutive relationships are incorporated into Hamilton's principle and nonlinear equations of motion are derived.

A.1 Material Overview

Magnetostrictive materials are an active material that can be described through the methodology presented in this thesis. Magnetostrictors are a nonlinear material where the strain is proportional to the square of the magnetic field. Like electrostrictors, magnetostrictors offer large actuation strains, high stiffness, and a quick response. Although linearized models of

magneto-mechanical interaction have been developed (Kannan and Dasgupta, 1994) (Brown, 1966), nonlinear quantatative analytical models have not been presented. This section takes the nonlinear constitutive relationships for magnetostrictors and, through the methodology presented in this thesis, derives the nonlinear governing equations for a magnetomechanical system.

Magnetostrictors are composed of materials that exhibit a strong magnetic anisotropy, such as Terfenol. Magnetic anisotropy is a reflection that electron spins are not entirely free to act independently of their host atom; and the regular atomic order within a crystal exterts some influence on the magnetic order (Braithwaite and Weaver, 1990). More specificaly, the magnetic anisotropy relates the amount of atomic magnetization along the unpreferred crystalline direction versus the atomic magnetization along the preffered crystalline direction.

The direction of the magnetic anisotropy depends upon the strain in the crystal. Applying a magnetic field alters the exchange interaction between adjacent atomic magnets and changes the atomic spacing in the material, which is strain. In other words, upon the application of a magnetic field a state of minimum energy is achieved if the crystal is strained. This small change in the shape of the magnetic specimen is the magnetostriction effect (Wang, 1966). Since the magnetostrictive effect is closely aligned with the material anisotropy, the magneto-mechanical coupling is a strong function of pre-stress and temperature.

Although large strain magnetostrictive actuators are a relatively new and exotic development, magnetostriction is neither new nor exotic. Most magnetic materials exhibit a magnetostrictive effect. Although far smaller than Terfenol, iron, cobalt, and nickel produce magnetostrictive strains on the order of 0.001%. Magnetostriction is the major source of hum in conventional transformer cores. Due to the quadratic nonlinearity of magnetostrictors, the 60 Hz main frequency produces a 120 Hz sound wave and higher harmonics.

A.2 Constitutive Equations

Like electrostrictors, magnetostrictors can be linearized through the application of a large electromagnetic field. In the unsimplified expression, however, the dynamics of an unconstrained magnetostrictor can be expressed in a set of nondissipative nonlinear algebraic constitutive relationships (Carman, 1994).

$$\begin{aligned} B_m &= \mu^S_{mn} H_n + g_{ijnm} S_{ij} H_n \\ T_{ij} &= -\frac{1}{2} g_{ijnm} H_n H_m + C^H_{ijkl} S_{kl} \end{aligned} \tag{a.1}$$

The magnetic permeability, μ, relates the magnetic flux density, B, with the applied magnetic field strength, H. The magnetic permeability relays the strength of the ferromagnetic effect and is measured at constant strain. The stiffness at constant magnetic field, C^H, relays strain and stress. The magnetomechanical coupling term is given by g.

A.3 Equations of Motion

A.3.1 Hamilton's principle

The general equations of motion of the magnetostrictor are based upon Hamilton's principle. Hamilton's principle for a nonlinear electo-magnetically coupled mechanical system is given by

$$\int_{t_1}^{t_2} \left[\delta T^* - \delta U + \delta W^*_m - \delta W_e + \delta W \right] dt = 0. \tag{a.2}$$

The form of Hamilton's principle given in equation (a.2) differs from the form given in equation (5.1) because the independent parameters are strain and magnetic field instead of strain and electric field. As a result, the energy terms are defined slightly differently from the forms given in equations (5.7-5.10).

$$T^* = \int_V \int_0^{\dot{\xi}} d\dot{u}_j \rho \dot{u}_j \, dV \tag{a.3}$$

$$U = \int_V \int_0^{\xi} S'_{ij}(\xi) T_{ij}(S(\xi), E(\xi)) \, d\xi \, dV. \tag{a.4}$$

$$W_e = \int_V \int_0^{\bar{\xi}} D'_m(\xi) E_m\big(S(\xi), D(\xi)\big)\, d\xi\, dV \tag{a.5}$$

$$W^*_m = \int_V \int_0^{\bar{\xi}} H'_m(\xi) B_m\big(S(\xi), H(\xi)\big)\, d\xi\, dV \tag{a.6}$$

$$\delta W = \int_A f_i\, \delta u_i\, dA - \sum_j E_j\, \delta q_j + \sum_k B_k \delta H \tag{a.7}$$

For a magnetostrictor, the electrical energy term given by equation (a.5) is negligible. The derivation of the general equations of motion closely follows that used for electrostrictors in section 5.2.1.

A.3.2 Variation of kinetic energy

The evaluation of the variations needs to be performed for each of the expressions in equation (a.2). The variation of the complementary kinetic energy is

$$\delta T^* = \int_V \delta \int_0^{\dot{u}} d\dot{u}^t \rho \dot{u}\; dV. \tag{a.8}$$

Bringing the variation inside of the integral gives

$$\delta T^* = \int_V \delta\dot{u}^t \rho \dot{u}\; dV. \tag{a.9}$$

Integrating by parts yields

$$\int_{t_1}^{t_2} \delta T^*\, dt = \int_V \delta u^t \rho \dot{u} \Big|_{t_1}^{t_2} dV - \int_{t_1}^{t_2} \int_V \delta u^t \rho \ddot{u}\, dV\, dt \tag{a.10}$$

where the first term must be zero. Hamilton's principle allows arbitrary variation of the path between the endpoints but requires the variation at the end points to be zero.

A.3.3 Variation of potential energy

The variation in the mechanical potential energy involves the coupled dynamics of the strain and stress variables. As a result, the variation of the coupled variables can be expressed in terms of a single dummy variable, ξ,

which reflects the current state of the system along the arbitrarily varying path. As given in equation (a.4), the variation in the potential energy is given by

$$U = \int_V \int_0^{\tilde{\xi}} S'_{ij}(\xi) T_{ij}\big(S(\xi), E(\xi)\big)\, d\xi\, dV. \tag{a.11}$$

Substituting the constitutive relationships as given in equation (a.1), the potential energy becomes

$$U = \int_V \int_0^{\tilde{\xi}} \underbrace{S'_{ij} C^H_{ijkl} S_{kl} - \frac{1}{2} g_{ijnm} S'_{ij} H_n H_m}_{\tilde{U}}\, d\xi\, dV. \tag{a.12}$$

Taking the variation with respect to each of the state variables yields

$$\begin{aligned} \delta U &= \int_V \int_0^{\tilde{\xi}} \left\{ \frac{\partial \tilde{U}}{\partial S_{kl}} \delta S_{kl} + \frac{\partial \tilde{U}}{\partial H_m} \delta H_m + \frac{\partial \tilde{U}}{\partial S'_{ij}} \delta S'_{ij} \right\} d\xi\, dV \\ &= \int_V \int_0^{\tilde{\xi}} \left\{ \left(C^H_{ijkl} S'_{ij}\right) \delta S_{kl} + \left(-g_{ijnm} S'_{ij} H_n\right) \delta H_m + \left(C^H_{ijkl} S_{kl} - \tfrac{1}{2} g_{ijnm} H_n H_m\right) \delta S'_{ij} \right\} d\xi dV. \end{aligned} \tag{a.13}$$

Integrating the last term in equation (a.13) by parts in order to transform the variation of S' into a variation of S yields

$$\begin{aligned} \delta U = \int_V \int_0^{\tilde{\xi}} &\left\{ \left(C^H_{ijkl} S'_{ij}\right) \delta S_{kl} + \left(-g_{ijnm} S'_{ij} H_n\right) \delta H_m + \left(-C^H_{ijkl} S'_{kl} + g_{ijnm} H'_n H_m\right) \delta S_{ij} \right\} d\xi \\ &+ \left(C^H_{ijkl} S_{kl} - \tfrac{1}{2} g_{ijnm} H_n H_m\right) \delta S_{ij} \Big|_0^{\tilde{\xi}} dV \end{aligned} \tag{a.14}$$

Let $\xi = \tilde{\xi}$ represent the present state of the system and $\xi = 0$ correspond to zero field and zero strain conditions:

$$\begin{aligned} &S\left(\xi = \tilde{\xi}\right) = S, \qquad H\left(\xi = \tilde{\xi}\right) = H, \\ &S(\xi = 0) = 0, \quad \text{and} \quad H(\xi = 0) = 0. \end{aligned} \tag{a.15}$$

Cancelling the redundant stiffness terms in the strain variation and rearranging equation (a.14) yields

$$\delta U = \int_V \left(C^H_{ijkl} S_{kl} - \tfrac{1}{2} g_{ijnm} H_n H_m\right) \delta S_{ij} + \int_0^{\tilde{\xi}} \left\{ \left(-g_{ijnm} S'_{ij} H_n\right) \delta H_m + \left(g_{ijnm} H'_n H_m\right) \delta S_{ij} \right\} d\xi\, dV \tag{a.16}$$

A.3.4 Variation of magnetic energy

The magnetic energy terms can be evaluated in a manner similar to the mechanical potential energy terms. Again, the arbitrary yet coupled magnetic field and magnetic flux variables require the introduction of a dummy variable, ξ, which indicates the state of the system along the path.

$$W_m^* = \int_V \int_0^{\tilde{\xi}} H'_m(\xi) B_m(S(\xi), H(\xi))\, d\xi\, dV \tag{a.17}$$

Substituting for magnetic flux from the constitutive relationship gives

$$W_m^* = \int_V \int_0^{\tilde{\xi}} \underbrace{\mu^S_{mn} H_n H'_m + g_{ijnm} S_{ij} H_n H'_m}_{W_m^*}\, d\xi\, dV. \tag{a.18}$$

Taking the variation with respect to each of the state variables yields

$$\begin{aligned}
\delta W_m^* &= \int_V \int_0^{\tilde{\xi}} \left\{ \frac{\partial \tilde{W}_m^*}{\partial S_{ij}} \delta S_{ij} + \frac{\partial \tilde{W}_m^*}{\partial H_n} \delta H_n + \frac{\partial \tilde{W}_m^*}{\partial H'_m} \delta H'_m \right\} d\xi\, dV \\
&= \int_V \int_0^{\tilde{\xi}} \left\{ \left(g_{ijnm} H_n H'_m\right) \delta S_{ij} + \left(\mu^S_{mn} H'_m + g_{ijnm} S_{ij} H'_m\right) \delta H_n \right. \\
&\qquad \left. + \left(\mu^S_{mn} H_n + g_{ijnm} S_{ij} H_n\right) \delta H'_m \right\} d\xi\, dV.
\end{aligned} \tag{a.19}$$

The variation of H′ needs to be transformed into a variation of H because the the variation of the magnetic field is defined to be zero at the endpoints. Variations of the derivative of the magnetic field, H′, are not explicitly defined. As a result, integrate equation (a.19) by parts to yield

$$\begin{aligned}
\delta W_m^* = \int_V \int_0^{\tilde{\xi}} &\left\{ \left(g_{ijnm} H_n H'_m\right) \delta S_{ij} + \left(\mu^S_{mn} H'_m + g_{ijnm} S_{ij} H'_m\right) \delta H_n \right. \\
&\left. - \left(\mu^S_{mn} H'_n + g_{ijnm} S'_{ij} H_n + g_{ijnm} S_{ij} H'_n\right) \delta H_m \right\} d\xi + \left(\mu^S_{mn} H_n + g_{ijnm} S_{ij} H_n\right) \delta H_m \Big|_0^{\tilde{\xi}}\, dV
\end{aligned} \tag{a.20}$$

Let $\xi = \tilde{\xi}$ represent the present state of the system and $\xi = 0$ correspond to zero field and zero strain conditions:

$$\delta W_m^* = \int_V \left(\mu^S_{mn} H_n + g_{ijnm} S_{ij} H_n\right) \delta H_m + \int_0^{\tilde{\xi}} \left\{ \left(g_{ijnm} H_n H'_m\right) \delta S_{ij} - \left(g_{ijnm} S'_{ij} H_n\right) \delta H_m \right\} d\xi\, dV \tag{a.21}$$

A.3.5 Equations of motion

At this point, each of the energy terms needed for Hamilton's principle have been expressed in terms of the constitutive relationships for magnetostrictors. Substituting these energy terms into equation (a.2) produces the equations of motion for a magnetostrictively coupled structure.

$$\int_{t_1}^{t_2}\left[\int_V \delta\mathbf{u}_j\rho\ddot{\mathbf{u}}_j\,dV - \int_V\left(C^H_{ijkl}S_{kl} - \tfrac{1}{2}g_{ijnm}H_nH_m\right)\delta S_{ij}\,dV\right.$$
$$\left. + \int_V\left(\mu^S_{mn}H_n + g_{ijnm}S_{ij}H_n\right)\delta H_m\,dV + \int_A f_i\delta u_i\,dA + \sum_k B_k\delta H_k\right]dt = 0. \qquad \text{(a.22)}$$

Now that the equations of motion for a magnetostrictively coupled system have been developed, the equations can be substituted into an assumed mode formulation. An actuator and a sensor equation will result. The process of applying assumed mode formulation was described in depth in chapter 5.